

AD-A083 653

GEORGIA INST OF TECH ATLANTA SCHOOL OF CIVIL ENGINEERING F/6 13/11
CAVITATION DAMAGE MECHANISMS: EXPERIMENTAL STUDY OF CAVITATION --ETC(U)
FEB 80 C S MARTIN, D C WIGGERT, H MEDLARZ F33615-77-C-2036

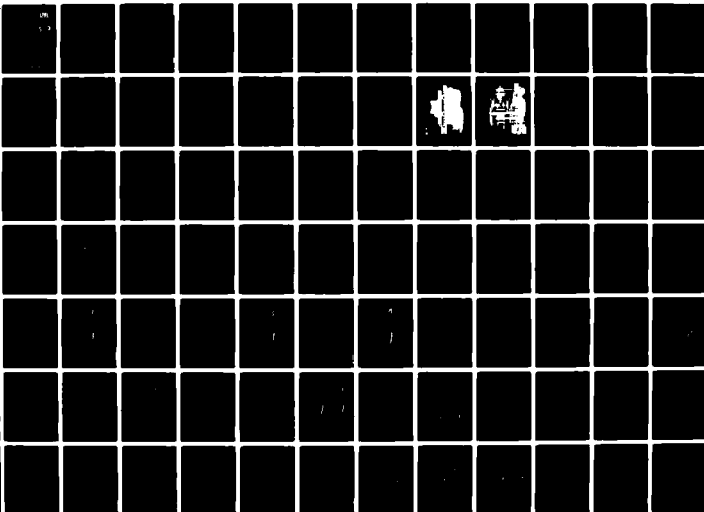
UNCLASSIFIED

AFAPL-TR-79-2121

NL

1 - 2

AD
A083653



ADA 083653

2

AFAPL-TR-79-2121

LEVEL II

CAVITATION DAMAGE MECHANISMS: EXPERIMENTAL STUDY OF CAVITATION
IN A SPOOL VALVE

C. S. Martin, D. C. Wiggert and H. Medlarz

School of Civil Engineering
Georgia Institute of Technology
Atlanta, Georgia 30332

DTIC
ELECTE
APR 28 1980
S D E

February 1980

TECHNICAL REPORT AFAPL-TR-79-2121
Final Report for Period August 1977 - September 1979

Approved for public release; distribution unlimited

AIR FORCE AERO PROPULSION LABORATORY
AIR FORCE WRIGHT AERONAUTICAL LABORATORIES
AIR FORCE SYSTEMS COMMAND
WRIGHT-PATTERSON AIR FORCE BASE, OHIO 45433

DDC FILE COPY

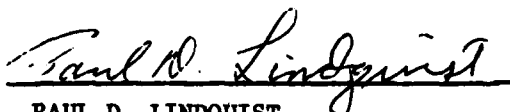
80 4 28 111

NOTICE


When Government drawings, specifications, or other data are used for any purpose other than in connection with a definitely related Government procurement operation, the United States Government thereby incurs no responsibility nor any obligation whatsoever; and the fact that the government may have formulated, furnished, or in any way supplied the said drawings, specifications, or other data, is not to be regarded by implication or otherwise as in any manner licensing the holder or any other person or corporation, or conveying any rights or permission to manufacture, use, or sell any patented invention that may in any way be related thereto.

This report has been reviewed by the Information Office (OI) and is releasable to the National Technical Information Service (NTIS). At NTIS, it will be available to the general public, including foreign nations.

This technical report has been reviewed and is approved for publication.



PAUL D. LINDQUIST
Power Systems Branch
Aerospace Power Division
Aero Propulsion Laboratory



B. L. MCFADDEN
Acting Chief, Power Systems Branch
Aerospace Power Division
Aero Propulsion Laboratory

FOR THE COMMANDER



JAMES D. REAMS
Chief, Aerospace Power Division
Aero Propulsion Laboratory

"If your address has changed, if you wish to be removed from our mailing list, or if the addressee is no longer employed by your organization please notify AFWAL/POOS, W-PAFB, OH 45433 to help us maintain a current mailing list".

Copies of this report should not be returned unless return is required by security considerations, contractual obligations, or notice on a specific document.

SECURITY CLASSIFICATION OF THIS PAGE (When Data Entered)

REPORT DOCUMENTATION PAGE		READ INSTRUCTIONS BEFORE COMPLETING FORM	
1. REPORT NUMBER AFAPL TR-79-2121	2. GOVT ACCESSION NO. AD-A083653	3. RECIPIENT'S CATALOG NUMBER 9	4. PERFORMING ORG. REPORT NUMBER
5. TITLE (and Subtitle) CAVITATION DAMAGE MECHANISMS: EXPERIMENTAL STUDY OF CAVITATION IN A SPOOL VALVE		6. PERIOD OF REPORT COVERED Final Technical rept. August 1977 - September 1979	
7. AUTHOR(s) C. S. Martin, D. C. Wiggert, and H. Medlarz		8. CONTRACT OR GRANT NUMBER(s) F33615-77-C-2036	
9. PERFORMING ORGANIZATION NAME AND ADDRESS School of Civil Engineering Georgia Institute of Technology Atlanta, Georgia 30332		10. PROGRAM ELEMENT, PROJECT, TASK AREA & WORK UNIT NUMBERS 12147	
11. CONTROLLING OFFICE NAME AND ADDRESS Air Force Aero Propulsion Laboratory Air Force Systems Command Wright-Patterson Air Force Base, Ohio 45433		12. REPORT DATE February 1980	
14. MONITORING AGENCY NAME & ADDRESS (if different from Controlling Office)		13. NUMBER OF PAGES 132	
		15. SECURITY CLASS. (of this report) Unclassified	
		15a. DECLASSIFICATION/DOWNGRADING SCHEDULE	
16. DISTRIBUTION STATEMENT (of this Report) Approved for public release; distribution unlimited.			
17. DISTRIBUTION STATEMENT (of the abstract entered in Block 20, if different from Report) Approved for public release; distribution unlimited.			
18. SUPPLEMENTARY NOTES			
19. KEY WORDS (Continue on reverse side if necessary and identify by block number) Directional control valve Dissolved gas Cavitation Incipient cavitation Pressure spectra Steady-state oscillation Acceleration spectra Damage mechanisms			
20. ABSTRACT (Continue on reverse side if necessary and identify by block number) Cavitation has been investigated in directional control valves in order to identify damage mechanisms characteristic of components of aircraft hydraulic systems. Extensive tests were conducted in a representative metal spool valve and in a model three times larger. Both valves are well instrumented for			

DD FORM 1 JAN 73 1473

EDITION OF 1 NOV 65 IS OBSOLETE

SECURITY CLASSIFICATION OF THIS PAGE (When Data Entered)

411354

TRE

the purpose of accurately measuring mean quantities as well as detecting the onset and extent of cavitation once it developed.

Non-cavitating data taken with both valves showed that the position of the high-velocity annular jet issuing from the orifice shifted orientation depending upon valve opening and Reynolds number. By means of high-frequency response pressure transducers strategically placed in the valve chamber of each test valve cavitation could be sensed by the correlation of noise with a cavitation index. Cavitation inception could be detected by comparing energy spectra for a fixed valve opening and a constant discharge. Another sensitive indicator of cavitation inception is the ratio of cavitating to non-cavitating spectral densities. The incipient cavitation index as defined in this investigation correlates well with the Reynolds number for both valves.

For developed cavitation fluctuating energy from a high-frequency response accelerometer indicated a sharp rise over the corresponding condition with no cavitation. In fact, once cavitation develops, an accelerometer properly located on the cavitating component can be as sensitive to cavitation noise as a pressure transducer. Energy levels under developed cavitation were affected to some extent by temperature differences. Several tests showed that dissolved gas had no effect on cavitation noise provided that the gas content did not exceed that corresponding to atmospheric conditions.

A limited number of tests were conducted under steady-state oscillation of the valve spool. There was no appreciable change in the cavitation noise provided that the cavitation index remained quite low. If the cavitation index was varied about a mean value corresponding to peak cavitation noise under steady-flow conditions then oscillating the valve resulted in lower noise levels. Further testing is recommended for the determination of valve characteristics under transient and steady-state oscillating conditions.

PREFACE

This final report is the result of a two-year contract between the Air Force Aero Propulsion Laboratory and the Georgia Institute of Technology. AFOSR Contract F33615-77-C-2036 was directly administered by Project Engineer Paul D. Lindquist of Wright-Patterson Air Force Base.

This experimental investigation was conducted in the Hydraulics Laboratory, School of Civil Engineering, Georgia Institute of Technology. The two co-principal investigators were Dr. C. S. Martin, Professor of Civil Engineering, Georgia Tech, and Dr. D. C. Wiggert, Associate Professor, Department of Civil Engineering, Michigan State University. Professor Wiggert was on sabbatical leave at Georgia Tech from September 1977 to August 1978, the period during which much of the testing was conducted. F. D. Lewis of Lockheed-Georgia designed the hydraulic test facility and supervised its construction.

H. D. Bates, senior research technician, assembled the hydraulic test facility and designed and built the model valve. Instrumentation installation and calibration was supervised by H. Medlarz, Graduate Research Assistant.

Of considerable aid in the initial conception and planning of the test facility and in the selection of data acquisition equipment and instrumentation was Dr. J. I. Craig, School of Aerospace Engineering, Georgia Tech. Professor Craig collaborated with and assisted the principal investigators throughout the course of the project.

r	
<input checked="checked" type="checkbox"/>	
1	
Library Codes	
Dist	Avail and/or special
A	

Direct contributions were made by Professor C. Brennen of the California Institute of Technology regarding the interpretation and analysis of results.

The purpose of this investigation was the assessment of cavitation damage mechanisms in a hydraulic flow system. This report is the culmination of the experimental phase of the program. A companion study entitled "Cavitation Damage Mechanisms: Review of the Literature," Reference [1], assesses the state of the art of cavitation in hydraulic systems with particular interest on such subsidiary factors as electrochemical and electromagnetic effects.

TABLE OF CONTENTS

SECTION	PAGE
I. INTRODUCTION	1
Brief Review of the Literature	2
II. DESCRIPTION OF TEST FACILITY	4
Test Valves.	6
Valve Modulator.	6
Hydraulic Oil.	10
III. INSTRUMENTATION.	11
Flow Meter	11
Pressure Transducers	11
Displacement Transducers	13
Accelerometer.	14
Temperature Detector	14
Dissolved Gas Meter.	14
IV. DATA ACQUISITION SYSTEM.	16
Mean Quantities.	16
Dynamic Quantities	18
V. DISCHARGE CHARACTERISTICS OF TEST VALVES	20
Test Results	20
Analysis of Results.	25
VI. TEST PROCEDURE FOR DYNAMIC MEASUREMENTS.	33
VII. NON-CAVITATING DYNAMIC CHARACTERISTICS	36
VIII. CAVITATION INCEPTION	49
Prototype Valve.	49
Model Valve.	55
Criterion for Cavitation Inception	62
Model Valve.	66
Prototype Valve.	66
Discussion of Results.	69
IX. DEVELOPED CAVITATION	72
Prototype Valve.	72
Effect of Temperature.	80
Effect of Valve Opening.	80
Repeatability of Testing	83
Model Valve.	83
Correlation of Results	91
Effect of Dissolved Gas.	99

TABLE OF CONTENTS

SECTION	PAGE
X. CAVITATION WITH PULSATING FLOW	103
XI. IMPACT OF RESULTS ON AIRCRAFT HYDRAULIC SYSTEMS.	110
XII. CONCLUSIONS.	114
XIII. RECOMMENDATIONS.	116
APPENDIXES	
A. PHYSICAL PROPERTIES OF HYDRAULIC OIL	119
B. THERMODYNAMIC EFFECT	125
C. BUBBLE RESONANCE	128
REFERENCES	131

LIST OF ILLUSTRATIONS

FIGURE	TITLE	PAGE
1	Schematic of Hydraulic Test Facility.	5
2	Cutaway and Spool of Prototype Valve.	7
3	Side View of Model Valve.	8
4	Longitudinal Section of Model Valve	9
5	Calibration Curve for Flow Meter.	12
6	Calibration Curve for Temperature Detector.	15
7	Data Acquisition System	17
8	Definition of Valve and Jet Characteristics	21
9	Discharge Characteristics of Prototype Valve.	23
10	Discharge Characteristics of Prototype Valve.	24
11	Non-Cavitating and Cavitating Discharge Characteristics of Model Valve.	26
12	Variation of Discharge Coefficient with Reynolds Number with No Cavitation	29
13	Variation of Discharge Coefficient with Reynolds Number under Cavitating Conditions.	30
14	Variation of Discharge Coefficient with Cavitation Index.	32
15	Non-Cavitating Mean-Square Energy Versus Discharge for Prototype Valve at a Fixed Opening.	39
16	Non-Cavitating Energy Spectra for Prototype Valve at a Fixed Opening.	40
17	Non-Cavitating Mean-Square Energy Versus Discharge for Model Valve at a Variable Opening and Constant Pressure Difference.	42
18	Non-Cavitating Energy Spectra for Model Valve at Two Values of Opening b and Constant Pressure Difference	43
19	Non-Cavitating Mean-Square Energy Versus Discharge for Model Valve at a Fixed Opening.	45

LIST OF ILLUSTRATIONS

FIGURE		PAGE
20	Non-Cavitating Energy Spectra for Model Valve at a Fixed Opening.	46
21	Non-Cavitating Mean-Square Energy Versus Discharge for Model Valve at a Fixed Opening	47
22	Non-Cavitating Energy Spectra for Model Valve at a Fixed Opening.	48
23	Mean-Square Energy Versus Cavitation Index for Prototype Valve at a Fixed Opening and Constant Discharges	50
24	Mean-Square Energy Versus Cavitation Index for Prototype Valve at a Fixed Opening and $Q = 11$ gpm.	51
25	Non-Cavitating and Cavitating Energy Spectra for Prototype Valve at a Fixed Opening and $Q = 11$ gpm.	53
26	Ratio of Cavitating to Non-Cavitating ($\sigma_o = 0.647$) Spectral Density for Prototype Valve at a Fixed Opening	54
27	Area under Ratio of Cavitating to Non-Cavitating Mean-Square Spectral Density Curve for Fluctuating Pressure Versus Cavitation Index for Prototype Valve at a Fixed Opening and $Q = 12$ gpm	56
28	Mean-Square Energy Versus Cavitation Index for Model Valve at Two Fixed Openings.	57
29	One Non-Cavitating and Two Cavitating Energy Spectra for Model Valve at a Fixed Opening	58
30	One Non-Cavitating and Two Cavitating Energy Spectra for Model Valve at a Fixed Opening	59
31	Non-Cavitating and Cavitating Energy Spectra for Model Valve at a Fixed Opening	61
32	Ratio of Cavitating to Non-Cavitating ($\sigma_o = 0.421$) Spectral Density for Model Valve at a Fixed Opening	63
33	Area under Ratio of Cavitating to Non-Cavitating Mean-Square Spectral Density Curve Versus Cavitation Index for Model Valve at a Fixed Opening	64
34	Area under Ratio of Cavitating to Non-Cavitating Mean-Square Spectral Density Curve Versus Cavitation Index for Model Valve at a Fixed Opening	65
35	Incipient Cavitation Index Versus Reynolds Number for Model and Prototype Valves	67

FIGURE	LIST OF ILLUSTRATIONS	PAGE
36	Mean-Square Energy Versus Cavitation Index for Prototype Valve at a Fixed Opening.73
37	Effect of Cavitation on Energy Spectra for Prototype Valve at a Fixed Opening.74
38	Ratio of Cavitating to Non-Cavitating ($\sigma_o=0.647$) Spectral Density for Prototype Valve at a Fixed Opening.76
39	Energy Spectra for Prototype Valve at a Fixed Opening77
40	Comparison of Two Cavitating Energy Spectra for Prototype Valve at a Fixed Opening ($\sigma_o=0.492$)78
41	Area under Ratio of Cavitating to Non-Cavitating Mean-Square Spectral Density Curve Versus Cavitation Index for Prototype Valve at a Fixed Opening.79
42	Effect of Temperature on Mean Square Energy for Prototype Valve at a Fixed Opening.81
43	Effect of Valve Opening on Mean Square Energy for Prototype Valve82
44	Comparison of Mean Square Energy Results for Tests Run at Different Times under Slightly Different Temperatures.84
45	Mean-Square Energy Versus Cavitation Number for Model Valve at an Opening $b=0.101$ mm.85
46	Energy Spectra and Ratio of Cavitating to Non-Cavitating ($\sigma_o=0.421$) Spectral Density for Model Valve at an Opening $b=0.101$ mm.87
47	Area under Ratio of Cavitating to Non-Cavitating Mean-Square Spectral Density Curve Versus Cavitation Index for Model Valve at an Opening $b=0.101$ mm.88
48	Mean-Square Energy Versus Cavitation Number for Model Valve at an Opening $b=0.207$ mm.89
49	Energy Spectra and Ratio of Cavitating to Non-Cavitating ($\sigma_o=0.666$) Spectral Density for Model Valve at an Opening $b=0.207$ mm.90
50	Area under Ratio of Cavitating to Non-Cavitating Mean-Square Spectral Density Curve Versus Cavitation Index for Model Valve at an Opening $b=0.207$ mm.92
51	Cavitating Mean-Square Energy Versus Discharge for Prototype Valve at a Fixed Opening.93

FIGURE	LIST OF ILLUSTRATIONS	PAGE
52	Cavitating Energy Spectra and Coherence Between Fluctuating Pressure and Acceleration for Prototype Valve at a Fixed Opening94
53	Cavitating Mean-Square Energy Versus Discharge for Model Valve at a Variable Opening.96
54	Summary of Test Data Comparing Mean-Square Energy Versus Cavitation Index for Model Valve97
55	Dimensionless Representation of Test Data for Model Valve.	.98
56	Effect of Dissolved Gas Content on Mean-Square Energy Levels in Prototype Valve.	100
57	Effect of Dissolved Gas Content on Mean-Square Energy Levels in Model Valve.	102
58	Effect of Spool Oscillation on Energy Spectra ($\sigma = 0.055$).	107
59	Effect of Spool Oscillation on Energy Spectra ($\sigma = 0.190$).	108
60	Correlation of Erosion with Cavitation Noise. (Ramamurthy and Bhaskaran [19]).	111
A1	Effect of Temperature on Vapor Pressure of MIL-H-5606 Hydraulic Oil.121
A2	Effect of Temperature on Kinematic Viscosity of MIL-H-5606 Hydraulic Oil122
A3	Effect of Pressure on Solubility of Air in MIL-H-5606 Hydraulic Oil123
B1	Thermodynamic Function for Water and MIL-H-5606 Hydraulic Oil.126
C1	Resonance Frequencies for Bubbles in MIL-H-5606 Hydraulic Oil.129

LIST OF TABLES

TABLE	TITLE	PAGE
1	Summary of Tests for Mean Flow Characteristics of Test Valves.22
2	Summary of Cavitation Tests with Prototype Valve.34
3	Summary of Cavitation Tests with Model Valve.35
4	Summary of Pulsating Flow Results	105
A-1	Typical Properties of MIL-H-5606 Hydraulic Oil.	120

SUMMARY

Cavitation has been investigated in directional control valves in order to identify damage mechanisms characteristic of components of aircraft hydraulic systems. Extensive tests were conducted in a representative metal spool valve and in a model three times larger. Both valves are well instrumented for the purpose of accurately measuring mean quantities as well as detecting the onset and extent of cavitation once it developed.

Non-cavitating data taken with both valves showed that the position of the high-velocity annular jet issuing from the orifice shifted orientation depending upon valve opening and Reynolds number. By means of high-frequency response pressure transducers strategically placed in the valve chamber of each test valve cavitation could be sensed by the correlation of noise with a cavitation index. Cavitation inception could be detected by comparing energy spectra for a fixed valve opening and a constant discharge. Another sensitive indicator of cavitation inception is the ratio of cavitating to non-cavitating spectral densities. The incipient cavitation index as defined in this investigation correlates well with the Reynolds number for both valves.

For developed cavitation fluctuating energy from a high-frequency response accelerometer indicated a sharp rise over the corresponding condition with no cavitation. In fact, once cavitation develops, an accelerometer properly located on the cavitating component can be as sensitive to cavitation noise as a pressure transducer. Energy levels under developed cavitation were affected to some extent by

temperature differences. Several tests showed that dissolved gas had no effect on cavitation noise provided that the gas content did not exceed that corresponding to atmospheric conditions.

A limited number of tests were conducted under steady-state oscillation of the valve spool. There was no appreciable change in the cavitation noise provided that the cavitation index remained quite low. If the cavitation index was varied about a mean value corresponding to peak cavitation noise under steady-flow conditions then oscillating the valve resulted in lower noise levels. Further testing is recommended for the determination of valve characteristics under transient and steady-state oscillating conditions.

The test program showed that maximum cavitation noise occurred for values of the cavitation index less than approximately 0.25. Minimum damage would be anticipated for valves operating well above this value of the cavitation index inasmuch as the review of the literature clearly demonstrated an excellent correlation of peak erosion with peak cavitation noise.

SECTION I

INTRODUCTION

Cavitation is not nearly as well documented in oil hydraulic systems as it is in such water hydraulic systems as centrifugal pumps, propellers, hydraulic turbines, and hydrofoils. In aircraft hydraulic systems cavitation most frequently occurs in system valves, pumps, and actuators. Large differences in pressure is a frequent cause of small-scale cavitation in chambers of four-way spool valves, while high frequency motion of a valve-controlled actuator can lead to large-scale cavitation in the cylinder. Another source of cavitation in aircraft hydraulic systems is the improper filling of the pistons on an axial-piston pump. Either during transient loading or under steady-state operation cavitation can occur in the return chamber of directional control valves because of the large pressure drop across the orifice. It is of interest to know the potential cavitation damage as well as any effect of cavitation on system performance under both steady and unsteady flow conditions. Criteria need to be established for the onset of cavitation, and damage mechanisms -- whether hydrodynamic, chemical, electrical, or thermodynamic -- should be identified once the cavitation becomes developed. Effects of bubble composition and the size and population of nuclei on cavitation inception should be included in any investigation of damage mechanisms. The dynamic type flow networks found in aircraft hydraulic systems dictates that special attention be given to transient as well as steady-state oscillation of valves.

An experimental investigation was undertaken to study cavitation damage mechanisms in aircraft hydraulic systems. The purpose of the investigation was to identify mechanisms which lead to damage. A test facility was designed which allowed for the measurement of hydraulic parameters under both non-cavitating and cavitating conditions. Diagnostic techniques were developed to detect the onset and the extent of cavitation. The principal thrust of this experimental study was to develop techniques for detecting collapse pressure intensities and their radiation. Considerable effort was also expended in attempting to assess the influence of other factors such as dissolved gas content, electrochemical and thermodynamic effects.

While the influence of dissolved gases was studied experimentally in this project, and the influence of temperature on the thermodynamics of bubble growth was approached analytically (Appendix B), the principal effort devoted to the assessment of subsidiary, or non-hydrodynamic, effects was a critical evaluation of the existing literature on the subject. The result of this effort is the companion volume "Cavitation Damage Mechanisms: Review of the Literature," [1].

Brief Review of the Literature

The main literature source summarizing the state-of-the art of cavitation, primarily in water flowing systems, is the book Cavitation, published in 1970 by Knapp, Daily and Hammitt, [2].

The amount of literature on cavitation in oil hydraulic components is rather sparse. The major publications in the English language are referred to in the book by McCloy and Martin [3]. There is also important literature in German, principally from the fluid power group at the

Technical University of Aachen. Cavitation was investigated to a limited extent by MacLellan et al. [4] in their laboratory study in an enlarged two-dimensional model of a piston type control valve. Later but more complete work on cavitation in spool valves was reported by McCloy and Beck [5], who established criteria for cavitation inception in two valves, both two dimensional, one with water and the other with oil as the test liquid. Backé and Benning [6], Backé and Riedel [7], and Riedel [8] all report on cavitation in short orifices using hydraulic oil. The effect of gas content and orifice length on desinent and incipient cavitation is reported by Lichtarowicz and Pearce [9]. Flow pattern changes under both non-cavitating and cavitating flow conditions were documented by McCloy and Beck [10].

SECTION II

DESCRIPTION OF TEST FACILITY

Cavitation has been investigated in two directional-control valves in order to identify damage mechanisms characteristic of components of aircraft hydraulic systems. Tests have been conducted in both a metal prototype valve and a plexiglass model three times its size. A common test facility was designed that allowed for control of flow, upstream pressure, downstream pressure, dissolved gas content, and spool position. The common hydraulic test loop shown in Figure 1 consisted of a 75-hp axial piston pump with a pressure regulator, a high pressure supply line, a flow meter, a bypass system, the particular test valve and its instrumentation, downstream valves for back pressure control, and a low pressure return line to the pump. The pump had a maximum flow capacity of 0.0025 cms (40 gpm) and a maximum supply pressure of 34.5 MPa (5000 psi). Most data were taken with supply pressures less than 18.6 MPa (2700 psi) and flow rates less than 0.00189 cms (30 gpm). By means of pressure regulators the supply pressure to the model was always maintained less than 3.45 MPa (500 psi). Manually operated ball valves and gate valves downstream of the respective test valve were used to control the back pressure in the chamber of the test valve. A high pressure filter with an absolute rating of $3\mu\text{m}$ was in continuous use for control of contaminants.

An auxiliary system consisting of a vacuum tank, tubing and valves, and a rubber bag storage reservoir was used to degas the oil. Oil was pumped from the closed bag through a nozzle on top of the vacuum tank and allowed to film down the sides of the tank. The dissolved air

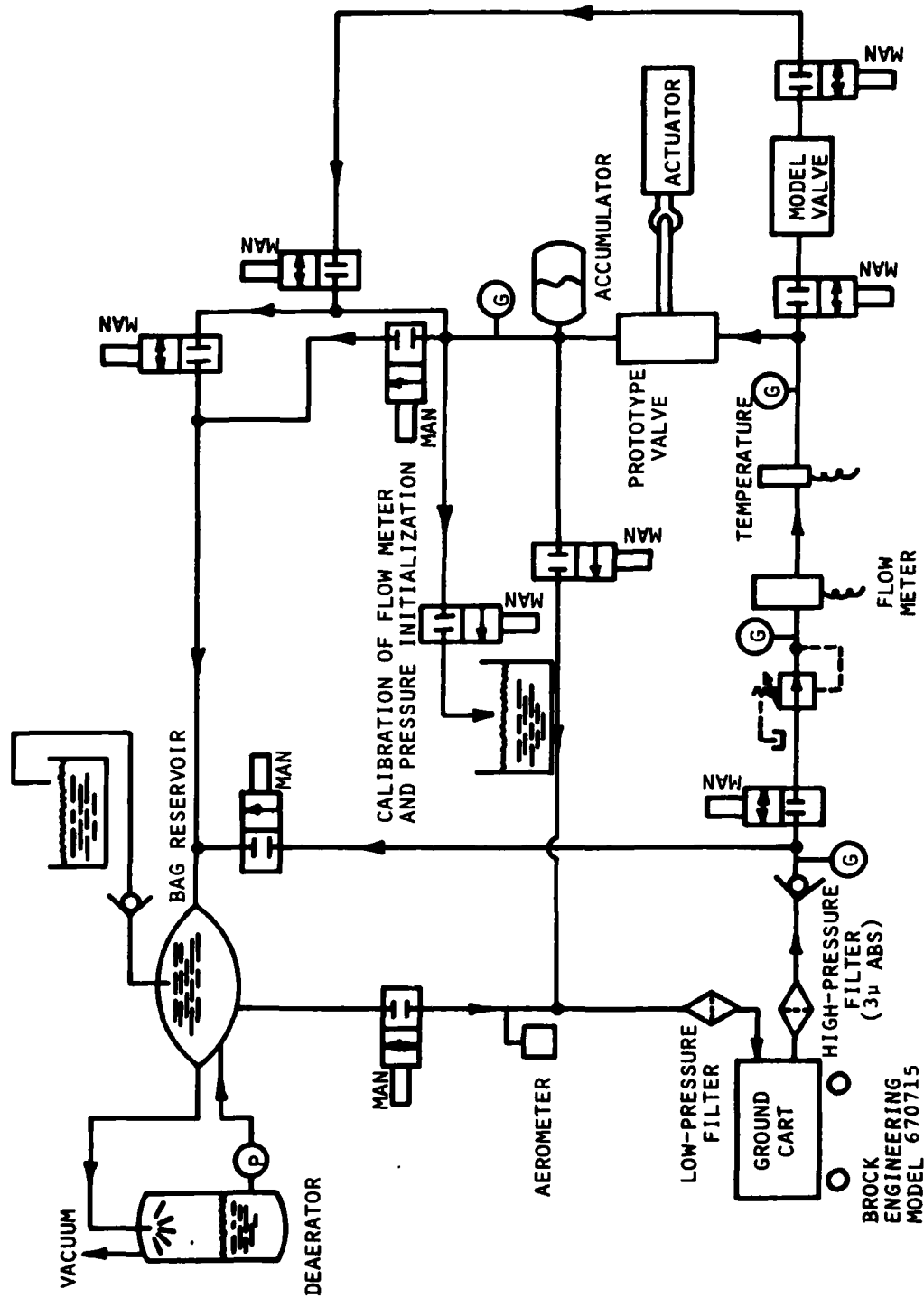


Figure 1. Schematic of Hydraulic Test Facility

content was monitored by use of an Aire-Ometer, a commercial device similar to a Van Slyke apparatus, which uses a filming technique to remove the gas. At room temperature and atmospheric pressure the dissolved gas content of the oil employed in this investigation varied between 9.5 and 10 percent by volume. The minimum value achieved after several hours of degassing was 4 percent.

Test Valves

In order to facilitate the continuous positioning of the spool as well as the mounting of instrumentation on the spool itself, a simple industrial four-way lever-operated spool valve was chosen as the prototype. A cutaway of this valve, which has a spool diameter of 19.05 mm (0.75 inch), is shown in Figure 2. In order to maximize the pressure differential across the valve, only one half of the valve was used, resulting in effect a two-way valve.

A photograph of the plexiglass model, which had a spool diameter of 57.2 mm (2.25 inches) is shown in Figure 3. The size of the valve chamber, lands, and ports of the model valve were scaled up from the metal prototype valve. Figure 4 is a longitudinal view of the body of the model valve. The opening of the annular space could be controlled by the mechanism attached to the end of the spool. A similar mechanism was installed on the end of the prototype valve. The supply and return ports in the vicinity of the model spool were made to scale with the prototype valve.

Valve Modulator

For the pulsating flow tests conducted using the prototype valve the

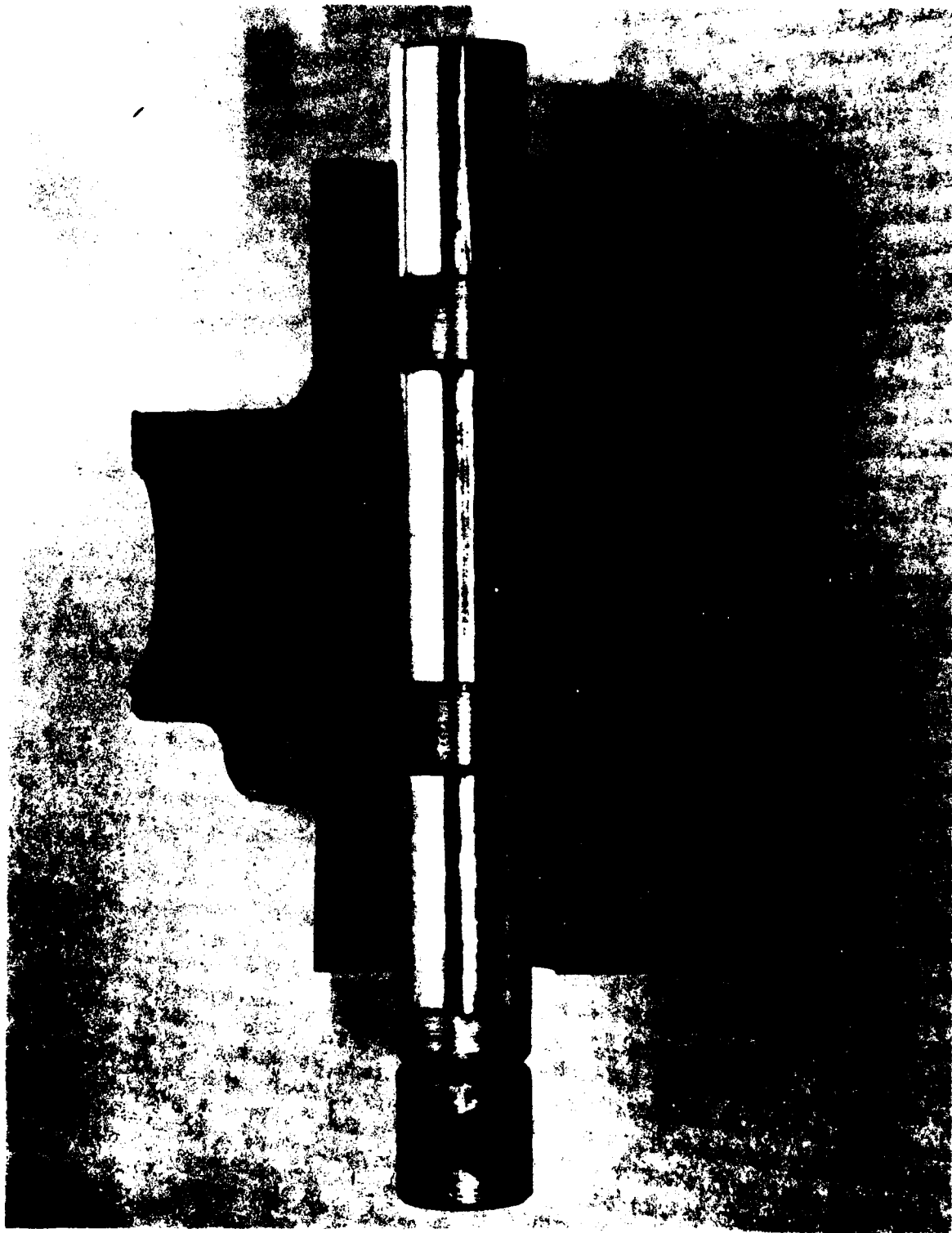


Figure 2. Cutaway and Spool of Prototype Valve

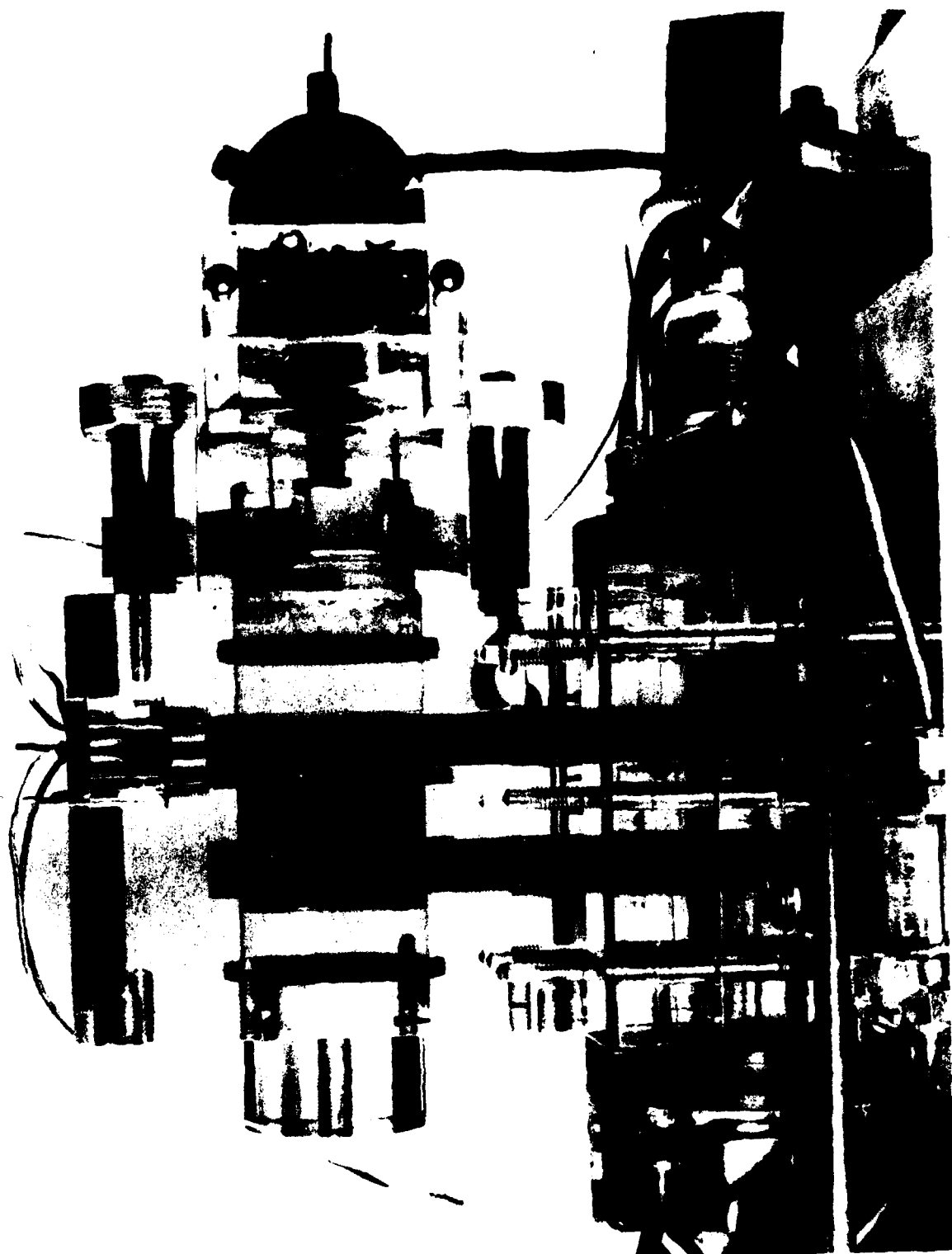


Figure 3. Side View of Model Valve

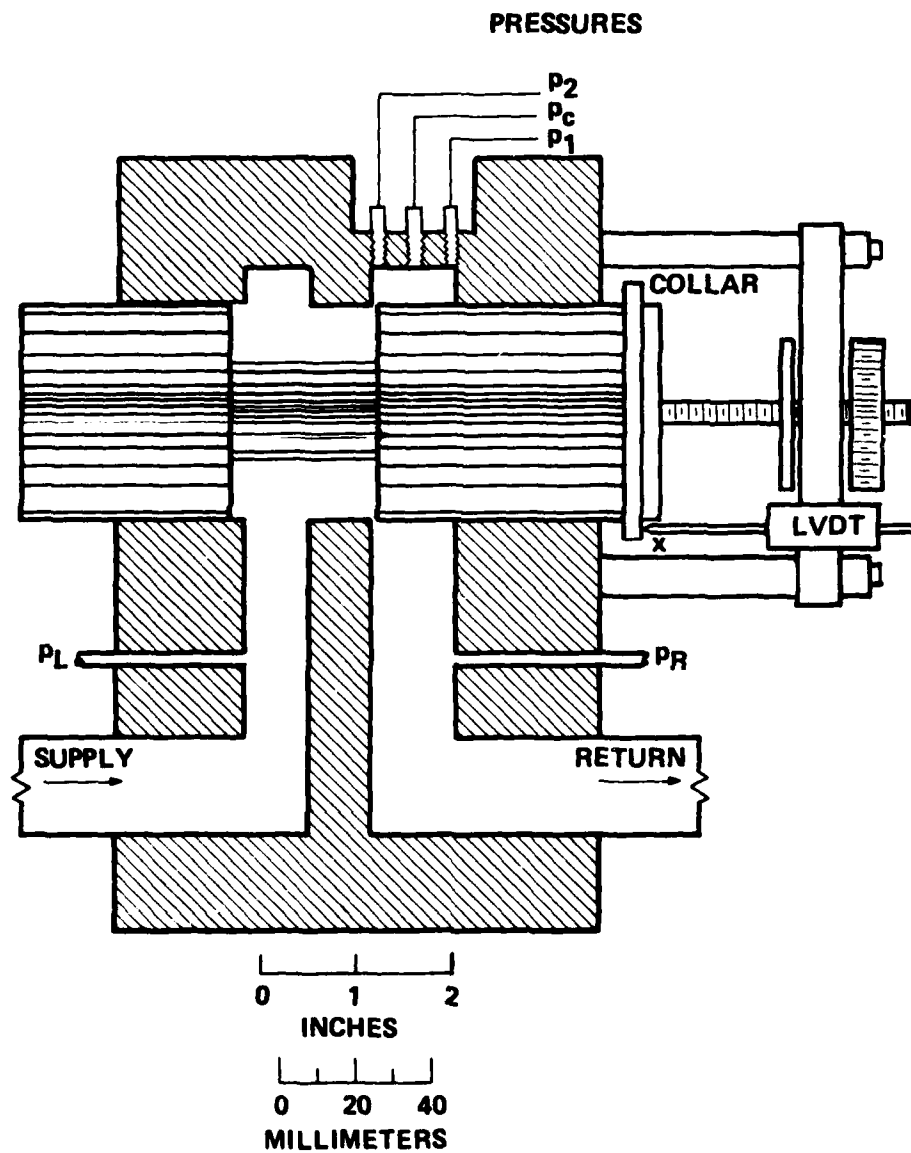


Figure 4. Longitudinal Section of Model Valve

actuator shown in Figure 1 was controlled by an MTS system which supplied the electrical signal to a Moog Model 73-103 servovalve. The actuator was directly connected to one end of the spool of the prototype valve shown in Figure 2. Feedback to the MTS system consisted of a differential pressure transducer and a linear variable differential transformer (LVDT) attached directly to the actuator.

Hydraulic Oil

As recommended by the sponsor MIL-H-5606C hydraulic oil, which is becoming the standard oil used in military aircraft hydraulic systems, was used throughout the test program. Some of the more important physical properties of the oil -- viscosity, vapor pressure, density, gas solubility, specific heat, and thermal conductivity -- are included in Appendix A.

SECTION III

INSTRUMENTATION

Flow Meter

For the steady flow results reported here mean flow rates and pressures were measured to characterize the overall test conditions, while dynamic pressures and acceleration were monitored to assess the onset and extent of cavitation. For both test valves a drag type flow meter, Ramapo Model V-1-SB, was used to measure the flow rate. This instrument consists of a circular target mounted on the end of a cantilever beam, which has strain gages attached to it. Targets with ranges of 1-10 gpm and 4-40 gpm were installed, depending upon the sensitivity desired. A 5-volt DC power supply was employed for excitation. The output signal was then amplified by means of a Neff Model 122-222 amplifier. Each target was calibrated in place gravimetrically. Figure 5 shows a typical calibration curve for the 4-40 gpm target.

Pressure Transducers

Pressure transducers were used to measure mean upstream (load-- p_L), differential (Δp), chamber (p_c), and downstream (return -- p_R) pressures. Figure 4 shows the location of the pressure taps for the model valve. In this case the differential pressure is defined by $p_L - p_R$. For the model the load pressure p_L was not measured directly.

The load, return, and differential pressure were measured by either Sensotec Model A5 strain-gage or Pace Models KP15 or P3D variable reluctance diaphragm pressure transducers. The mean chamber

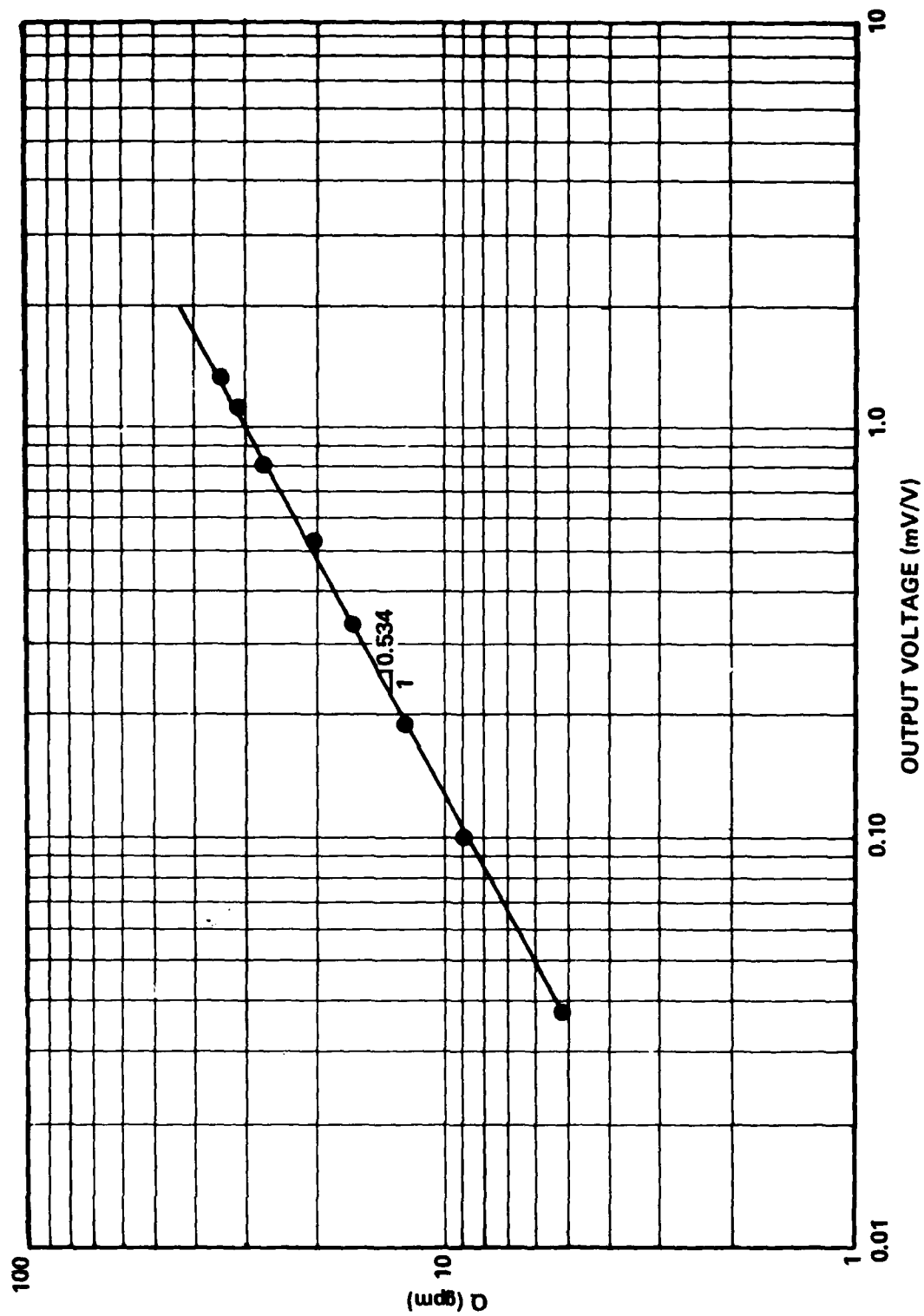


Figure 5. Calibration Curve for Flow Meter

pressure p_c for each valve was sensed by Kulite Model XTMS semiconductor pressure transducers. As shown in Figure 4 transducer P_c is located exactly in the middle of the model chamber. For the prototype valve the chamber transducer is located somewhat downstream of the center of the port. For all mean pressure transducers the power supply and signal conditioning were furnished by Hewlett-Packard Model 8805A carrier amplifiers, which provided an excitation frequency of 2400 Hz. Each transducer and amplifier assembly was calibrated by means of a dead weight tester.

Fluctuating pressures in the chamber of each valve were measured for the detection of cavitation by high-frequency response piezoelectric pressure transducers, PCB Model 105 A12. These transducers were flush mounted in the chamber of each valve, as shown in Figure 4 for the model valve. The diameter of the sensing surface is 2.51 mm (0.099 inch). The transducers had a resonant frequency in air of 250 kHz and a nominal sensitivity of 5 mV/psi.

The larger size model allowed for the installation of two PCB transducers, referred to as P_1 and P_2 on Figure 4. The single piezoelectric transducer in the prototype valve chamber is called P_1 . This transducer is located somewhat downstream of the middle of the chamber. For a very limited number of tests a second PCB transducer, referred to as P_2 , was flush mounted in the rectangular return passage of the prototype valve.

Displacement Transducers

An accurate determination of the position of the specific valve was essential because of the relative small openings in practice. For each valve a linear variable displacement transducer (LVDT) was used to

measure the relative position x of the spool. Each LVDT, which was excited by a 6-volt DC supply, was calibrated by means of accurate dial gages and a sensitive voltmeter.

Accelerometer

For the detection of mechanical effects in the spool related to cavitation a high-frequency response quartz accelerometer was mounted on the end of the spool of the prototype valve. The miniature accelerometer is a MB Model 306 with an undamped natural frequency of 120 kHz and a sensitivity of 7.64 mV/g.

Temperature Detector

An Edison resistance temperature detector and a Fluke Model 8000A multimeter were used to monitor the oil temperature immediately upstream of the test valve in question. From the nonlinear curve furnished by the manufacturer, Figure 6, the oil temperature was computed.

Dissolved Gas Meter

The dissolved gas content of the oil could be determined before and after each test by use of an Aire-Ometer, Seaton-Wilson Model AD-4003. This device uses a filming technique and a vacuum to release the dissolved gas from solution. Oil samples were taken from the vacuum tank and oil reservoir during degassing and from the suction line, as shown on Figure 1, before and after testing.

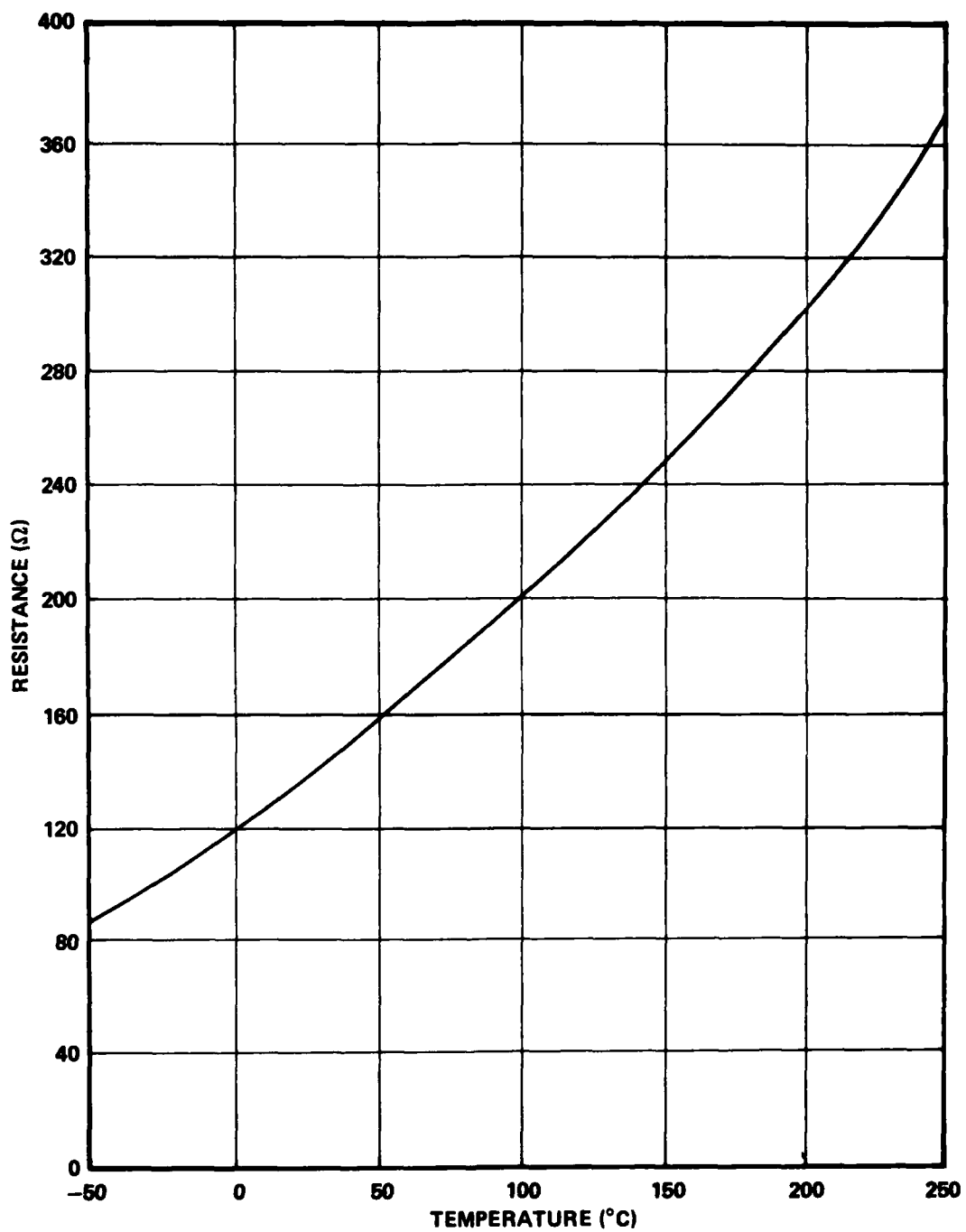


Figure 6. Calibration Curve for Temperature Detector

SECTION IV

DATA ACQUISITION SYSTEM

The data acquisition system used to sample the so-called mean signals will be described with reference to Figure 7. The test valve shown in the illustration could either be the model or the prototype valve. For the model valve there was no measurement of load pressure p_L , nor any accelerometer signal \ddot{x} . On the other hand for the prototype valve usually only one piezoelectric pressure transducer (P_1) was used.

Mean Quantities

The central device regarding the collection of mean quantities to characterize the flow conditions is a HP Model 9825A Desktop Computer. This computer controlled the HP Model 3495 Scanner and the HP Model 3455 Digital Voltmeter, both of which are programmable. The analog signal from any of the six input channels shown in Figure 7 could be transferred through the multiplexer by the controller to the $6\frac{1}{2}$ digit voltmeter, which digitized the signal and transferred the data to the computer. For a given channel twenty samples were averaged to obtain a mean value. The voltages were converted to engineering units by calibration constants which were either input into the computer or retrieved from memory. The resistance output of the Fluke multimeter was keyed into the computer for the computation of temperature from the calibration curve for the temperature. Once the six input channels were scanned and the values computed, the results were transmitted by an interface bus to a TI Model 735 terminal, which was used as a printer. For each flow rate or test

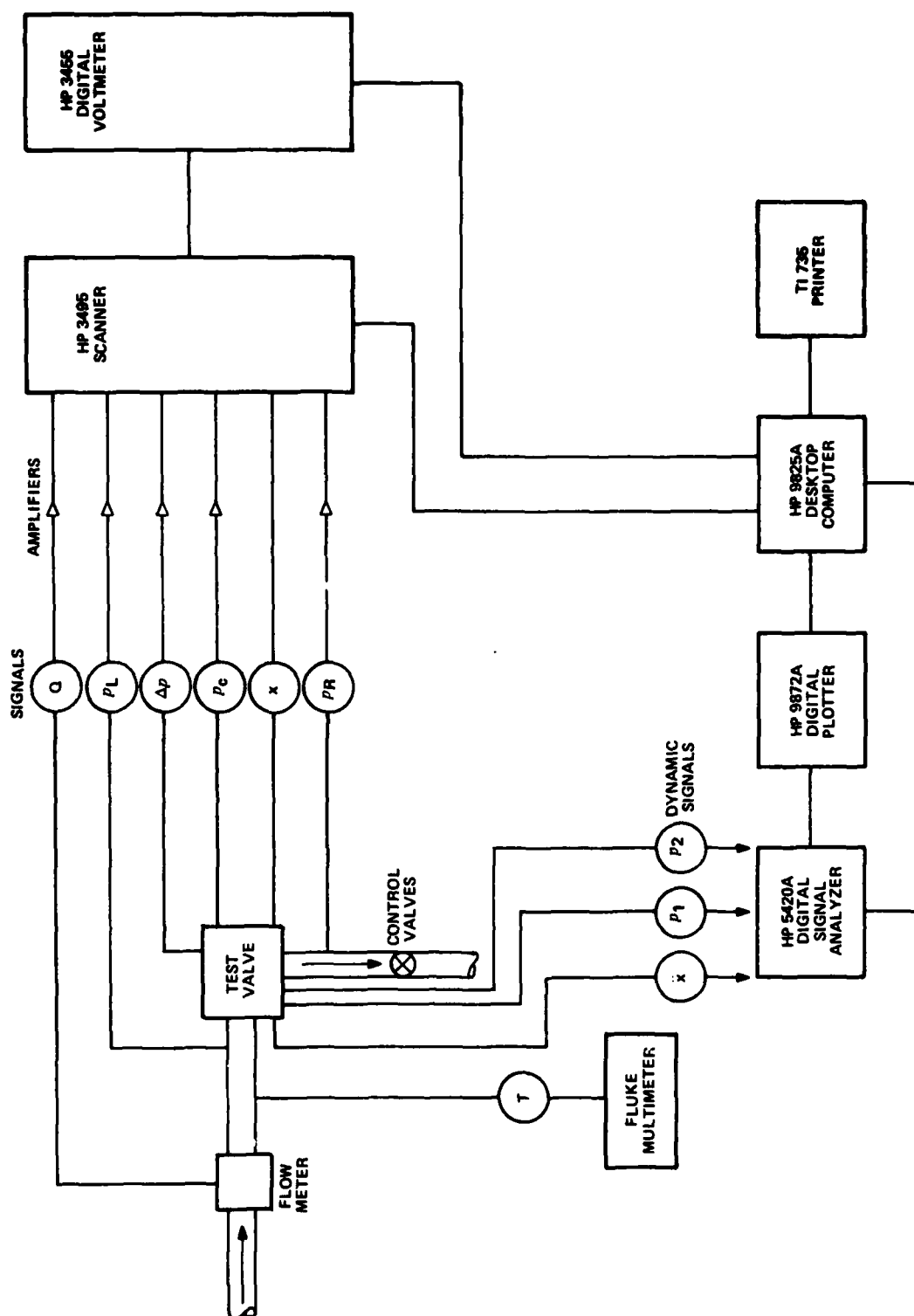


Figure 7. Data Acquisition System

condition all of the mean quantities which were printed out could be maintained in the memory of the computer, or discarded. At the completion of the entire test series the data were then stored on a cassette tape of the desktop computer for future retrieval and analysis.

The four-color HP Model 9872A Digital Plotter, which could be controlled by the 9825A Desktop Computer, was utilized for the correlation of data. As mentioned later the plotter could also be controlled by the HP 5420A Signal Analyzer for the plotting of energy spectra.

Dynamic Quantities

As illustrated on Figure 7 the dynamic quantities monitored in this investigation are the fluctuating pressures p_1 and p_2 and the fluctuating spool acceleration \ddot{x} . Any two of these signals could be simultaneously input into the HP 5420A Digital Signal Analyzer, which is an all digital instrument capable of providing both time and frequency domain analysis of complex analog signals in the range of DC to 25.6kHz. In the time domain the analyzer offers such measurements as time-record averaging, probability density function, and auto and cross correlation functions. The various measurement tools available in the frequency domain are linear spectrum, auto and cross spectra, transfer function and coherence function. The calibration constants for the particular instrument could be keyed into the analyzer for direct calculation and display in the appropriate engineering units. The frequency bandwidth could be chosen for the particular application. The analyzer has the capability of instant viewing of both channels on a CRT, and storage of results if desired on a tape cassette, as well as being able to be controlled by the desktop computer. The user can preselect the type of time series analysis most

conducive for the specific study -- either sinusoidal, random, or transient. The results could be plotted on the plotter shown in Figure 7.

Only auto power spectra of the pressure transducer and accelerometer signals are reported here as they proved to be the most meaningful as regard to the detection of cavitation. All data reported were collected with the maximum frequency band width available -- 0 to 25.6 kHz. Preliminary testing was conducted to determine the stationarity of the dynamic signals. Although in a few runs during the initial testing period up to 100 ensemble averages were taken, it was later found that 50 averages were more than adequate.

The time resolution was $9.77\mu\text{s}$ and the width of each frequency channel 100 Hz. Although the time length of each sample was 10 ms, processing time increased the elapsed time. Since the measurement bandwidth was below the real-time bandwidth of the analyzer, overlap processing of the ensembles resulted. By choosing the random option the signals were processed using a modified Hanning-type window.

SECTION V

DISCHARGE CHARACTERISTICS OF TEST VALVES

The mean flow characteristics of each valve were determined by direct measurement before embarking upon the main cavitation study. It was essential to know accurately the value of the discharge coefficient of the valve in question because of the difficulty in measuring the valve opening with the desired precision. Once the value of the discharge coefficient was known for the particular test conditions the valve opening could then be calculated from the known flow rate and pressure difference across the valve, both of which could be measured quite accurately.

Test Results

For both valves steady flow tests were conducted by maintaining a constant pressure difference Δp across the valve for various openings, defined as b in Figure 8, which defines the essential geometric and flow characteristics of a spool valve. For each test the flowrate Q , the axial position of the respective valve x , the return pressure p_R , the pressure differential, and the oil temperature were measured.

Extensive testing was conducted under both non-cavitating and cavitating conditions in order to determine the effect of such factors as viscosity and cavitation on the discharge characteristics of each test valve. A summary of the test conditions is provided by Table 1.

Typical results for the prototype valve as plotted in Figures 9 and 10. The cavitation index is normally defined as the ratio of a

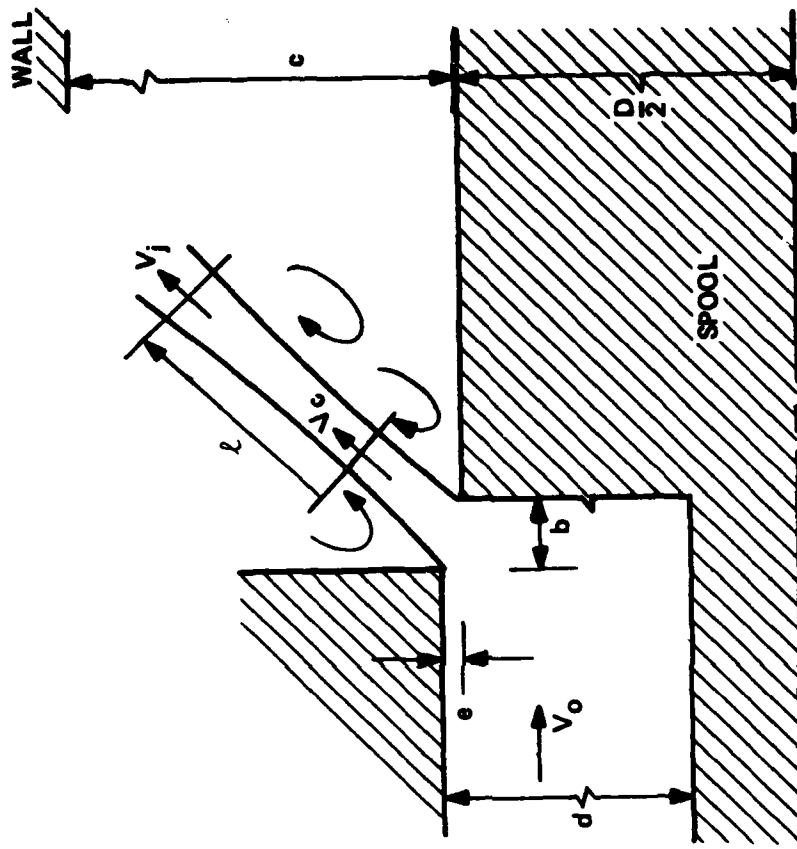


Figure 8. Definition of Valve and Jet Characteristics

TABLE 1
SUMMARY OF TESTS FOR MEAN
FLOW CHARACTERISTICS OF TEST VALVES

<u>Date</u>	<u>Run</u>	<u>*Valve Position</u>	<u>Range of T(°C)</u>	<u>Range of Q(gpm)</u>	<u>Nominal Values of Δp(psi)</u>	<u>Range of P_R (psi)</u>
a) Prototype						
4/07/78	1	V	48-62	0.2-10.4	500,1000	0
4/11	1	V	44-54	0.2-10.0	1500,2000	0
4/11	2	V	45-55	0.4-10.2	2500	0
4/11	3	V	31-57	0.4-10.5	1500,2000,2500	0
4/11	4	V	45-60	0.3-10.2	250,750	0
4/13	1	V	52-59	0.3-10.2	500,1000,1500,2500	0
4/20	1	V	55-65	0.5-10.6	500,1000,1250,1500	0
4/21	1	F	52-64	3.9-10.2	100,200,400,600,800	0-1100
4/25	1	V	59-65	1.4-10.0	200,400	0-1000
4/25	2	V	56-63	1.9-9.7	400,600	0-1000
4/25	3	V	60-65	2.8-9.9	1000,1500	0-1000
4/27	1	V	53-60	2.8-9.9	1500	0-1000
5/01	1	V	57-66	0.8-9.9	500	0-200
5/01	2	V	54-62	0.9-10.1	1000	0-200
5/01	5	V	48-58	0.7-10.1	1500	0-200
b) Model						
6/22/78	1	V	55-56	6.3-25.3	142	48-240
11/08	1	V	30-34	3.8-26.8	142	20-108
11/21	1	V	32-33	4.7-26.2	202	0-16

*F - Fixed Spool Position
V - Variable Spool Position

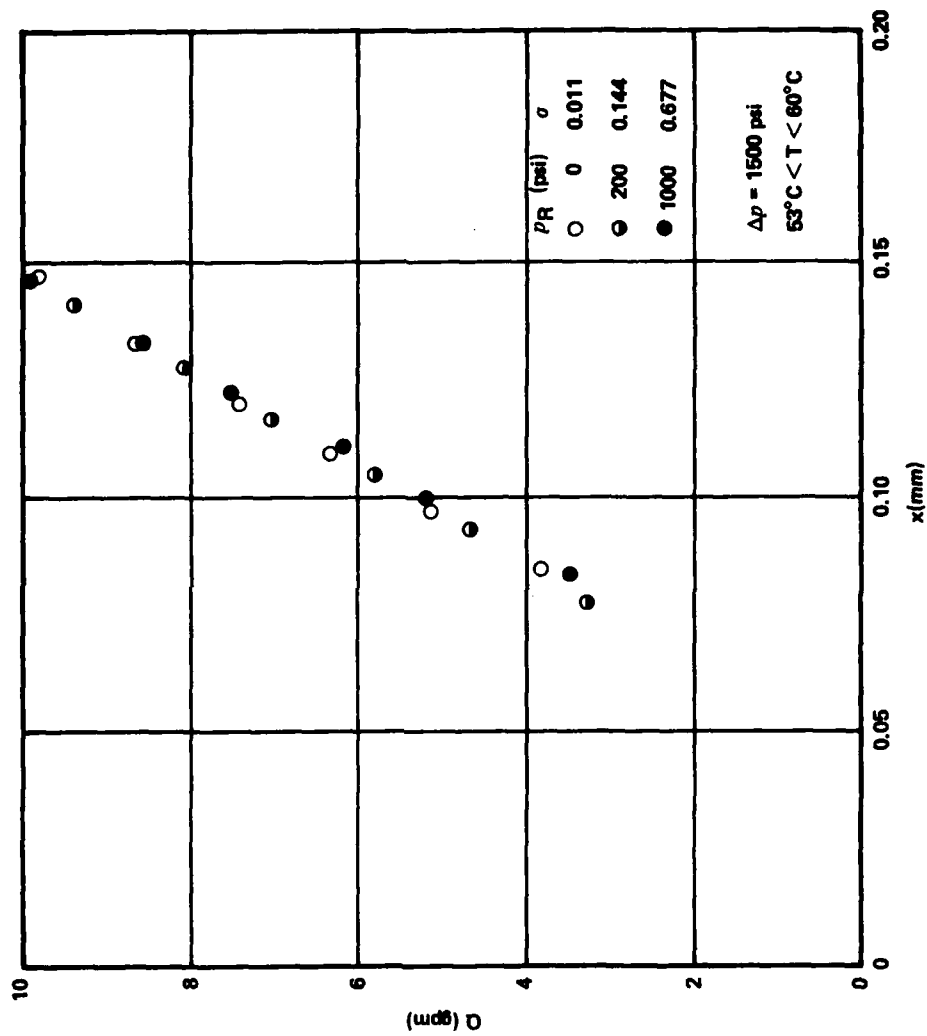


Figure 9. Discharge Characteristics of Prototype Valve

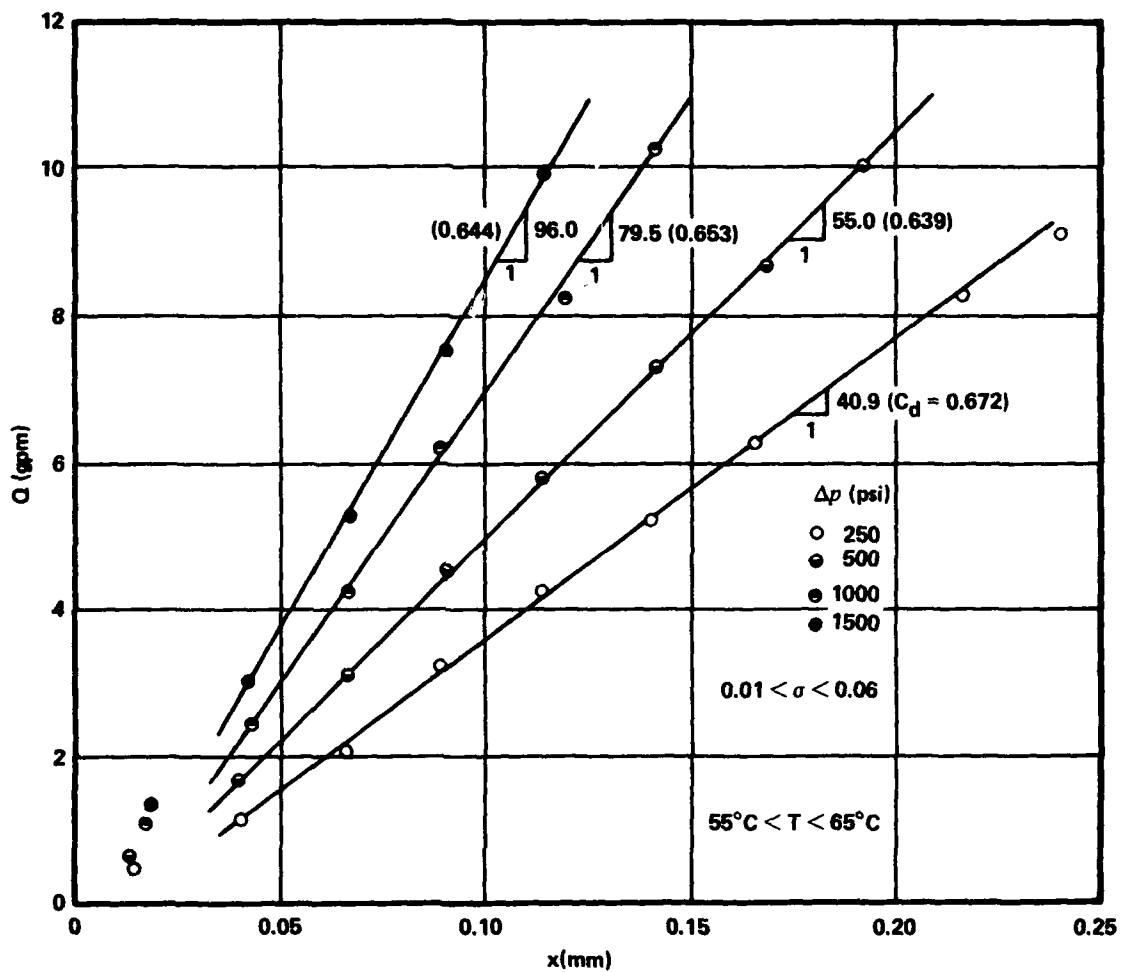


Figure 10. Discharge Characteristics of Prototype Valve

reference pressure minus the vapor pressure of the liquid to a dynamic pressure, the latter of which is referenced to the approach velocity V_o . A more appropriate dynamic pressure for the spool valve would be that based on the jet velocity V_j which is not measured directly, but instead directly related to Δp . The cavitation number is defined as

$$\sigma = \frac{p_c - p_v}{\Delta p} \quad (1)$$

Figure 9, which represents data taken under both non-cavitating and cavitating flow conditions, suggests that cavitation plays only a minor role on the mean flow characteristics of a spool valve. The four sets of data depicted on Figure 10 all correspond to rather developed cavitation.

For the model valve Figure 11 represents both non-cavitating and cavitating data. Because of an increasing return pressure with the greater flow rates the cavitating data shown in Figure 11 do not correspond to the ideal test conditions of a constant cavitation number σ .

Analysis of Results

Free streamline theory is applied to the annular jet issuing from the orifice shown in Figure 8. Assuming inviscid flow from the approach region

$$\frac{V_o^2}{2} + p_L = \frac{V_c^2}{2} + p_c \quad (2)$$

in which ρ is the fluid density, V_o is the approach velocity, and V_c is the jet velocity in the vena contracta. For the test program considered here the opening b is much less than the annular dimension d , resulting in

$$V_c = \sqrt{\frac{2\Delta p}{\rho}} \quad (3)$$

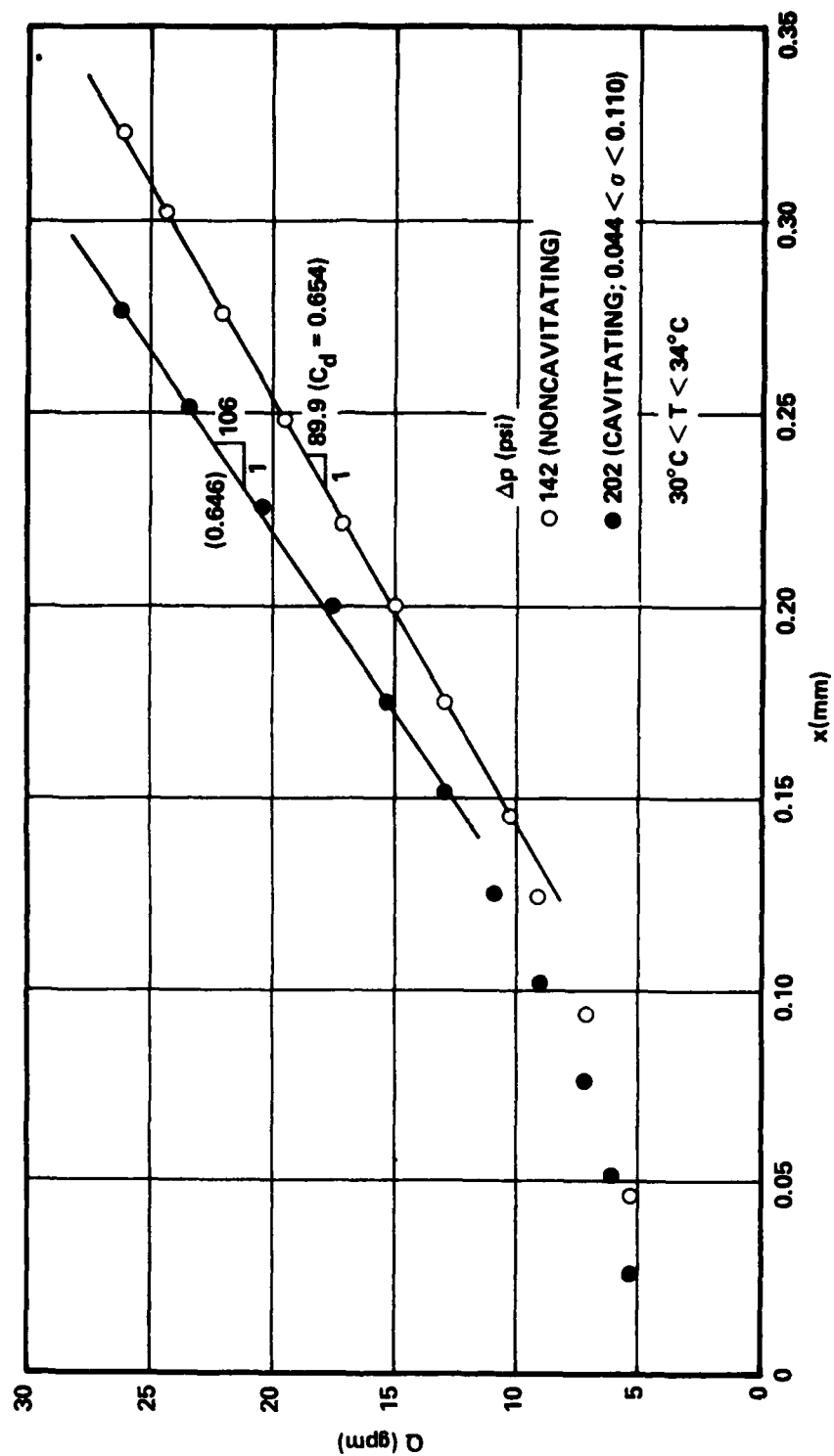


Figure 11. Non-Cavitating and Cavitating Discharge Characteristics of Model Valve

where $\Delta p = p_L - p_R$, the nominal pressure difference measured by the differential pressure transducer. The volumetric flow rate through the valve

$$Q = A_c V_c \quad (4)$$

in which A_c is the area of the contracted jet, which is usually defined in terms of the area of the annular orifice, or

$$A_c = C_c A = C_c \pi D b \quad (5)$$

in which C_c is the contraction coefficient and D is the diameter of the spool. The resulting relationship for the flow rate is

$$Q = C_d \pi D b \sqrt{\frac{2\Delta p}{\rho}} \quad (6)$$

in which C_d is the discharge coefficient, which in the case for which $b \ll d$, is equal to C_c . The above equation suggests a linear relationship between Q and b .

Because of the relatively small values of b employed in this study and the inherent difficulty in maintaining the desired accuracy in the measurement of b directly for a fixed opening, tests were instead conducted by varying b while holding Δp constant. In this instance the coefficient of discharge could be computed from

$$C_d = \frac{dQ/dx}{\pi D \sqrt{\frac{2\Delta p}{\rho}}} \quad (7)$$

in which x is the axial position of the spool, as measured by the LVDT. As shown by Figures 9-11, tests conducted at a constant Δp and varying x yielded nearly linear relationships between Q and x , allowing for the determination of C_d from the slope of the curve.

In general it would be expected that the discharge coefficient would be a function of a Reynolds number and the cavitation index, or

$$C_d = C_d(R, \sigma) \quad (8)$$

For simplicity the Reynolds number is defined on the basis of the average velocity at the annular opening instead of in terms of V_c at the vena contracta. The length dimension chosen in the definition is b , yielding

$$R = \frac{\rho(Q/A)b}{\mu} = \frac{Q}{\pi D\nu} \quad (9)$$

in which μ and ν are the dynamic and kinematic viscosities of the liquid, respectively. For a given temperature Eq. (9) suggests that the Reynolds number is independent of the valve opening b at a constant discharge.

For the linear portion of the curves of Figures 9-11 the slopes of the respective lines were determined by both (1) visual adjusting and (2) least-square curve fitting. Extensive testing over a range of R from 150 to 1500 under noncavitating conditions showed that C_d was independent of viscous effects, yielding an average value of C_d based upon Eq. (7) of 0.68 for the prototype valve versus 0.66 for the model valve, Figure 11.

In order to determine the variation of C_d with the Reynolds number Eq. (6) had to be used for correlation rather than Eq. (7). Figure 12 shows the scatter of data using the less accurate determination of C_d by Eq. (6), but suggests that there is no effect of a Reynolds number. Under the entire range of cavitating conditions for the prototype valve, the data of Figure 13 indicates likewise that viscosity has no influence on the discharge coefficient under cavitating conditions for $200 < R < 1500$.

The values of C_d based upon least-squares curve fitting of 0.68 and 0.66 for the prototype and model valve, respectively, are close to the theoretical value of 0.677 calculated by von Mises using two-dimensional

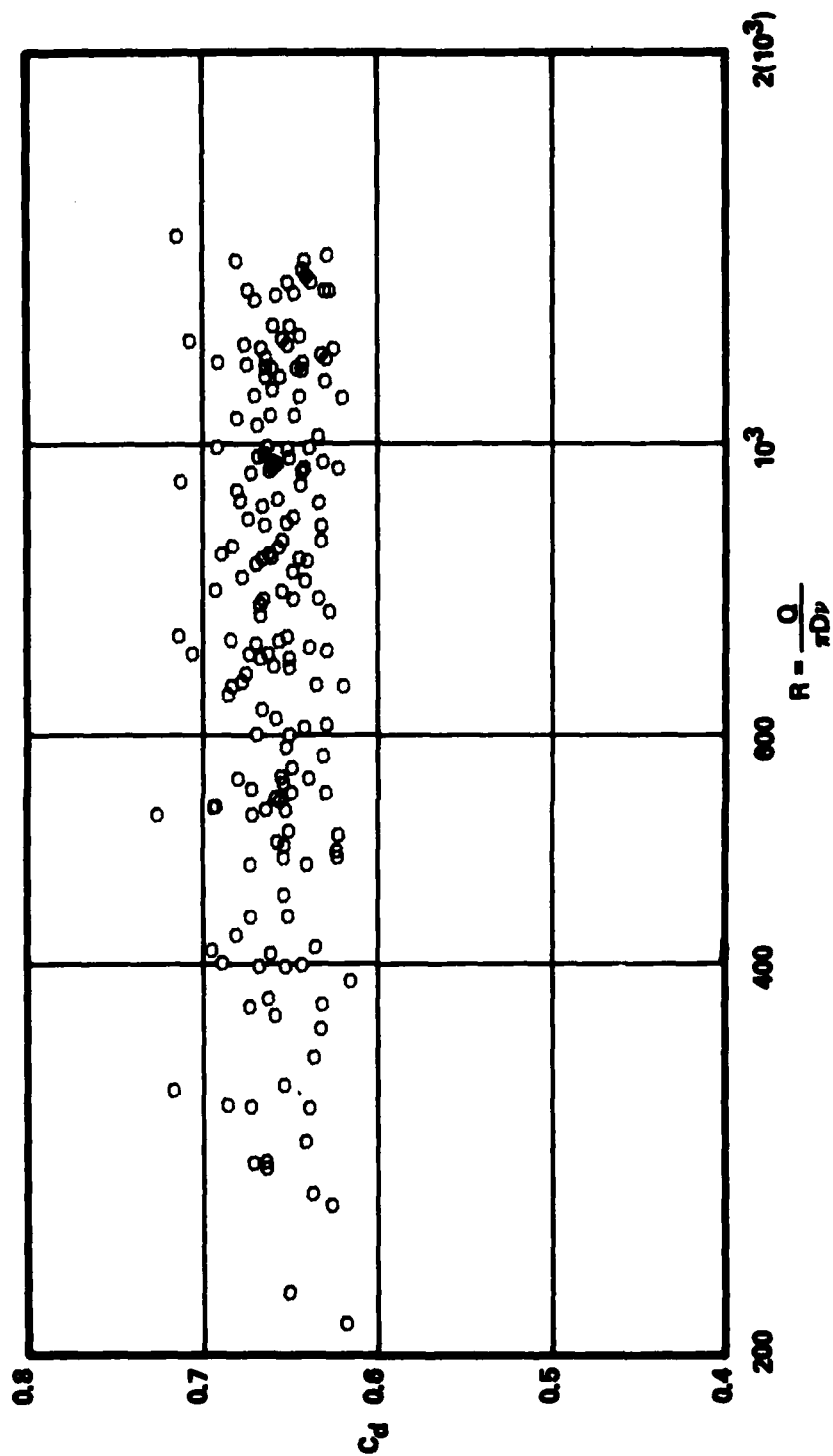


Figure 12. Variation of Discharge Coefficient with Reynolds Number with No Cavitation

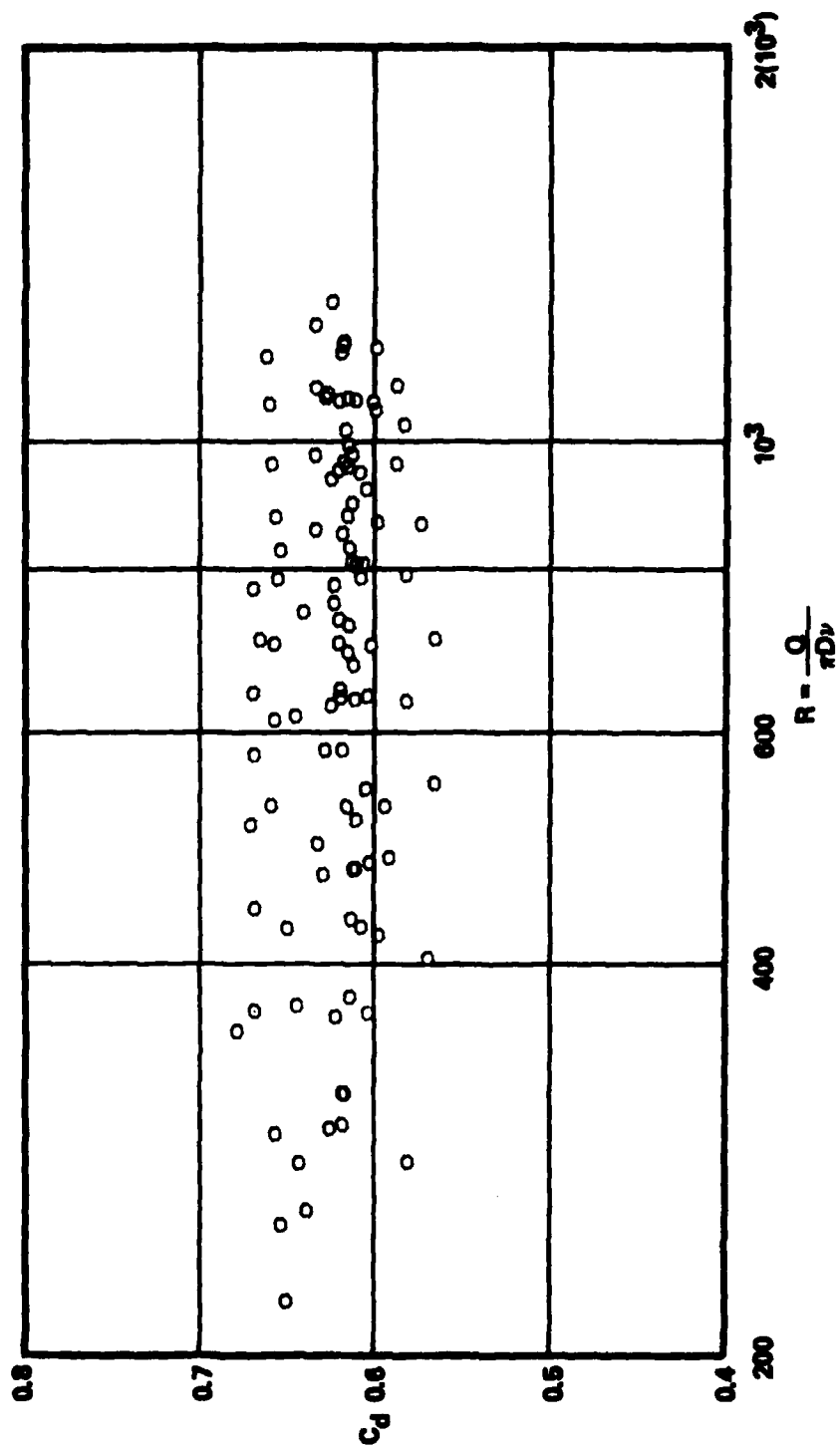


Figure 13. Variation of Discharge Coefficient with Reynolds Number under Cavitating Conditions

inviscid theory. A summary of the theory is reported by Robertson [11]. Experimental results published by Beck and McCloy [5] show a similar trend. Apparently the Reynolds number defined by Eq. (9) must be less than approximately 100 before viscous effects commence to influence the mean flow characteristics of the valve.

As shown by a number of researchers in the study of cavitation in pipe orifices, cavitation has to become quite extensive before there is any effect on C_d . The data shown in Figure 14, which were computed using least-squares curve fitting and Eq. (7), indicate a weak influence of cavitation on the discharge characteristics of the prototype valve over a wide range of σ .

The opening b during any test was computed from Eq. (6) using measured values of Q and Δp . The coefficient of discharge was approximated by the data of Figure 14, and assumed to be independent of the Reynolds number.

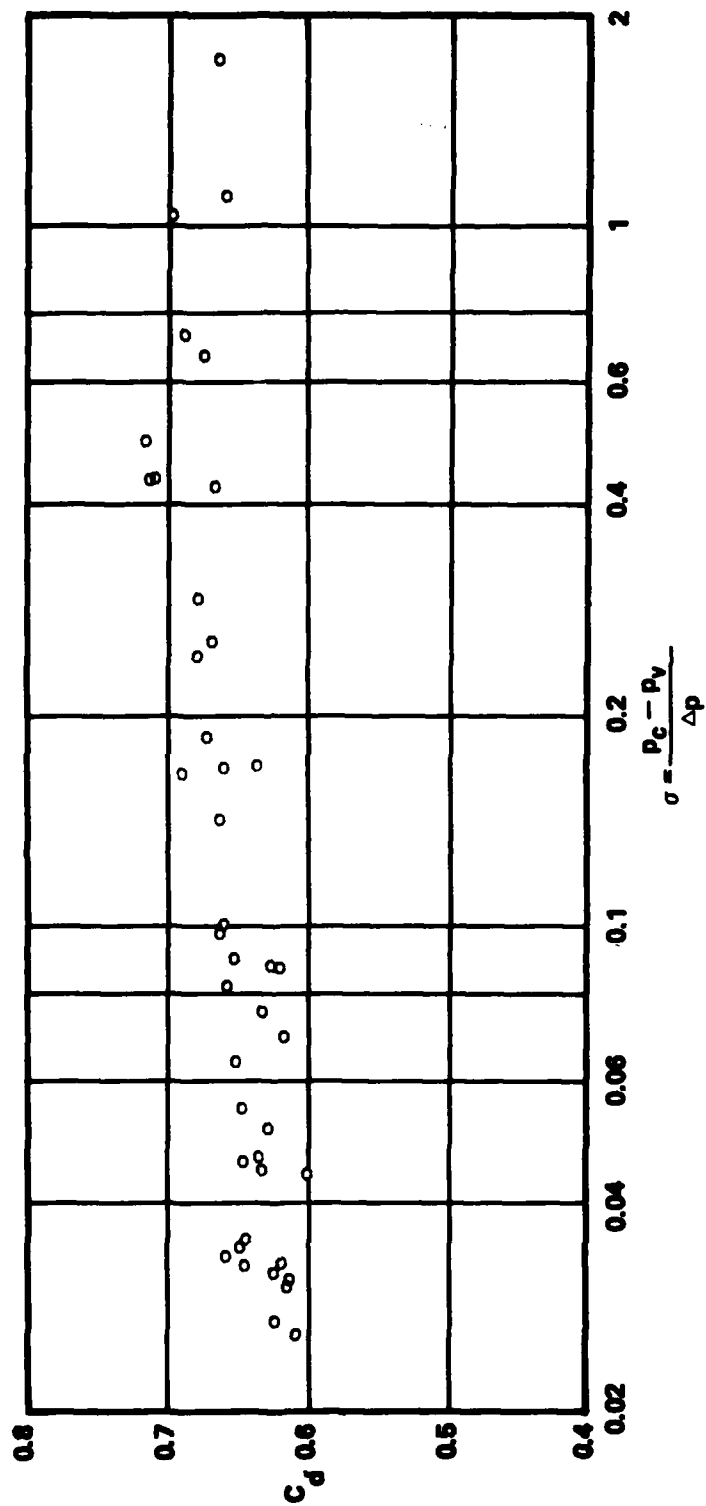


Figure 14. Variation of Discharge Coefficient with Cavitation Index

SECTION VI

TEST PROCEDURE FOR DYNAMIC MEASUREMENTS

Once the mean flow characteristics of each valve were determined a test program was initiated to assess both cavitation inception and developed cavitation. The principal instruments used in detecting and defining cavitation were the two transducers P_1 and P_2 for the model valve and transducer P_1 and the accelerometer for the prototype valve. Most of the individual tests were conducted for a constant discharge Q with the spool locked in a fixed position x . Cavitation at various degrees could be established by controlling both the upstream pressure regulator and the downstream ball and needle valves. Once the mean quantities as indicated by the desktop computer corresponded to the desired flow, valve position, and back pressure, the dynamic signals were fed into the signal analyzer.

Although occasionally the cross spectrum and coherence between P_1 and P_2 for the model or P_1 and X for the prototype valve were measured, the most frequent and useful measurements were the auto power spectra for the two channels. The power spectral density function for the auto spectra will be in units of $\sqrt{P'^2}/\Delta f$ for the pressure transducers and $[(d^2x'/dt^2)^2]^{1/2}/\Delta f$ for the accelerometer. By means of cursors the total energy over any frequency range could be quickly extracted from the analyzer, facilitating the real-time analysis and the establishment of criteria for cavitation inception.

Summaries of the test conditions for the entire set of cavitation tests are listed in Tables 2 and 3 for the prototype and model valves, respectively.

TABLE 2
SUMMARY OF CAVITATION TESTS
WITH PROTOTYPE VALVE

Date	Run (Tests)	*Valve Position	Range of T(°C)	Range of Q(gpm)	Range of Δp (psi)	Range of P_R (psi)	**Transducers	HP5420A Tape (Records)
5/12/78	1(17)	F	47-56	9.0	660-760	0-970	P1	1(27-41)
5/12	2(27)	F	42-55	1.3-10.1	10-740	0-1000	P1	1(42-68)
5/15	1(16)	F	50-52	9.0	670-730	0-140	P1	1(69-82)
5/26	1(5)	F	52-55	9.0	570-600	200-400	A1,P1	2(1-30)
5/26	2(12)	F	54-56	9.0	590-680	0-180	A1,P1	2(31-84)
5/30	1(18)	F	53-55	9.0	560-650	0-400	A1,P1	3(1-96)
6/01	1(13)	F	53-56	4.0-10.0	65-750	0-300	A1,P1	4(1-45)
6/01	2(10)	F	51-55	1.0-10.0	5-720	450	A1,P1	4(46-75)
6/13	1(13)	F	60-61	9.0	1850-2020	0-300	A1,P1	4(79-120)
6/30	1(5)	F	64-65	9.0	1890-2080	210-310	A1,P1	5(1-6)
6/30	2(14)	F	63-64	9.0	1690-1830	0-260	A1,P1	5(7-32)
7/02	1(7)	F	59-62	9.0	1980-2230	300-820	A1,P1	5(33-46)
7/05	1(11)	F	56-61	9.0	1040-1200	0-320	A1,P1	5(50-93)
7/07	1(13)	F	51-56	9.0	1050-1200	0-415	A1,P1	5(94-120)
7/12	2(5)	F	51-58	4.0-11.9	180-1840	720-810	A1,P1	and 6(1-20)
7/12	3(5)	F	51-57	4.0-10.0	300-2070	780-820	A1,P1	6(21-30)
8/10	1(11)	F	50-53	8.8-9.1	900-1840	0-1250	A1,P1	6(31-40)
7/31	1(13)	O	47-51	6.9-9.9	640-1140	5	A1,P1	6(41-58)
8/01	1(8)	O	46-47	8.4-9.2	1240	5	A1,P1	+ 1(1-86)
8/13	1(11)	O	42-46	5.8-9.4	1160-1220	75-230	A1,P1	+ 2(1-27)
8/14	1(20)	O	42-47	7.9-9.3	1150-1220	140-170	A1,P1	+ 2(28-61)
2/06/79	1(11)	F	16-20	7.0-11.1	320-810	0-450	A1,P1	+ 2(62-102)
2/22	1(14)	F	26-28	9.0	550-660	0-290	A1,P1,P2	6(59-78)
2/28	1(37)	F	26-37	7.0-11.0	320-930	80-400	P1,P2	6(79-120)
3/15	1(26)	F	30-32	11.0	805-860	170-500	A1,P1	7(1-70)
3/21	1(50)	F	40-43	11.0	820-910	0-920	A1,P1	7(71-120)
3/21	2(28)	F	35-39	9.0,10.0	560-710	190-810	A1,P1	8(1-94)
3/23	1(27)	F	34-43	12.0,13.0	1000-1200	420-1020	A1,P1	9(1-56)
3/27	1(31)	F	32-34	11.0	825-950	0-870	A1,P1	9(57-108)
								10(1-62)

*F - Fixed Spool Position
O - Oscillating Spool
V - Variable Spool Position

**A1 - Accelerometer
P1 - Piezoelectric Pressure Transducer in Chamber
P2 - Piezoelectric Pressure Transducer in Return Passage

+ Oscillatory Flow Tapes

TABLE 3
SUMMARY OF CAVITATION TESTS
WITH MODEL VALVE

Date	Run (Tests)	*Valve Position	Range of T(°C)	Range of Q(gpm)	Range of Δp(psi)	Range of P _R (psi)	**Transducers	HP 5420A Tape (Records)
6/23/78	1(11)	F	51-56	20.1-20.5	118-151	10-64	P1	1(1-11)
8/16	1(9)	V	38-42	3.2-26.6	78-201	1-68	P1,P2	1(12-47)
8/16	2(12)	F	43-45	9.6-10.3	55-185	2-139	P1,P2	1(48-75)
8/23	1(7)	F	40-43	10.0	87-104	5-68	P1,P2	1(76-120)
8/24	1(7)	F	39-42	10.0	135-204	4-98	P1,P2	2(1-56)
8/30	1(25)	F	41-43	9.9-10.2	138-196	5-59	P1,P2	2(57-100)
9/29	1(13)	F	38-40	10.0	146-214	3-57	P1,P2	2(101-120)
10/20	1(18)	F	35-36	10.0	138-221	3-72	P1,P2	3(1-34)
10/31	1(16)	F	36-37	6.8-13.0	107-259	1-67	P1,P2	3(35-98)
11/03	1(10)	F	36-37	7.1-13.0	79-232	3-54	P1,P2	3(99-110)
11/08	1(14)	V	30-34	3.8-26.8	140-144	45-108	P1,P2	4(1-28)
11/10	1(14)	F	35-36	5.9-15.7	67-273	30-132	P1,P2	4(29-52)
11/10	2(18)	F	34-37	9.0-26.1	18-200	65-158	P1,P2	4(53-88)
11/17	1(18)	F	34-36	10.0	161-224	3-52	P1,P2	4(89-120)
11/21	1(13)	V	32-33	4.7-26.2	201-203	1-16	P1,P2	5(1-26)
11/29	1(16)	F	22-25	20.0	151-170	9-75	P1,P2	5(27-58)
11/30	1(12)	F	25-26	6.9-15.3	76-258	12-89	P1,P2	5(59-78)
12/01	1(12)	F	30-31	9.5-23.4	30-232	3-110	P1,P2	5(79-98)
1/11/79	1(14)	F	25-27	20.0	158-173	10-77	P1,P2	6(1-26)
1/16	1(18)	F	21-26	20.0	145-184	10-63	P1,P2	6(27-60)
1/30	1(9)	V	24-25	20.0	83-215	31-79	P1,P2	6(61-78)
1/31	1(14)	V	16-18	10.0, 20.0	35-243	5-52	P1,P2	6(79-102)
7/03	1(34)	F	41-45	20.0	147-218	10-88	P1,P2	7(1-82)
7/16	1(20)	F	43-45	20.0	147-226	10-94	P1,P2	7(83-120)
7/25	1(27)	F	38-39	20.0	146-217	10-91	P1,P2	8(1-52)
7/30	1(26)	F	40-44	10.0	158-215	3-65	P1,P2	8(53-104)

*F - Fixed Spool Position

V - Variable Spool Position

**P1 - Piezoelectric Pressure Transducer Distant from Opening

P2 - Piezoelectric Pressure Transducer Near Opening

SECTION VII

NON-CAVITATING DYNAMIC CHARACTERISTICS

Prior to the establishment of criteria for the inception of cavitation the level of fluctuations of pressure and acceleration had to be understood for non-cavitating flow in each valve. Extensive testing was conducted to correlate energy levels of pressure fluctuations with flow rate and valve opening. Care was taken to insure that the chamber pressure p_c was large enough to inhibit any cavitation. This was accomplished by monitoring the total mean-square energy over the entire spectra for various values of σ . It was found that, for a constant discharge Q and valve opening b , the total energy did not vary if σ was above a certain threshold value, to be discussed later. The tests under non-cavitating conditions were also of value in observing changes in the jet flow pattern for different conditions.

The pressure transducers P_1 and P_2 in the model and P_1 in the prototype chamber experience the acoustical noise from the confined jet issuing from the annular orifice. The fact that the discharge coefficient is constant over the range of Reynolds numbers tested would suggest a turbulent jet. As shown by McCloy and Beck [10] in their study of jet hysteresis the jet can either reattach on the surface of the spool or on the wall of the port, or issue freely. A shifting jet pattern was clearly indicated in the model chamber by observing the energy levels on the two transducers, which were located at the extremities of the cavity.

The dynamics of an unconfined plane jet issuing from a nozzle are fairly well documented, albeit at higher Reynolds numbers than experienced with the two valves. As experimentally shown by Albertson et al. [12],

and later by Gutmark and Wygnanski [13], the mean centerline velocity of a plane jet decreases as the square root of the ratio of the initial jet diameter to the axial distance. In terms of the definition sketch on Figure 8

$$\frac{V_j}{V_c} = K \sqrt{\frac{b}{l}} \quad (10)$$

in which K is a constant for plane jets at large Reynolds number, and l is the axial distance from the nozzle, or from the vena contracta in the case of an orifice. For a plane turbulent jet Gutmark and Wygnanski [13] found that the r.m.s. value of the fluctuating velocity u'_o on the centerline of the jet was a constant when normalized with V_j , or

$$\frac{\sqrt{u_o'^2}}{V_j} = \text{constant} \quad (11)$$

Reethof [14] states that a fluctuating mass flow rate with in-phase pressure fluctuations would correspond to a monopole source, for which the r.m.s. energy of fluctuating pressure in this case are assumed to be correlated by

$$\sqrt{p'^2} = B_1 \rho V_j^2 \quad (12)$$

in which B_1 is a dimensionless coefficient which would depend upon transducer location, Reynolds number, etc. If, instead the fluctuations emanate from dipole sources -- which may be related directly to fluctuating pressures

$$\sqrt{p'^2} = B_2 \rho V_j^2 \left(\frac{V_j}{a}\right) \quad (13)$$

in which a is the acoustic velocity. For a monopole source Eq. (12) along with the jet relationships (4,5,10) yield the mean-square energy

$$\overline{p'^2} = B_1^2 \left[\frac{K}{\pi C_c} \right]^4 \frac{\rho^2}{D^4 b^2 l^2} Q^4 \quad (14)$$

In the case of dipole sources

$$\overline{p'^2} = B_2^2 \left[\frac{K}{\pi C_c} \right]^6 \frac{\rho^2 Q^6}{D^6 b^3 l^3 a^2} \quad (15)$$

All non-cavitating spectra measured by transducer P_1 in the chamber of the prototype valve indicate that the mean-square energy can be correlated in terms of a dipole, or fluctuating pressure, source. The mean-square energies measured with this transducer correlate well with Q^6 , as shown by the two data sets in Figure 15. The data shown in Figure 15 were taken at virtually the same opening b , but quite different Reynolds numbers. If l is assumed to be fixed and to correspond to the distance from the orifice opening to transducer P_1 , then Eq. (15) can be reduced to

$$\overline{p'^2} = B_3 \rho^2 Q^6 \quad (16)$$

as a , D , and b are virtually constant. Although there is a Reynolds number variation for each data set the coefficient B_3 appears to be a constant for each. Energy spectra for two of the data points plotted on Figure 15 are presented in Figure 16. The slope of each curve can be approximated by -1 for the lower frequency range and -2 for the higher frequencies. As demonstrated by Lush [15] a dipole source will produce energy spectra with a -1 slope. As most of the energy is in the first half of the frequency range shown in Figure 16, the dipole source dominates, resulting in a relationship represented by Eq. (15). An examination of many non-cavitating spectra shows

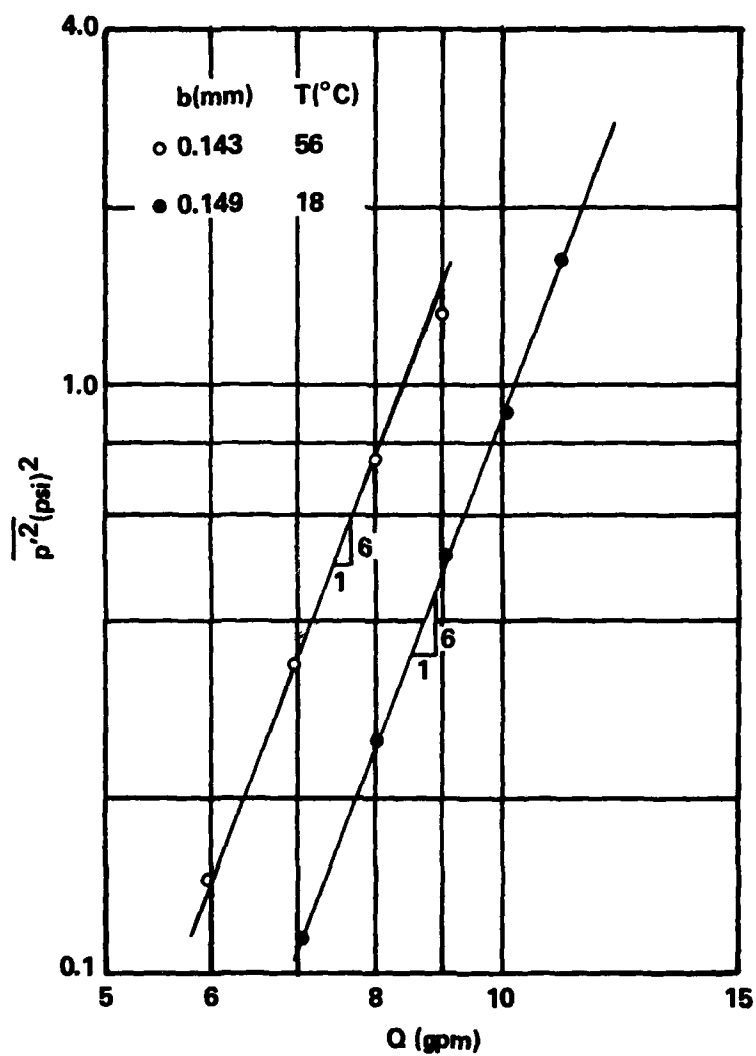


Figure 15. Non-Cavitating Mean-Square Energy Versus Discharge for Prototype Valve at a Fixed Opening

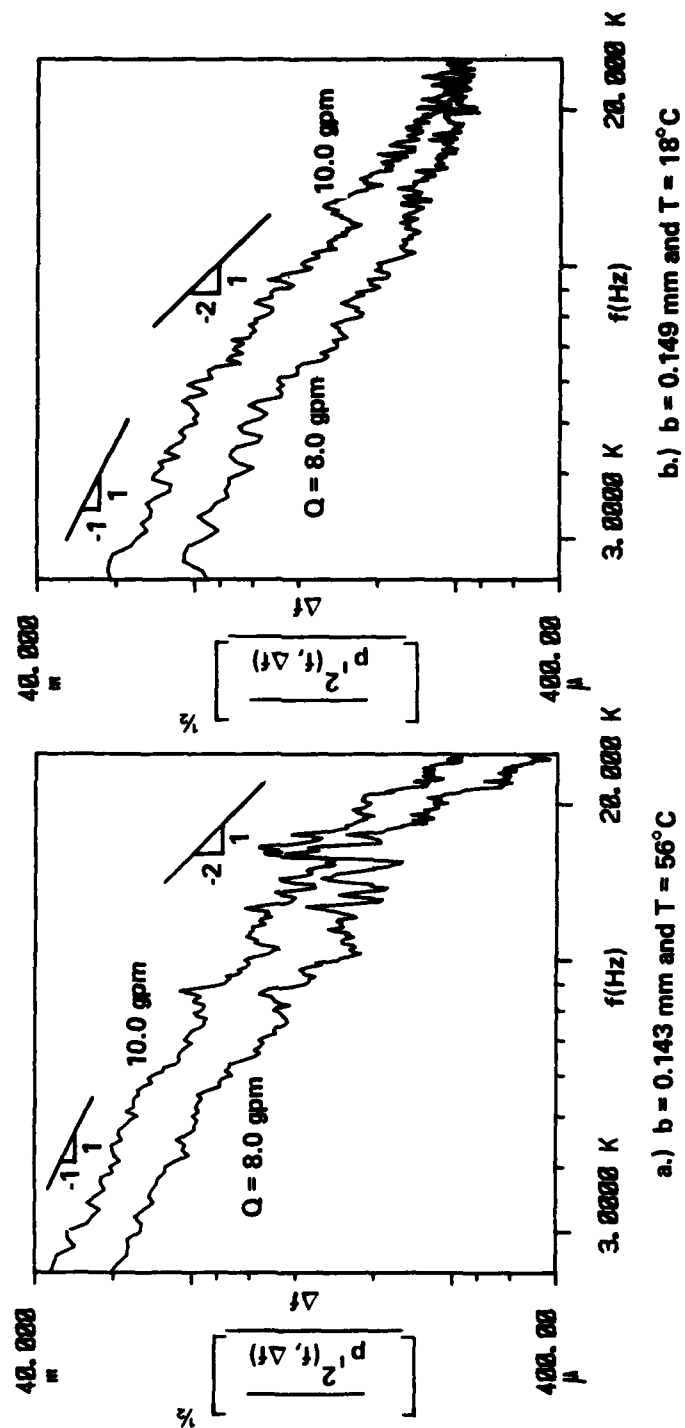


Figure 16. Non-Cavitating Energy Spectra for Prototype Valve at a Fixed Opening

that, as the flow rate and hence jet velocity V_j is increased for a fixed opening b , the extent of the spectrum corresponding to a -1 slope increases.

The two pressure transducers in the model were located such that any significant changes in the jet orientation could be noticed. The non-cavitating results presented here suggest that the jet did flip back and forth, confirming the conclusions of McCloy and Beck [10] that the jet may reattach to either the spool surface or the port wall, or issue freely at an angle depending upon the opening b and any clearance between the spool and the wall of the valve body.

The variation of mean-square energy with flow rate is shown in Figure 17 for various openings of the model valve. The pressure difference Δp was maintained constant under non-cavitating conditions. For a free jet for which Δp is a constant the velocity at the vena contracta V_c as given by Eq. (3) should have been a constant for all of the data shown in Figure 17. According to Eq. (10) the jet velocity at some position l from the vena contracta would increase directly with the square root of the opening b . The nearly constant output from transducer P_1 over the range of openings would indicate that the jet was not directed toward P_1 . For flows less than 15.5 gpm the jet is probably between P_1 and P_2 because of the relatively low energy levels. As shown by Figure 17 and the corresponding spectra in Figure 18 for transducer P_2 there is an apparent shift in the flow pattern as the flow increased slightly from 15.5 to 17.6 gpm. As the valve is opened further the energy level sensed by P_2 increases as the square of the flow, suggesting a monopole source in accordance with Eqs. (6) and (14) for a variable opening b . It is suspected that the increase in energy is either due to direct impingement of a reattached jet or the nearly direct effect of a free jet.

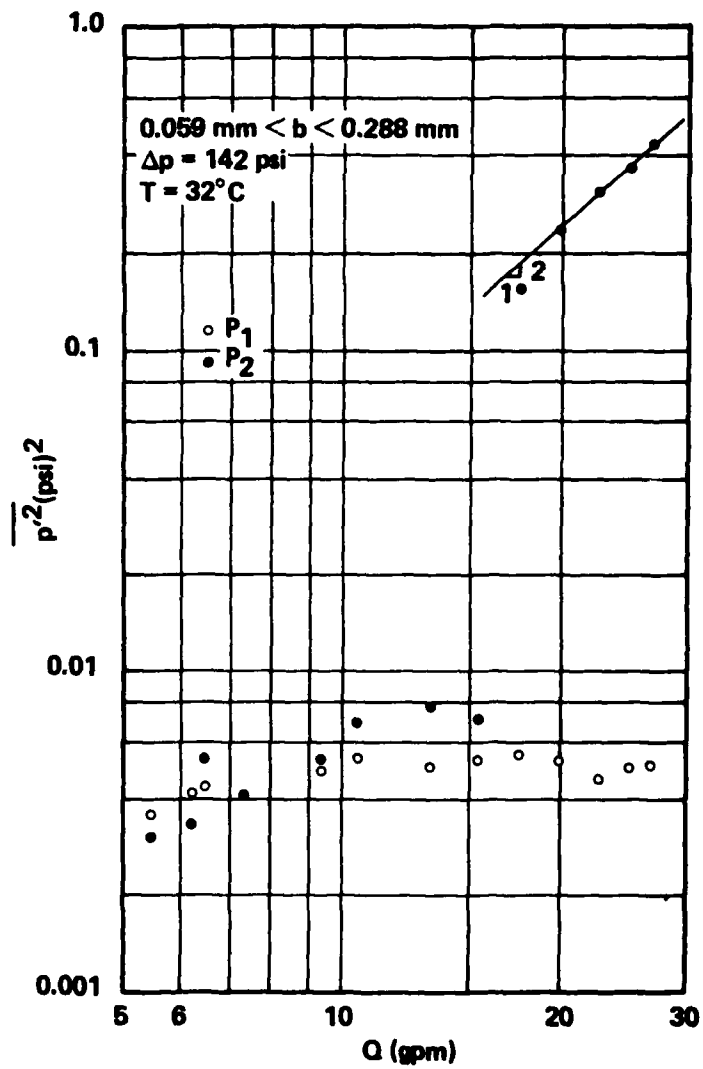


Figure 17. Non-Cavitating Mean-Square Energy Versus Discharge for Model Valve at a Variable Opening and Constant Pressure Difference

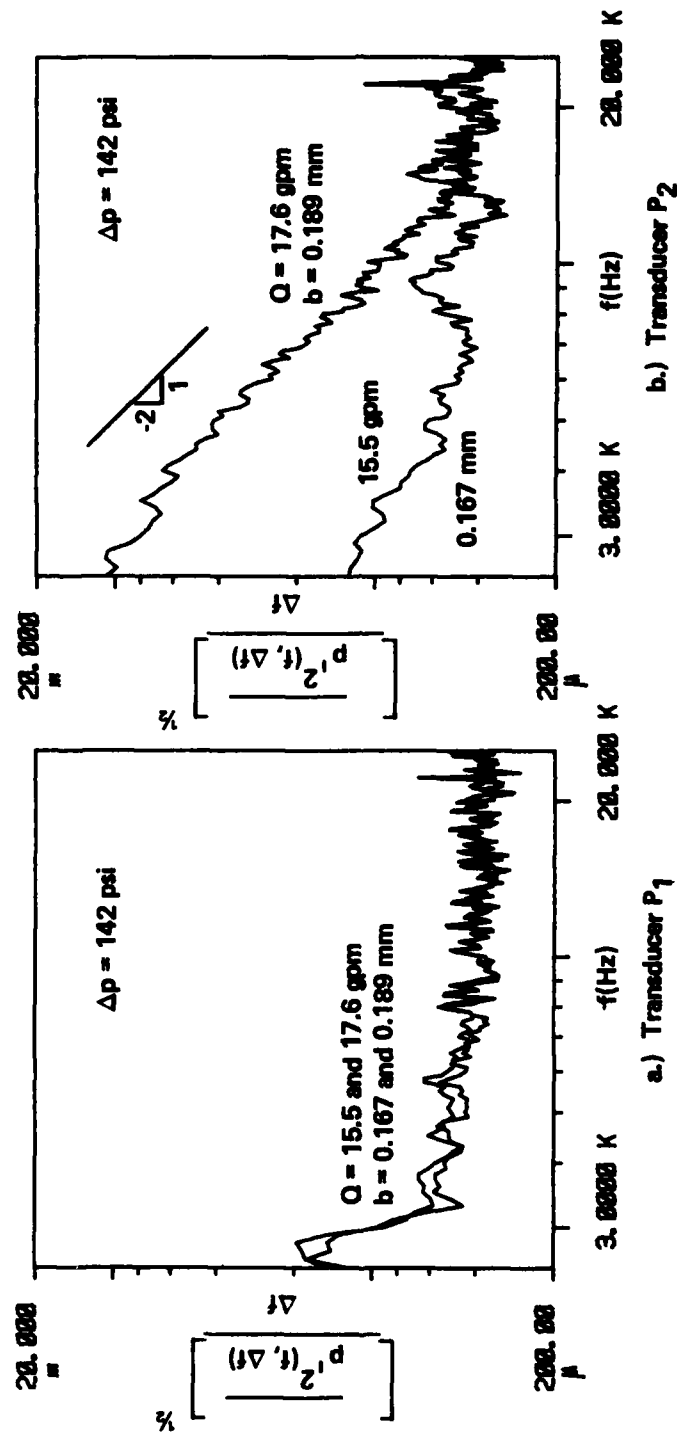


Figure 18. Non-Cavitating Energy Spectra for Model Valve at Two Values of Opening b and Constant Pressure Difference

The slope of the energy spectra at location P_2 can be approximated by -2 over a range of frequencies.

Non-cavitating data were collected with the model valve fixed at openings of $b = 0.108$ and 0.237 mm. For the smaller opening the plot of mean-square energy versus flow rate shown in Figure 19 and energy spectra for two of the higher flow rates plotted in Figure 20 indicated that the jet may have been free, and furthermore directed toward transducer P_1 . At the greater opening, however, the transducer P_1 hardly experienced any change in energy fluctuations as the flow increased, as shown in Figures 21 and 22a. There is some indication that the slope of the mean-square energy versus flow rate correlation changes from a dipole source (6 to 1) to a monopole source (4 to 1) at the higher flow rates. Portions of the jet-induced spectra plotted in Figure 22b can be approximated by slopes of -1, and others by -2.

The direct effect of pressure fluctuations from a jet are clearly shown in Figures 18b, 20a, and 22b for the model, in contrast to Figures 18a and 22a, for which there is little to no jet effect, but instead only background noise. The effect of any shifting of the jet is more evident in the larger model than in the prototype valve because of the size of the piezoelectric transducers relative to the length of the valve chamber.

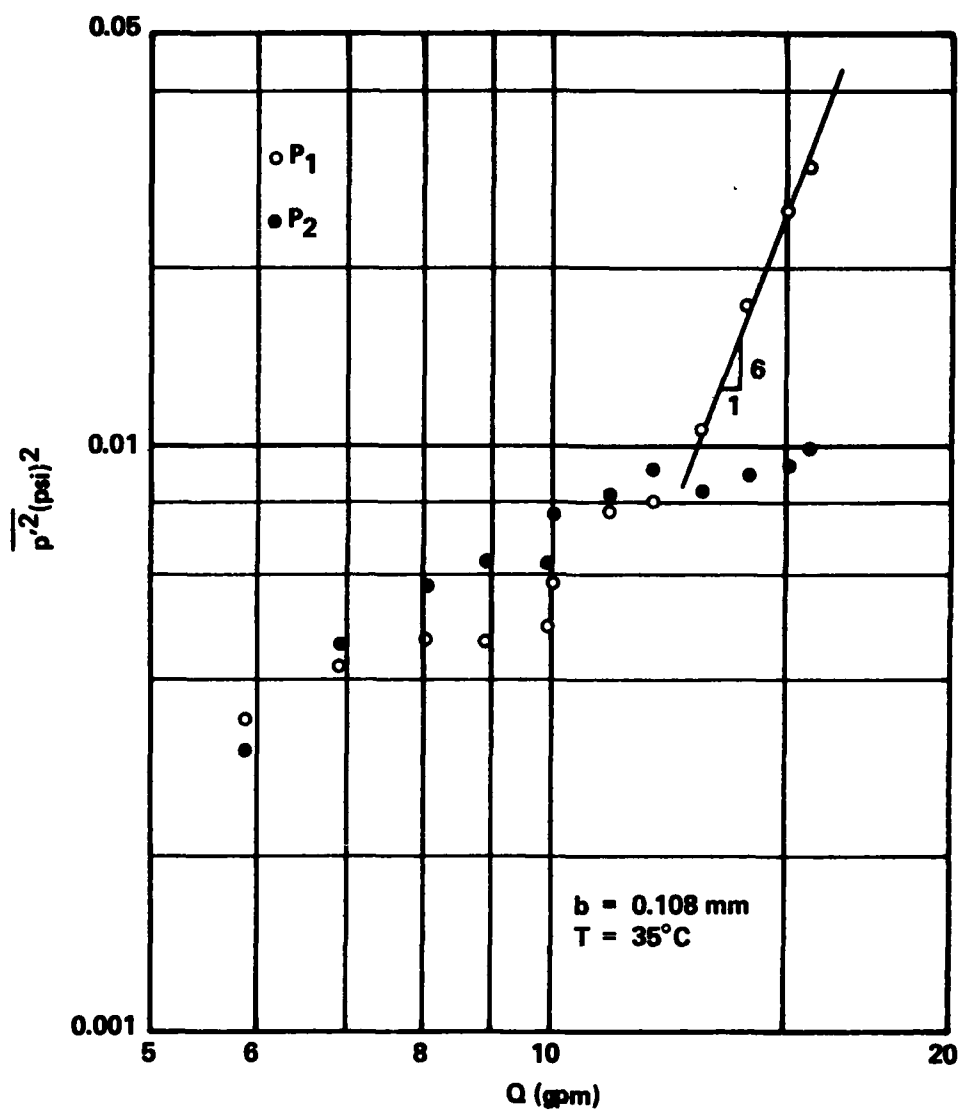


Figure 19. Non-Cavitating Mean-Square Energy Versus Discharge for Model Valve at a Fixed Opening

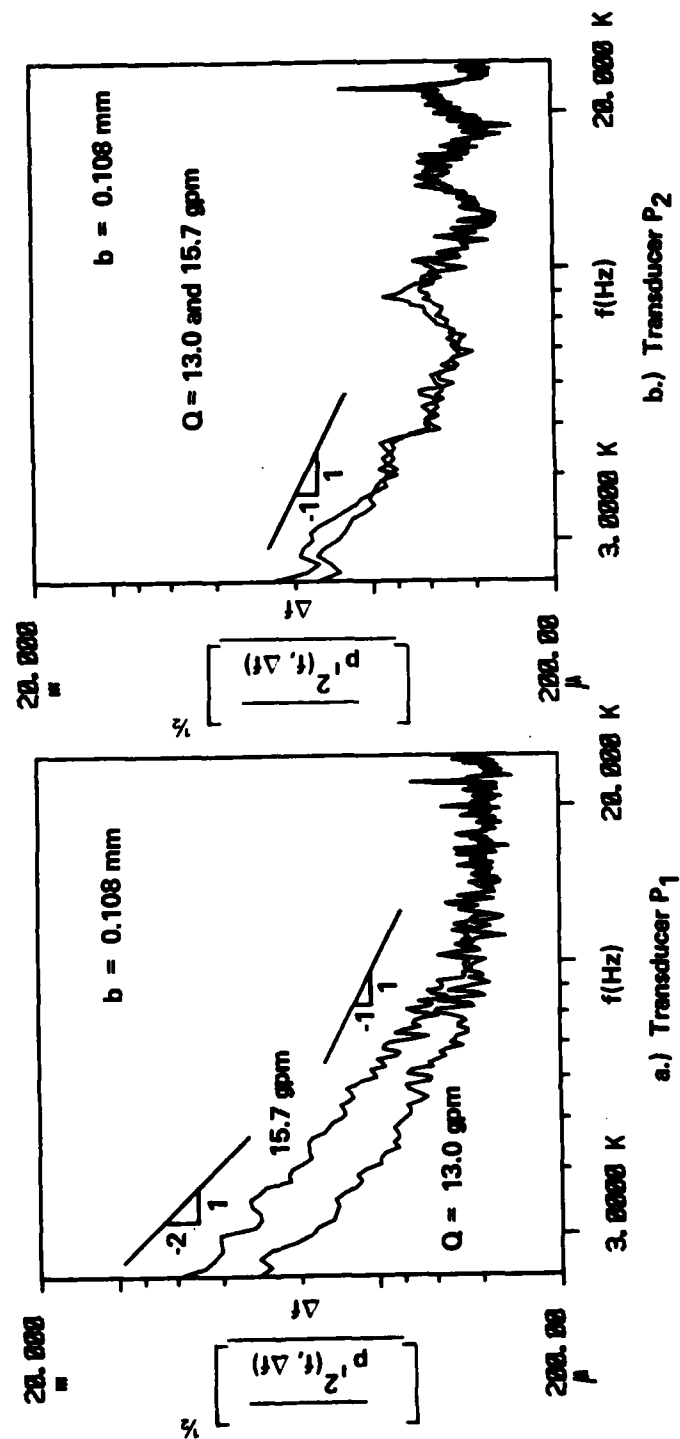


Figure 20. Non-Cavitating Energy Spectra for Model Valve at a Fixed Opening

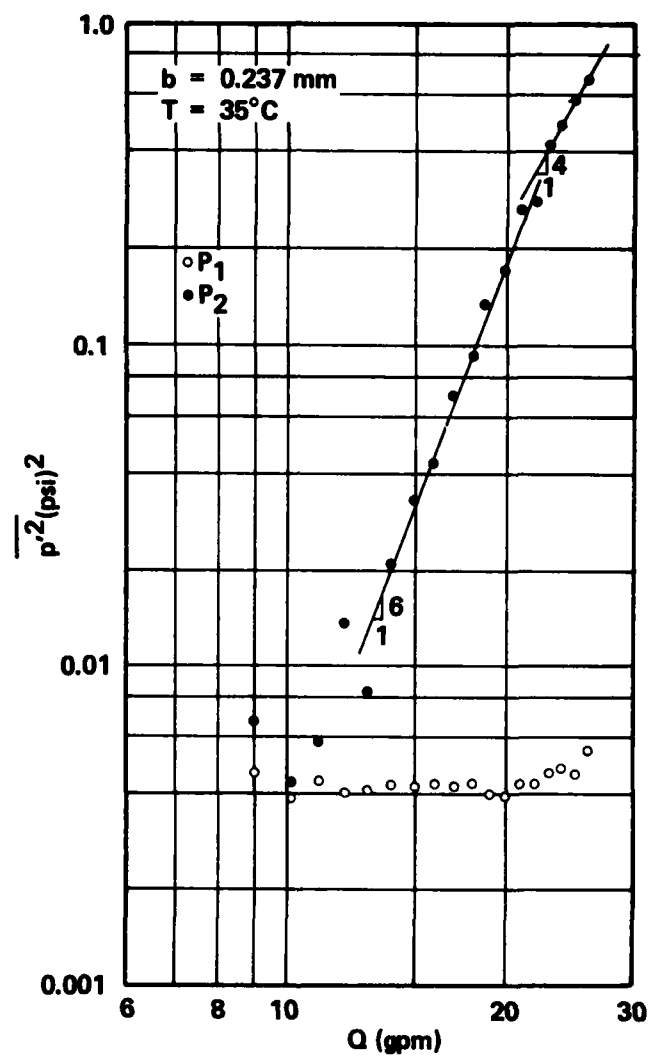


Figure 21. Non-Cavitating Mean-Square Energy Versus Discharge for Model Valve at a Fixed Opening

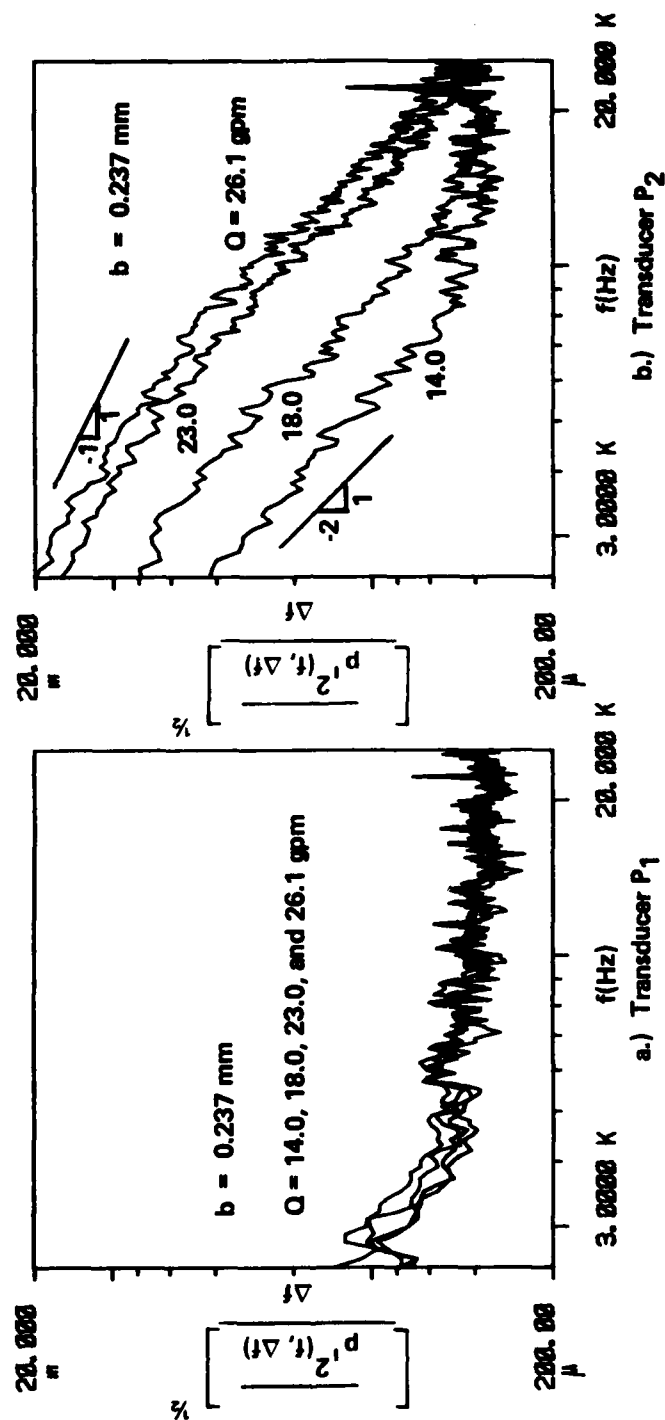


Figure 22. Non-Cavitating Energy Spectra for Model Valve at a Fixed Opening

SECTION VIII

CAVITATION INCEPTION

In order to define and determine the condition of cavitation inception, tests were conducted over a range of values of the cavitation number σ . Because of the sensitivity of pressure fluctuations to changes in jet velocity, care was taken to maintain the volumetric flow Q constant and to hold the respective spool at a fixed position. As shown by the non-cavitating energy spectra slight differences in valve opening b can lead to significant changes in energy levels if there is a direct effect of the jet. On the other hand, however, cavitation noise in the model valve can be several orders of magnitude greater than that due to a non-cavitating jet.

Prototype Valve

The results of varying σ as b and Q are maintained nearly constant are presented in Figure 23 for five flow rates. Although for each flow rate there is eventually a continual increase in the fluctuating energy measured by the pressure transducer P_1 and the accelerometer A_1 as the chamber pressure p_c is lowered, it is not clear where cavitation inception occurs. The definition of incipient cavitation is especially difficult with the prototype valve because of the relatively large jet energy under non-cavitating conditions. In order to illustrate this difficulty the data points for $Q = 11$ gpm are replotted on Figures 24a and b at a different scale. For reference each data point is given a number, which actually corresponds to a data file on a storage tape. The definition of cavitation inception would be very difficult if not

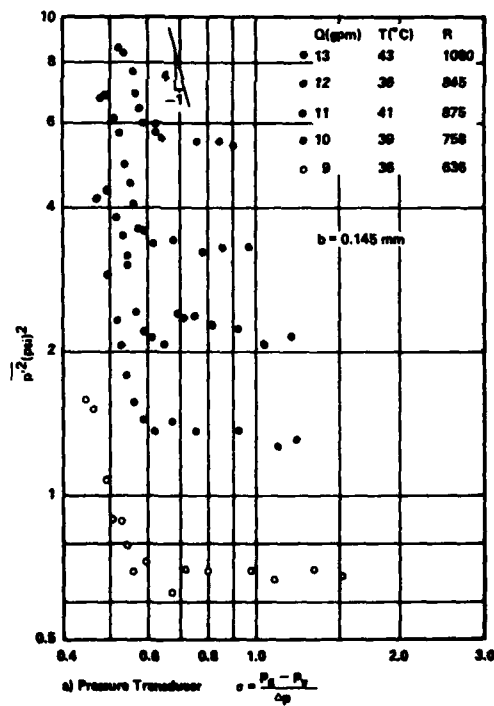
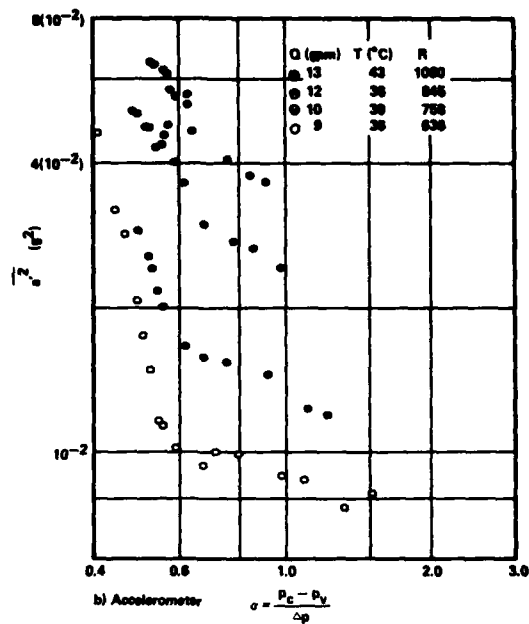


Figure 23. Mean-Square Energy Versus Cavitation Index for Prototype Valve at a Fixed Opening and Constant Discharges

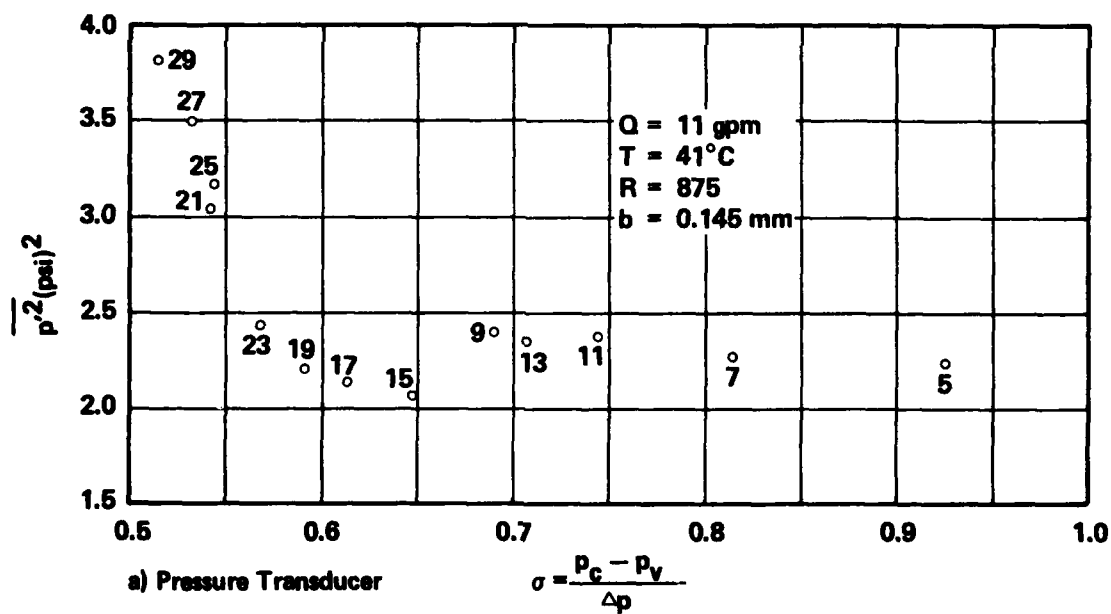
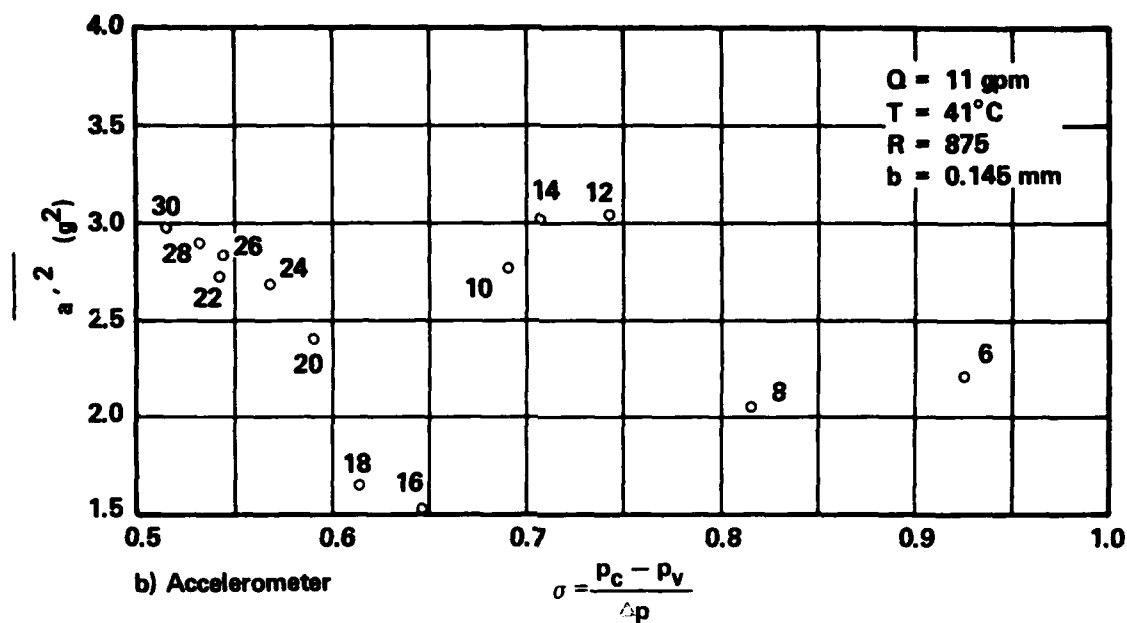


Figure 24. Mean-Square Energy Versus Cavitation Index for Prototype Valve at a Fixed Opening and Q = 11 gpm

impossible on the basis of mean-square energy, because of the sudden decrease in energy level from point 9 to point 15 for P_1 and corresponding points 10 to 16 for the accelerometer. It was discovered that an inspection of the respective energy spectra for each test proved more revealing than the total energy in the entire spectrum. In Figures 25a (P_1) and 25b (A_1) individual spectra for the seven points for which $\sigma > 0.6$ are superimposed on the left while the spectra for three values of σ are plotted on the right. The coincidence of the data on the left plot of pressure spectra suggests only non-cavitating jet noise. Apparently few if no cavitation events occurred for $\sigma=0.614$ (17 and 18) but many were present once the cavitation number was slightly reduced to 0.591 (19 and 20). Due to the relatively high energy levels at the low frequency end of the spectrum resulting from jet noise, small increases in the spectral density at the higher frequencies as a result of limited cavitation do not contribute much to the total energy over the entire pressure spectrum. The parameter total energy becomes more indicative of cavitation levels once cavitation becomes more extensive. Although the acceleration spectra under non-cavitating conditions are not as similar as the pressure spectra it is fairly evident at high frequencies that cavitation has occurred between $\sigma=0.614$ and 0.591.

The spectra in Figure 25 indicate that cavitation noise is restricted to the higher frequencies, but extends over a wider band as the cavitation number decreases. Another measure of cavitation noise is the ratio of the power spectral density of each frequency channel Δf under cavitating conditions to that under non-cavitating conditions. Choosing points 15 and 16 ($\sigma_0=0.647$) as the non-cavitating reference values, the ratio of power spectral densities are plotted in Figure 26 for points 17 and 18 ($\sigma=0.614$)

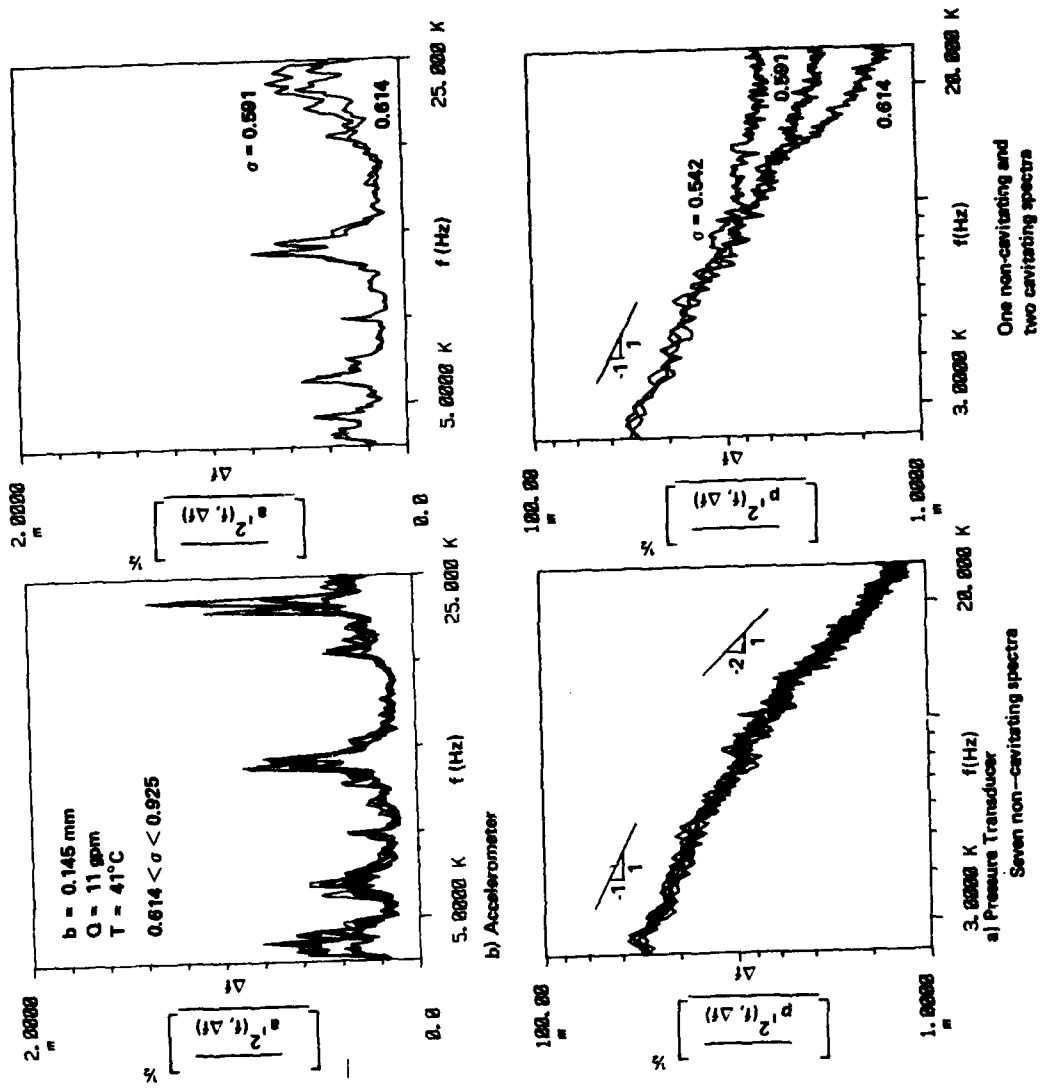


Figure 25. Non-Cavitating and Cavitating Energy Spectra for Prototype Valve at a Fixed Opening and $Q = 11$ gpm

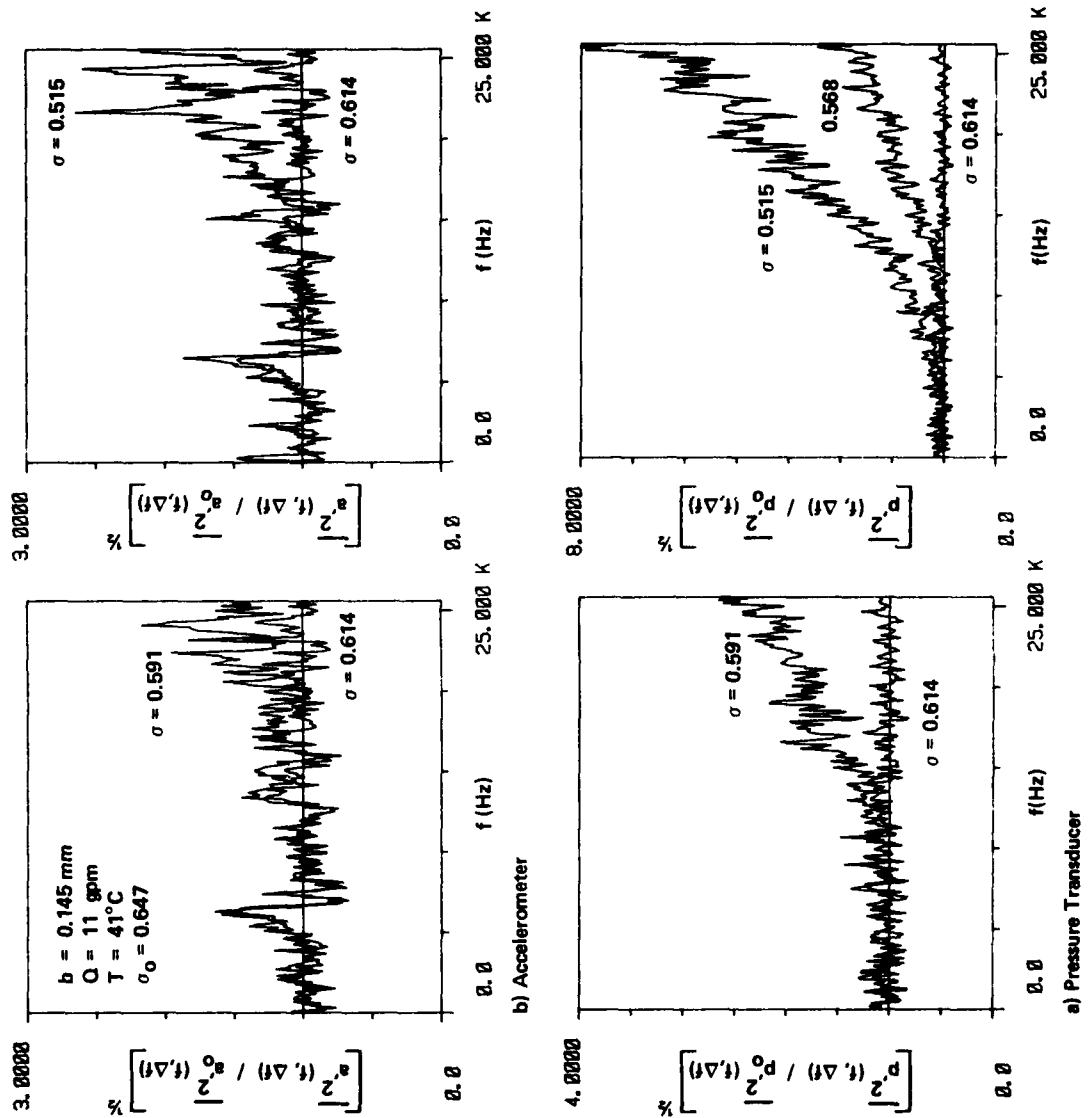


Figure 26. Ratio of Cavitating to Non-Cavitating ($\sigma = 0.647$) Spectral Density for Prototype Valve at a Fixed Opening

and points 19 and 20 ($\sigma=0.591$). Additional ratios of the power spectral density are presented in Figure 26 for lower values of the cavitation index, showing a progressive expansion of the cavitation noise to lower frequencies as σ is decreased. A sensitive measure of the extent of cavitation noise is the area under the curve of the ratio of power spectral density versus frequency, as shown on Figure 27 for transducer P_1 for a flow of $Q=12$ gpm. Similar correlations occurred for other flow rates. In comparing the sensitivity of the piezoelectric pressure transducer with the accelerometer it is clear that both sense the onset of cavitation, but the pressure transducer is probably a better detector for inception because (1) it is located close to the source and (2) the accelerometer is more sensitive to valve noise from the downstream throttling valves, especially for large values of p_R and hence σ . As will be demonstrated in the section on developed cavitation, as the effect of valve noise subsides as σ is lowered the accelerometer appears to be just as effective as the pressure transducer in sensing the radiation of cavitation noise.

Model Valve

The variation of mean-square energy versus the cavitation number is shown on Figure 28 for two openings of the model valve. Selected spectra are plotted in Figure 29 for the smaller opening ($Q=10$ gpm), and in Figure 30 for the larger opening ($Q=20$ gpm).

For $Q=10$ gpm there is only a limited effect of the jet under non-cavitating conditions, resulting in relatively low energy levels for the four pairs of data for P_1 and P_2 plotted on Figure 28. Once σ was lowered to 0.269, however, the noise increased approximately tenfold on both

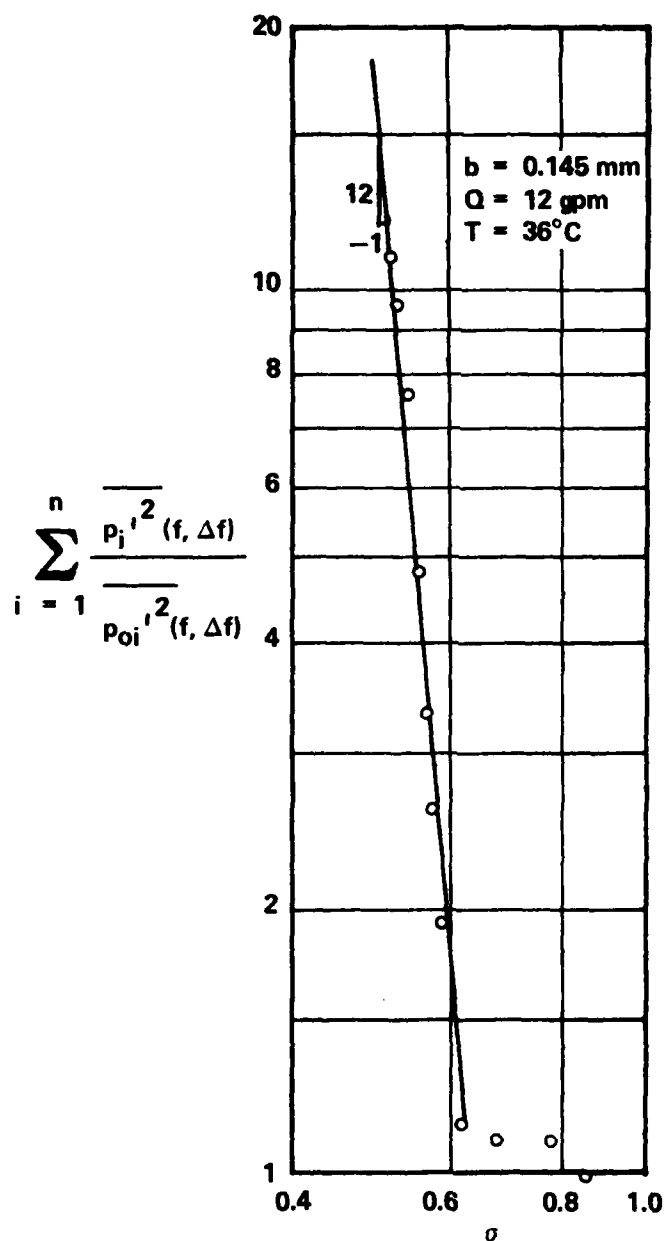


Figure 27. Area under Ratio of Cavitating to Non-Cavitating Mean-Square Spectral Density Curve for Fluctuating Pressure Versus Cavitation Index for Prototype Valve at a Fixed Opening and Q = 12 gpm

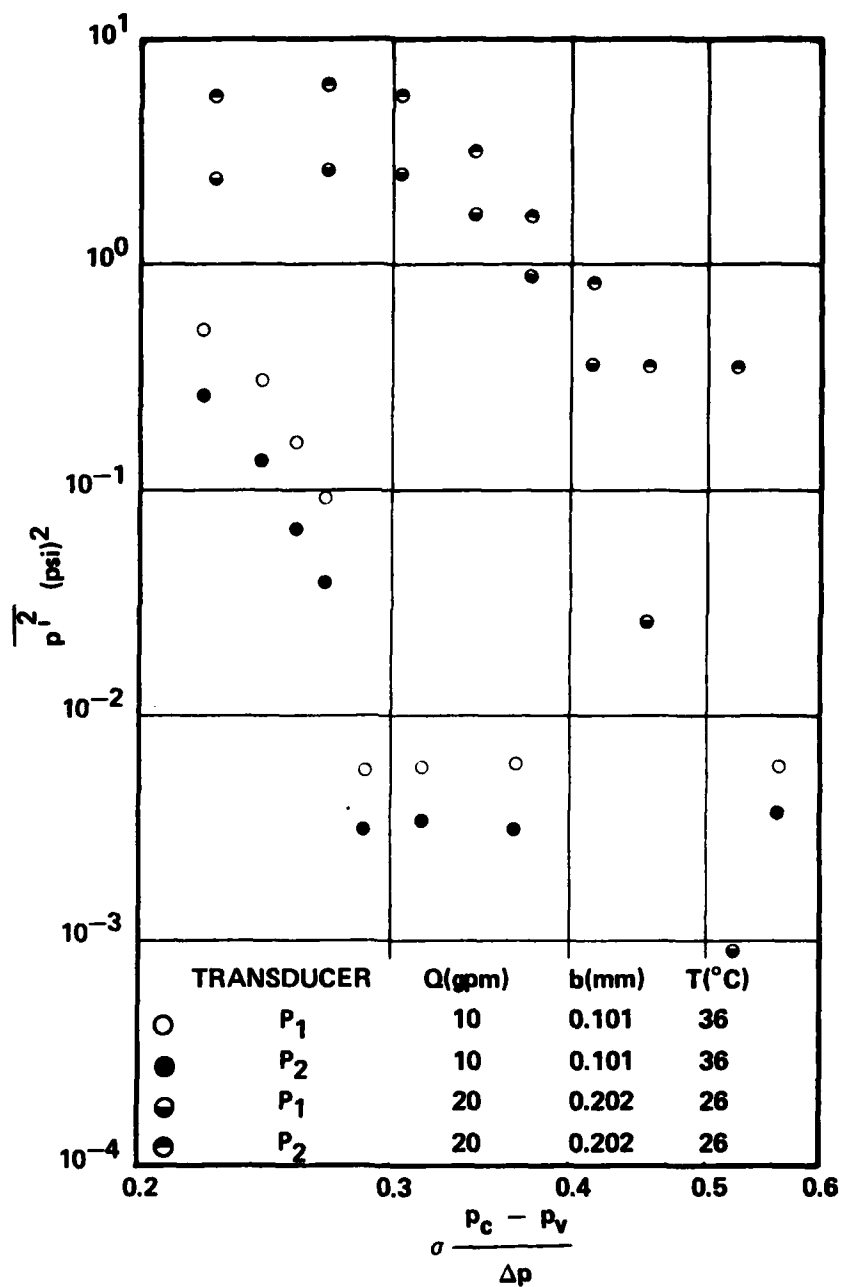


Figure 28. Mean-Square Energy Versus Cavitation Index for Model Valve at Two Fixed Openings

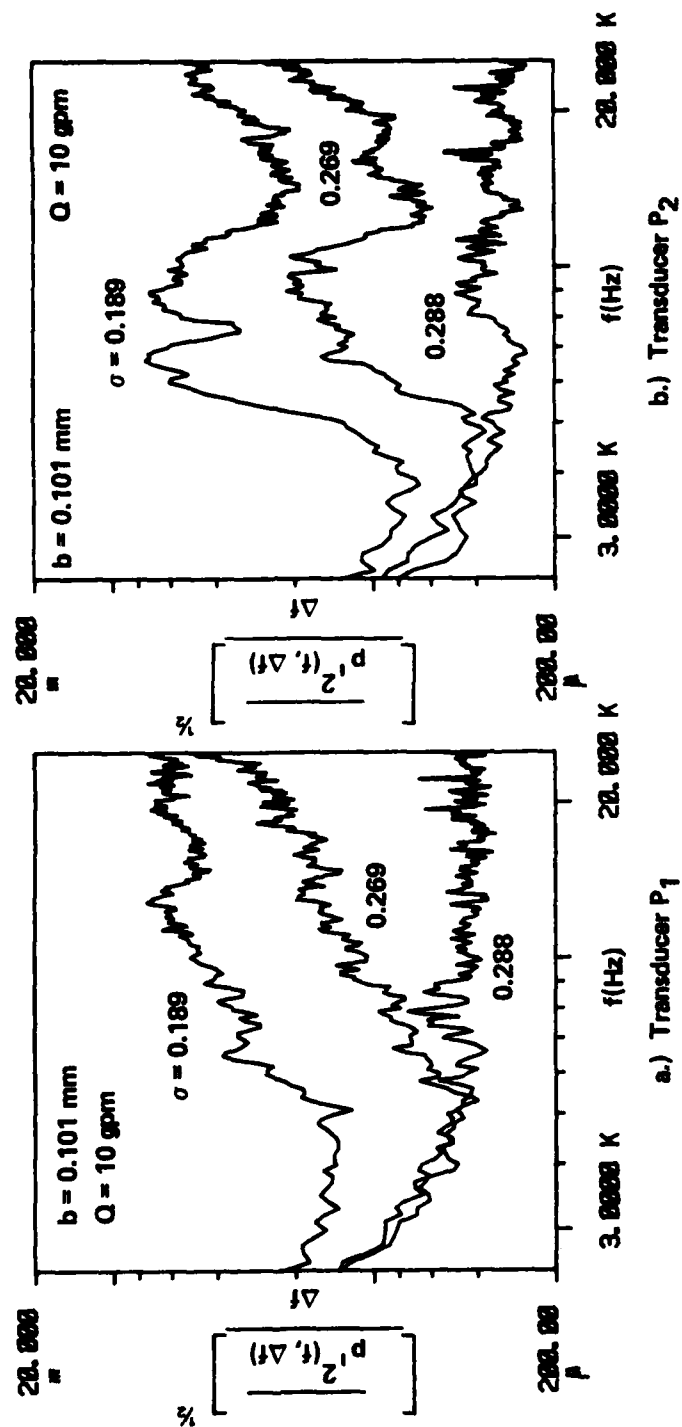


Figure 29. One Non-Cavitating and two Cavitating Energy Spectra for Model Valve at a Fixed Opening

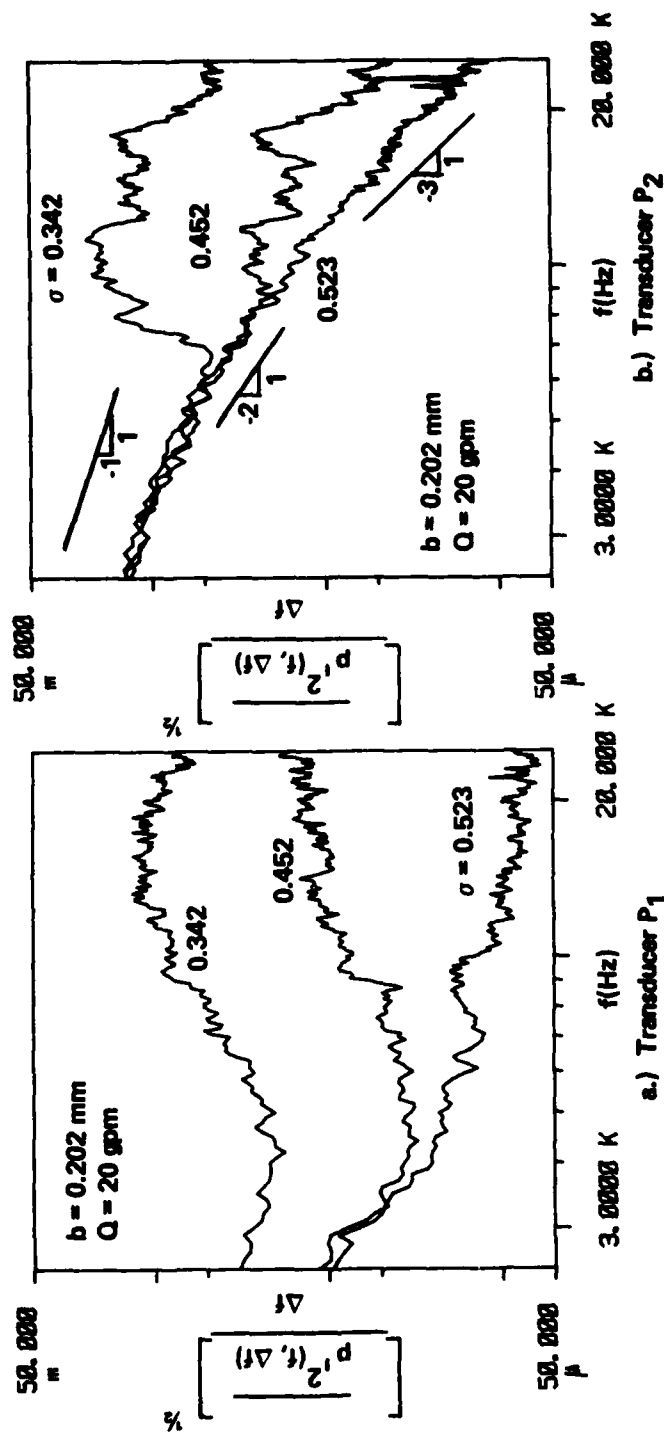


Figure 30. One Non-Cavitating and Two Cavitating Energy Spectra for Model Valve at a Fixed Opening

transducers. In contrast to the results for the prototype valve cavitation noise in the model valve is evident over a wider band of frequencies. A further lowering of the cavitation number increased the energy level at least another order of magnitude, as shown by Figure 28. From $\sigma=0.269$ to $\sigma=0.189$ the increase in noise is rather broadband, at least from $2.5 \text{ kHz} < f < 25 \text{ kHz}$. Figure 28 clearly demonstrates the dramatic sensitivity of the fluctuating pressure to the onset of cavitation events.

At the greater valve opening the jet has a direct effect on transducer P_2 , Figure 30b, under both non-cavitating and cavitating conditions. The energy level measured by transducer P_1 under non-cavitating conditions ($\sigma=0.523$ in Figure 28) is quite low compared to that indicated by P_2 . Transducer P_1 is much more sensitive to the onset of cavitation, however, because of the low background noise level under no cavitation. As the cavitation index was lowered from 0.523 through inception to a value of 0.452 the increase in noise measured by transducer P_1 was significantly greater than that sensed by transducer P_2 . As the cavitation number was lowered further the noise as measured by transducer P_1 continued to increase over a wide band. This increase was not sensed by transducer P_2 at the low frequencies because of the intense background noise of the jet, which may have been directed upon P_2 .

For another test series, for which the difference in the cavitation index $\Delta\sigma$ between tests was much closer, non-cavitating and cavitating spectra are shown in Figure 31 for pressure transducers P_1 and P_2 . The six spectra shown on the left plots suggest no cavitation for $\sigma \geq 0.385$. As shown by the plots on the right figure a slight lowering of σ to 0.373 resulted in an increase in the power spectrum at the higher

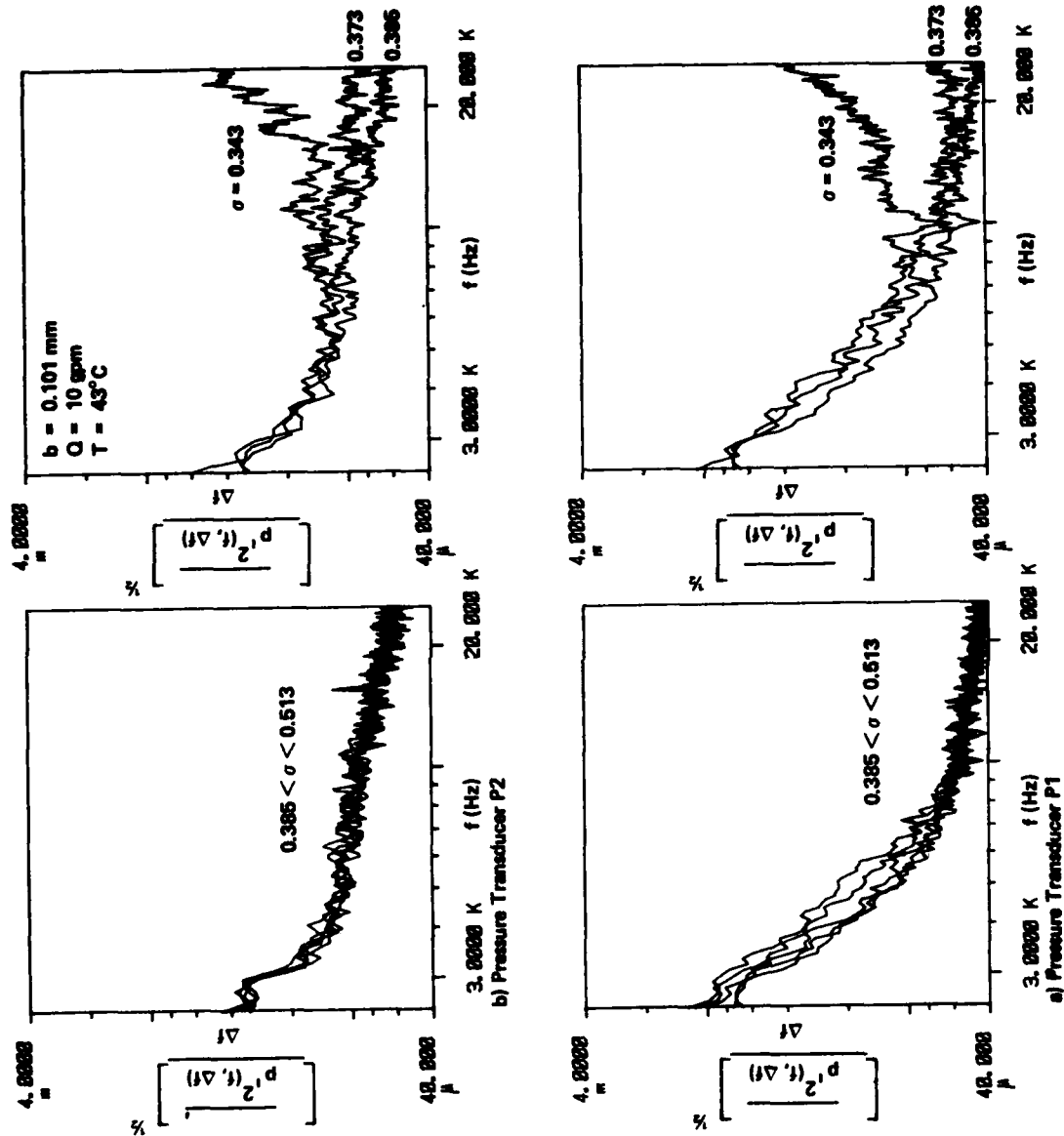


Figure 31. Non-Cavitating and Cavitating Energy Spectra for Model Valve at a Fixed Opening

frequencies. The ratio of the power spectral density for the same data shown in Figure 32 is also quite revealing regarding both the coincidence of non-cavitating results as well as the onset of cavitation. In fact, as illustrated by Figure 33 for this data set and by Figure 34 for another data set taken at a higher flow, the area under the curve of the ratio of power spectral density at any condition to a reference non-cavitating condition is quite sensitive to cavitation events. Over a range of σ of 0.15 in Figure 33 the area function varied by nearly four orders of magnitude. For the larger opening and corresponding greater flow rate for the data of Figure 34 the area function for P_1 also varied by nearly four orders of magnitude from $\sigma=0.6$ to $\sigma=0.4$, while for P_2 the increase was not as great because of the hydrodynamic jet noise caused by the jet being directed toward that transducer. Nevertheless, the area functions of Figures 33 and 34 are very sensitive indicators of cavitation events.

Criterion for Cavitation Inception

Attempts were made to formulate a criterion for the definition of incipient cavitation. Although the model was made of transparent walls for the purpose of visualization of the formation and collapse of bubbles, and the bubbles could be clearly seen as the valve was made to cavitate somewhat extensively, the onset of cavitation was extremely difficult to define visually because of the small openings, high jet velocities, and relatively small bubbles. After a number of somewhat unsuccessful attempts to establish incipient and desinent cavitation visually, reliance was placed upon the pressure transducers and the accelerometer, as well as aural sensing using a stethoscope. The identification of

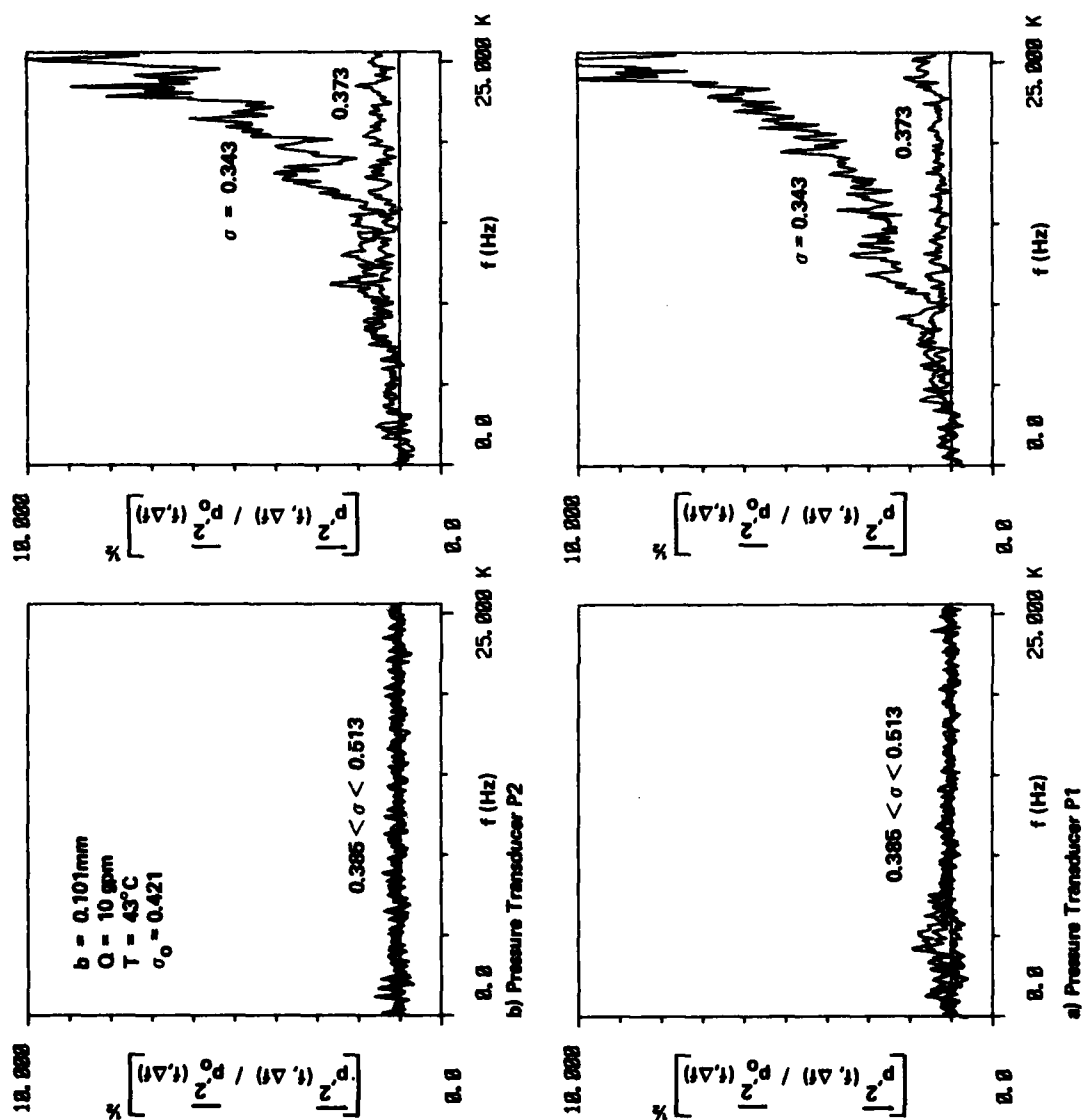


Figure 32. Ratio of Cavitating to Non-Cavitating ($\sigma = 0.421$) Spectral Density for Model Valve at a Fixed Opening

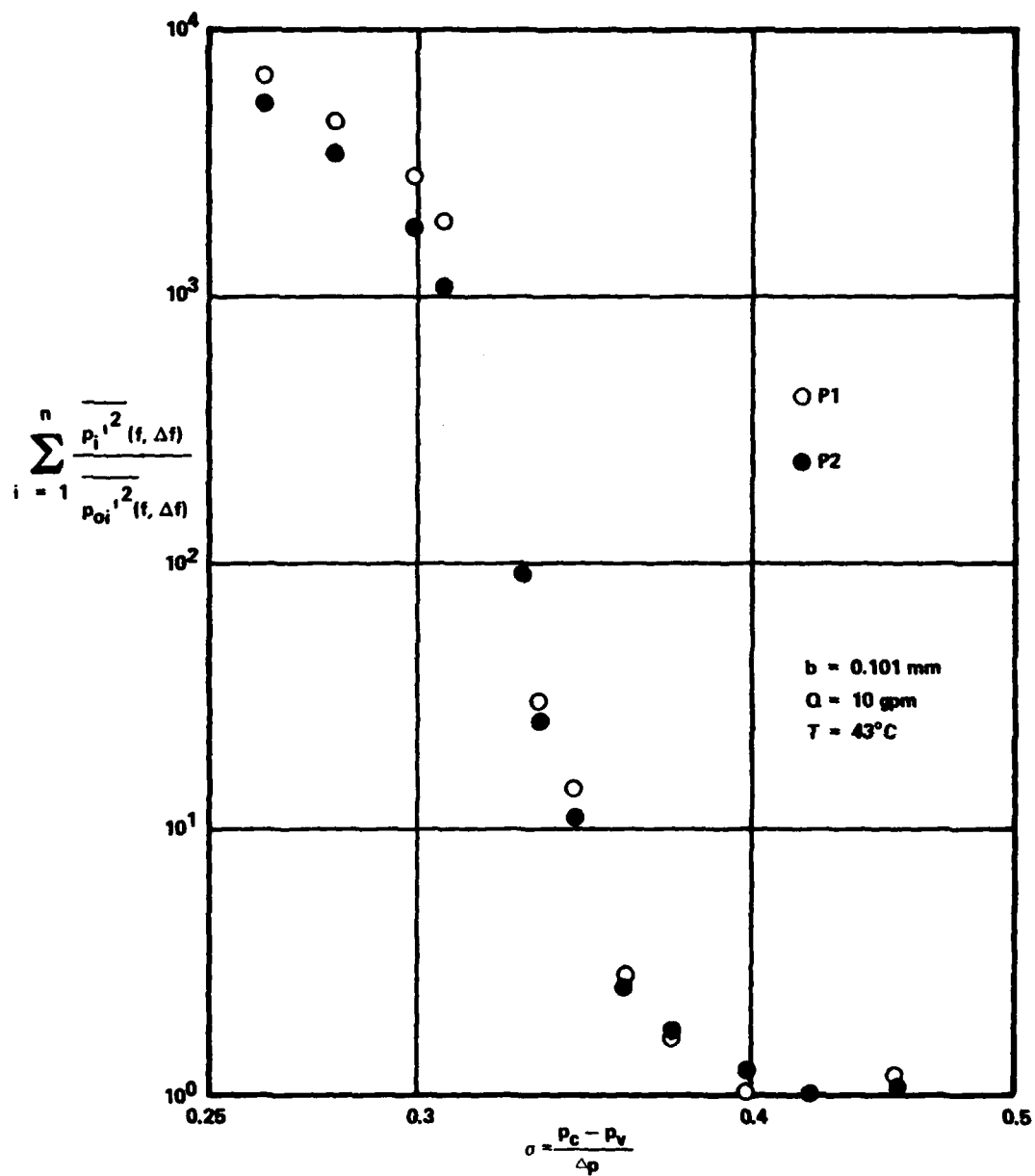


Figure 33. Area under Ratio of Cavitating to Non-Cavitating Mean-Square Spectral Density Curve Versus Cavitation Index for Model Valve at a Fixed Opening

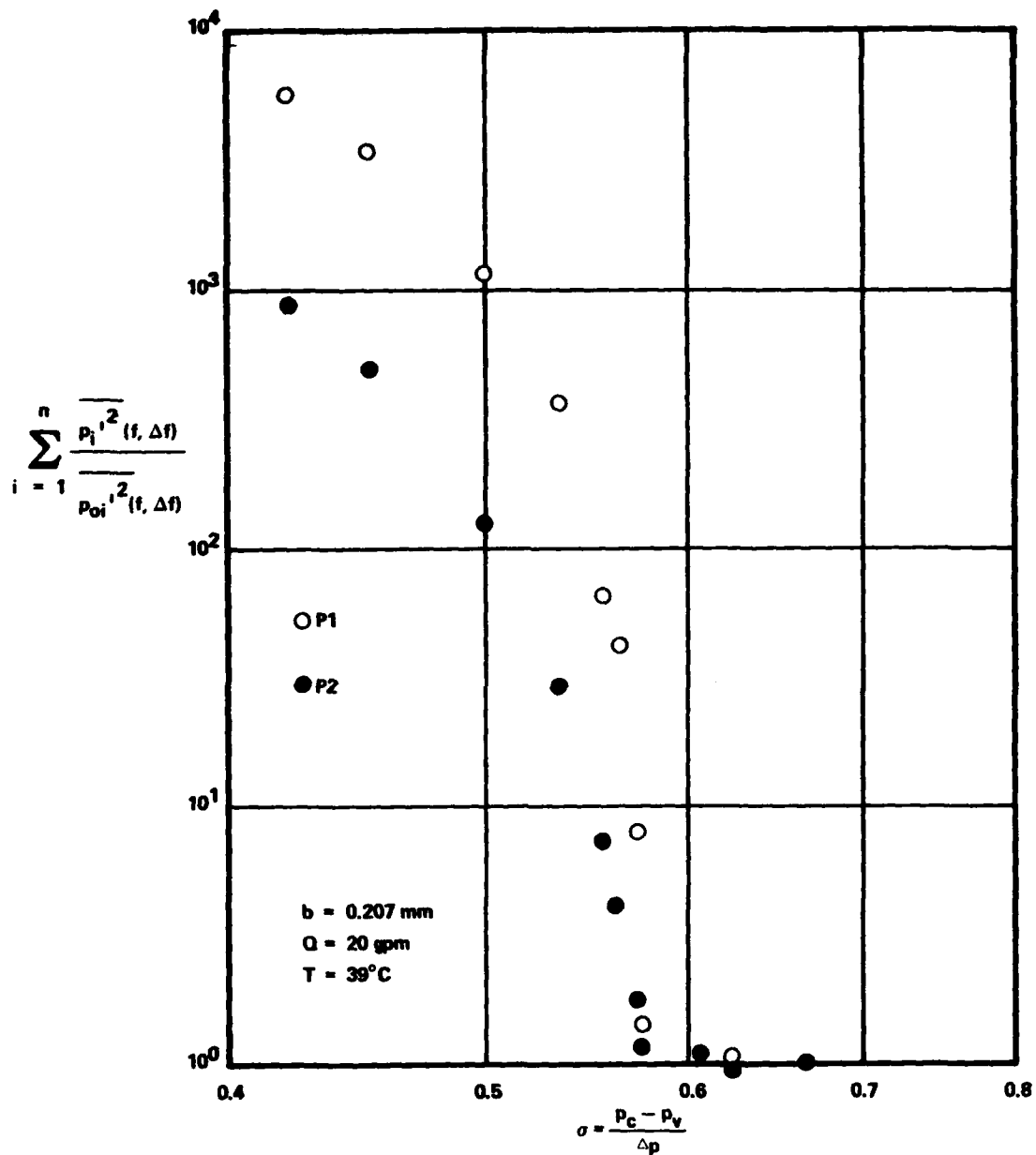


Figure 34. Area under Ratio of Cavitating to Non-Cavitating Mean-Square Spectral Density Curve Versus Cavitation Index for Model Valve at a Fixed Opening

inception was much easier in the model using transducer P_1 because of the dramatic change once cavitation commences. Because of the difficulty of separating jet noise from cavitation noise the criterion for inception used for the prototype valve differed slightly from that applied to the model valve, the latter of which will be discussed first.

Model Valve. -- Because of the relatively low levels of energy in the model under non-cavitating conditions, except when the jet was apparently directed onto transducer P_2 , it was not difficult to observe the occurrence of a few cavitation events by comparing cavitating with non-cavitating spectra. The data were taken by maintaining a constant flow with the spool locked in a fixed position. The cavitation number was reduced as the pressure difference Δp , and consequently the discharge Q , was maintained constant as nearly as possible. For each value of σ the dynamic signal for transducer P_1 was processed and the total fluctuating energy noted. It was observed that this value hardly changed under non-cavitating conditions. Cavitation inception was defined at the condition for which this nominal value increased by approximately 50 to 100 percent, which corresponded to only the slightest change in the cavitation index. Usually aural sensing by means of a stethoscope yielded the same value of the critical cavitation number. The cavitation number at the 50 to 100 percent energy increase is defined as the incipient cavitation index σ_1 , and is plotted as a function of the Reynolds number in Figure 35. The two sets of data correspond to a range of flow rates for each value of the fixed opening b .

Prototype Valve. -- As mentioned earlier a comparison of fluctuating energies measured by the pressure transducer in the chamber of the prototype valve did not clearly indicate the difference between cavitation

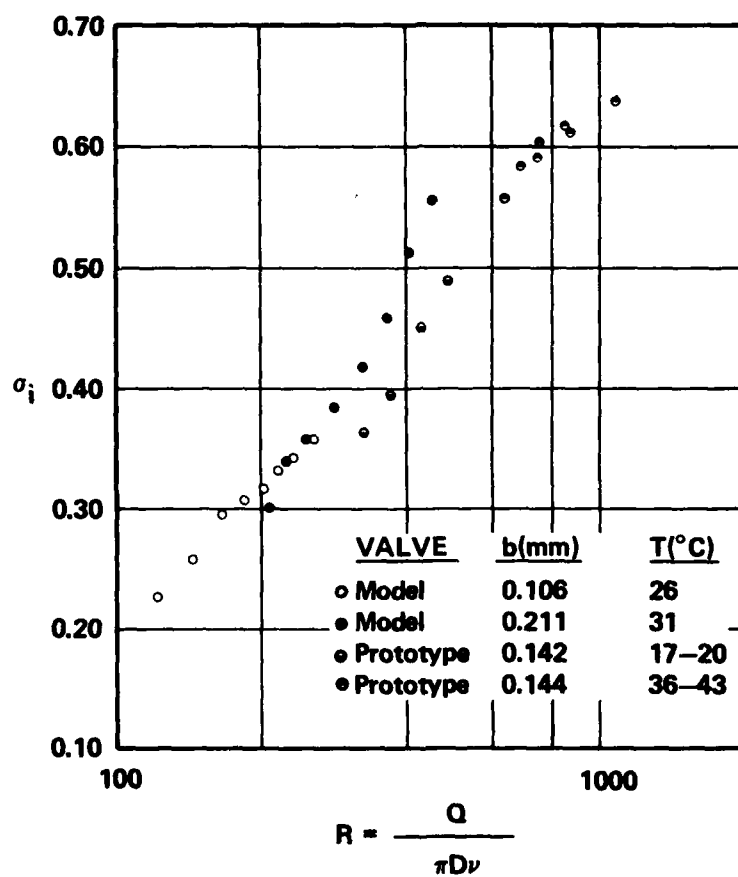


Figure 35. Incipient Cavitation Index Versus Reynolds Number for Model and Prototype Valves

inception or limited cavitation and no cavitation because of the high level of jet noise. The points shown on Figure 24 for $\sigma > 0.6$ illustrate the difficulty inherent with comparing solely mean-square energy, while the spectra on Figure 25 suggest there is no cavitation. Only by comparing spectra or by normalizing the spectral density with the corresponding non-cavitating spectra, Figure 26, could the presence of cavitation be determined. The criterion for incipient cavitation for the prototype valve was defined as the departure of the area under the normalized pressure spectral density curves versus cavitation number from the non-cavitating value, which usually varied from approximately 0.9 to 1.1, depending upon which non-cavitating test was chosen as the reference value. The value of σ_1 was obtained from expanded versions of Figure 27 by interpolating between the intersection of the extrapolated curve on the cavitating leg of the plot and the non-cavitating horizontal line. Various criteria yielded differences in the incipient cavitation number of only 0.005 to 0.01. The results of two series of tests at virtually the identical valve opening and nearly the same range of flow rates (7-13 gpm) are shown in Figure 35. The only difference in the two series was the oil temperature, which resulted in a significant difference in the range of Reynolds numbers.

Although the use of the area function was not employed for the model valve, inspection of Figures 33 and 34 illustrates that such a criterion could be as valid, or even more so, as it was for the prototype valve. The expanded σ scale on Figure 33 suggests that the effect of an increasing number of cavitation events as σ is lowered below σ_1 , which is somewhat of an arbitrary criterion, is to produce an exponential effect on the area function. The use of an energy spectrum with 50 ensemble averages

does yield a reasonable statistical summary of cavitation events, however.

Discussion of Results

The criteria of cavitation inception employed in this investigation corresponds to a few, but unknown number, of cavitation events during the 50 ensemble averages taken over the sampling period. Single bubble formation in the transparent model could not be observed under these conditions. In fact, the cavitation index corresponding to the formation of a series of bubbles around the annulus was approximately 0.18 less than the values shown on Figure 35. Even a desinent cavitation number defined at the condition of the elimination of all visible bubbles was 0.10 smaller than the corresponding values of σ_1 depicted on Figure 35. Because of the smallness of the bubbles, the high jet velocity, and apparently few cavitation events, bubbles at the condition σ_1 are difficult to observe.

No attempt was made to measure the size of free nuclei in the oil, although the high pressure filter limited the absolute size of any contaminant to 3 μm . Because of the continual filtering of the test liquid the nuclei size and distribution probably did not vary much from test to test, as was evident from a comparison of energy spectra from test series to test series at the same conditions. As shown by the data on Figure 15 for two different temperatures there is an apparent viscous effect on the non-cavitating energy spectra. Since cavitation inception is affected by the level of turbulence, as shown by Arndt [16,17], the variation of σ_1 with Reynolds number shown in Figure 35 can be directly correlated with the non-cavitating fluctuating energy shown in Figure 15. The data of McCloy and Beck [5] indicate a similar trend of σ_1 versus R for two two-dimensional models. Their incipient

cavitation index was based on the aural detection of the initial presence of a sharp crackling sound. For the range of Reynolds numbers the critical values of σ_1 reported by McCloy and Beck [5] are 0.05 to 0.10 lower than the corresponding ones plotted on Figure 35, however. Perhaps the criterion employed in this investigation corresponds to a smaller number of cavitation events at σ_1 . The effect of viscosity on cavitation inception is also evident in the results of Backé and Riedel [7] and Riedel [8], who evidently defined inception at the condition of the change in the discharge coefficient of an orifice, or a situation corresponding to wider spread cavitation. Noise data taken by Rouse [18] with a water jet issuing from a nozzle yielded $\sigma_1 = 0.55$ from a plot of noise versus σ . Intermittent bursts of noise were observed for values of σ as high as 0.7, however. Obviously, the criterion employed for cavitation inception is somewhat subjective.

For the range of values of dissolved air content present in this study there was no apparent effect of hysteresis on σ_1 . The critical σ_1 did not appear to depend upon whether the downstream pressure was being decreased or increased. As discussed later, for dissolved air content at the two extremes experienced in the investigation - 4.5 and 9.0 percent by volume - there was no apparent difference in σ_1 nor cavitation noise over the entire range of the cavitation index. Evidently the low residence time of the bubbles in the jet and valve chamber precluded any significant effect of gaseous cavitation. Even for the lowest values of the cavitation number experienced by the model valve, the bubbles disappeared as the flow left the downstream port, suggesting the presence of only vaporous cavitation.

Although the accelerometer mounted on the end of the spool of the

prototype valve was not quite as sensitive to the onset of cavitation, it proved to be quite a good indicator of the level of cavitation once inception occurred. As the cavitation index was lowered toward σ_1 , as represented by Figure 23b, there was a very gradual increase in the fluctuating acceleration levels, making the formulation of a criterion of cavitation inception on the basis of the accelerometer quite difficult. The low level response on the accelerometer for $\sigma > \sigma_1$ is attributed to mechanical effects caused by the method utilized to vary σ -- the operation of downstream valves.

SECTION IX

DEVELOPED CAVITATION

Attention has been focused on flow conditions corresponding either to no cavitation or to moderate cavitation for values of the cavitation index σ slightly less than the incipient value σ_1 . As the return pressure p_R is lowered more and more for a constant discharge Q , for which the pressure difference increases moderately, cavitation becomes more extensive and attains a developed state. For both test valves extensive testing was conducted over the maximum range that σ could be varied.

Prototype Valve

Figure 36 shows the same test data plotted in Figures 23 and 24 as well as the remaining data for that particular data set, which was very closely spaced, and covered a wide range of values of the cavitation index. Over the approximate range of $0.4 < \sigma < 0.5$ the fluctuating pressure energy (Figure 36a) is on virtually a plateau, whereas the accelerometer (Figure 36b) registers a steady rise. The cavitation number at peak energy is 0.229 for the accelerometer, but 0.187 for the pressure transducer. Because of the effect of the annular jet under non-cavitating conditions the peak pressure energy at $\sigma = 0.187$ is no more than approximately four times the non-cavitating value, while the peak energy registered by the accelerometer is nearly two orders of magnitude greater than the non-cavitating value.

Figure 37 shows the pressure and acceleration energy spectra for a

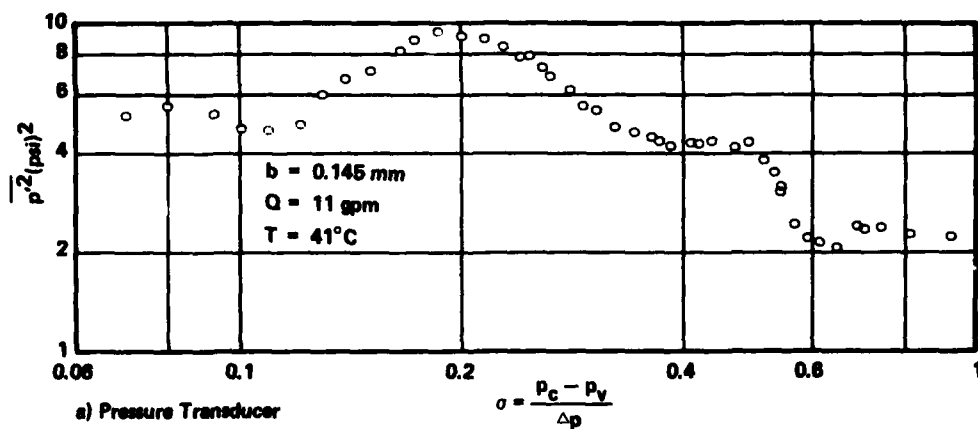
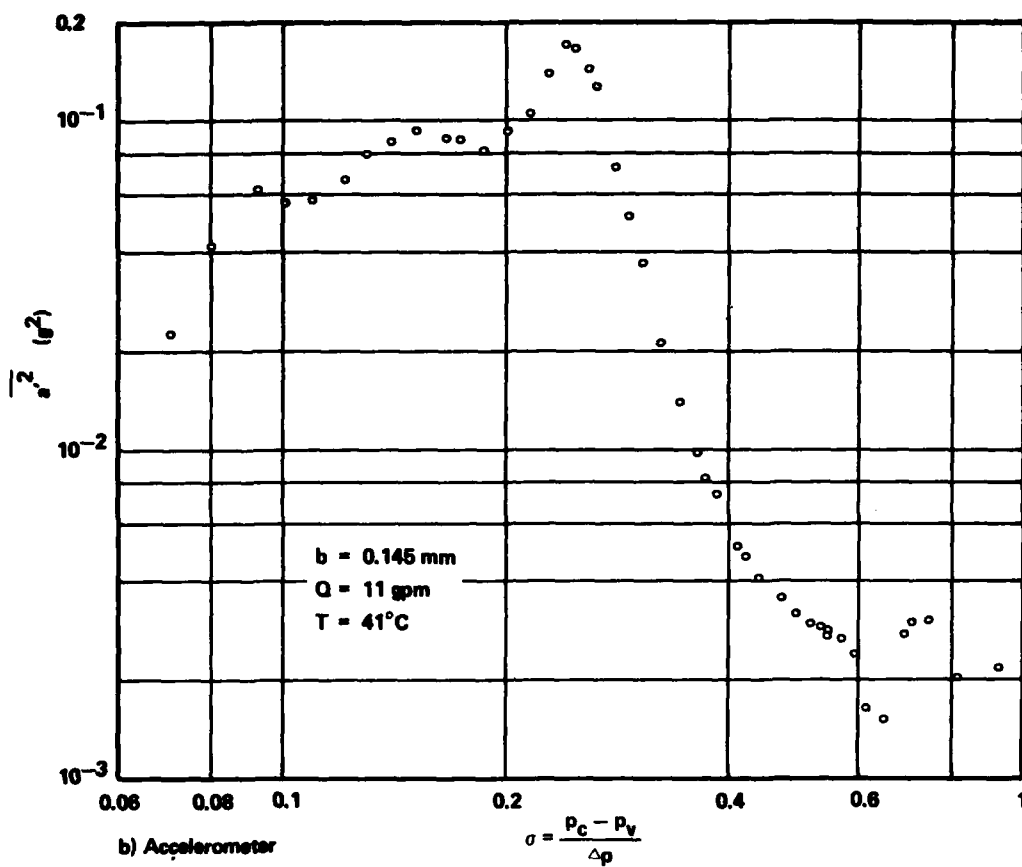


Figure 36. Mean-Square Energy Versus Cavitation Index for Prototype Valve at a Fixed Opening

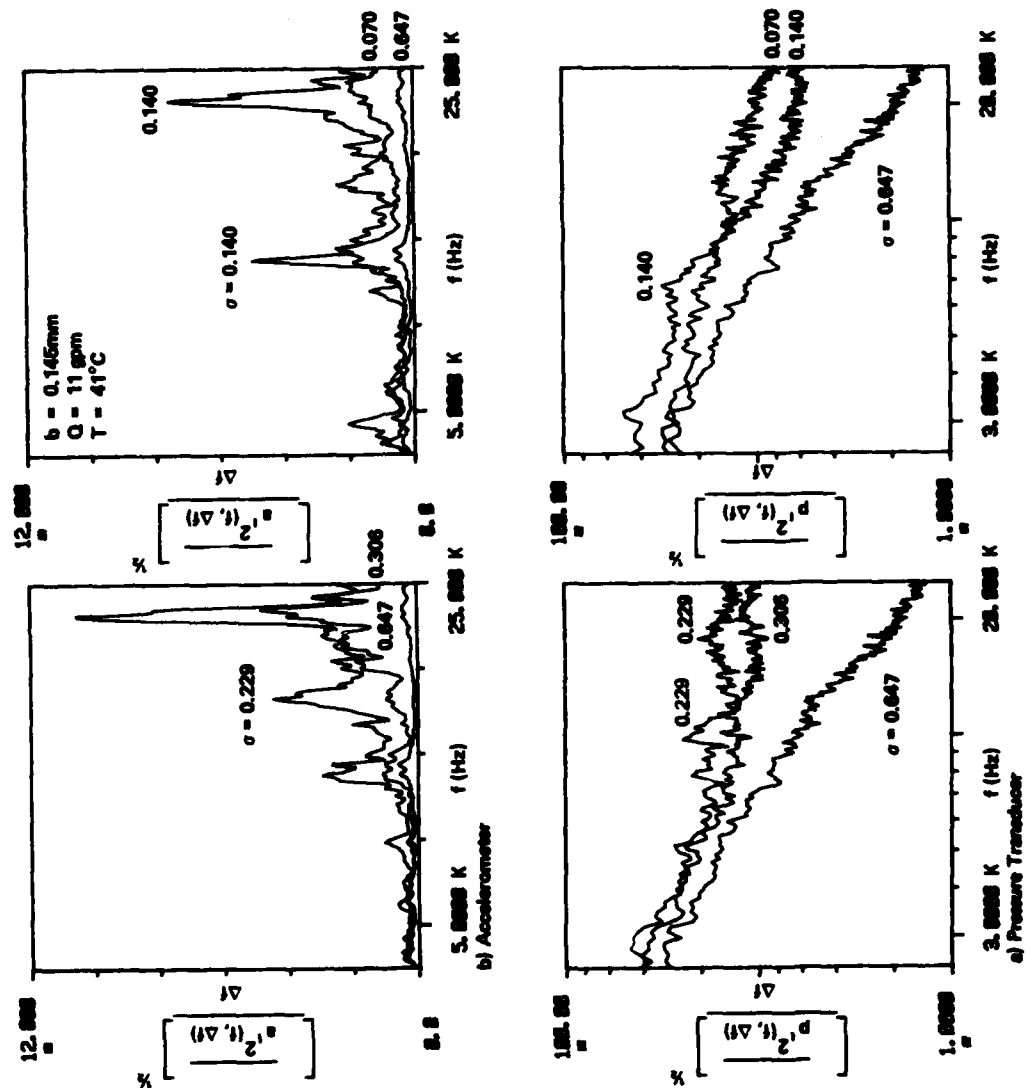


Figure 37. Effect of Cavitation on Energy Spectra for Prototype Valve at a Fixed Opening

few selected values of σ , followed by the ratio of spectral densities in Figure 38, using $\sigma_0 = 0.647$ as the non-cavitating reference spectrum. Additional data from this same test are plotted in Figures 39 and 40. The pressure spectra show an increase in the higher frequency energy as σ is lowered from the non-cavitating value of 0.647, to the energy plateau value of 0.492, to 0.229, and then a decrease as σ approaches the 0.187 value corresponding to peak total energy. Only for the relatively low values of σ is there a very noticeable increase in the energy at the lower frequencies compared to the non-cavitating jet noise, as shown by the ratios of spectral density on Figure 38. Figures 39 and 40 are included to compare the pressure spectra at the energy plateau ($\sigma = 0.492$) with the conditions of peak energy ($\sigma = 0.187$) and minimum cavitation number ($\sigma = 0.070$).

The sharp peaks of the acceleration spectra suggest that the changing cavitation pattern and attendant bubble collapse pattern and acoustic energy radiation excites various modes and corresponding frequencies of the spool valve, or mechanical support system. The peak in the mean-square acceleration in Figure 36 at $\sigma = 0.229$ can be attributed to some mechanical resonance at $f = 23$ kHz, as shown by the spectrum on Figure 37b.

The area under the pressure and acceleration spectral density ratios of all data points plotted in Figure 36 has been normalized with respect to the bandwidth used in the analysis and plotted in Figure 41. The area function illustrates a greater sensitivity of the pressure transducer subsequent to cavitation inception than the accelerometer, but shows similar peaks and relative effect once cavitation is well developed. It is evident that either instrument would prove to be useful in predicting

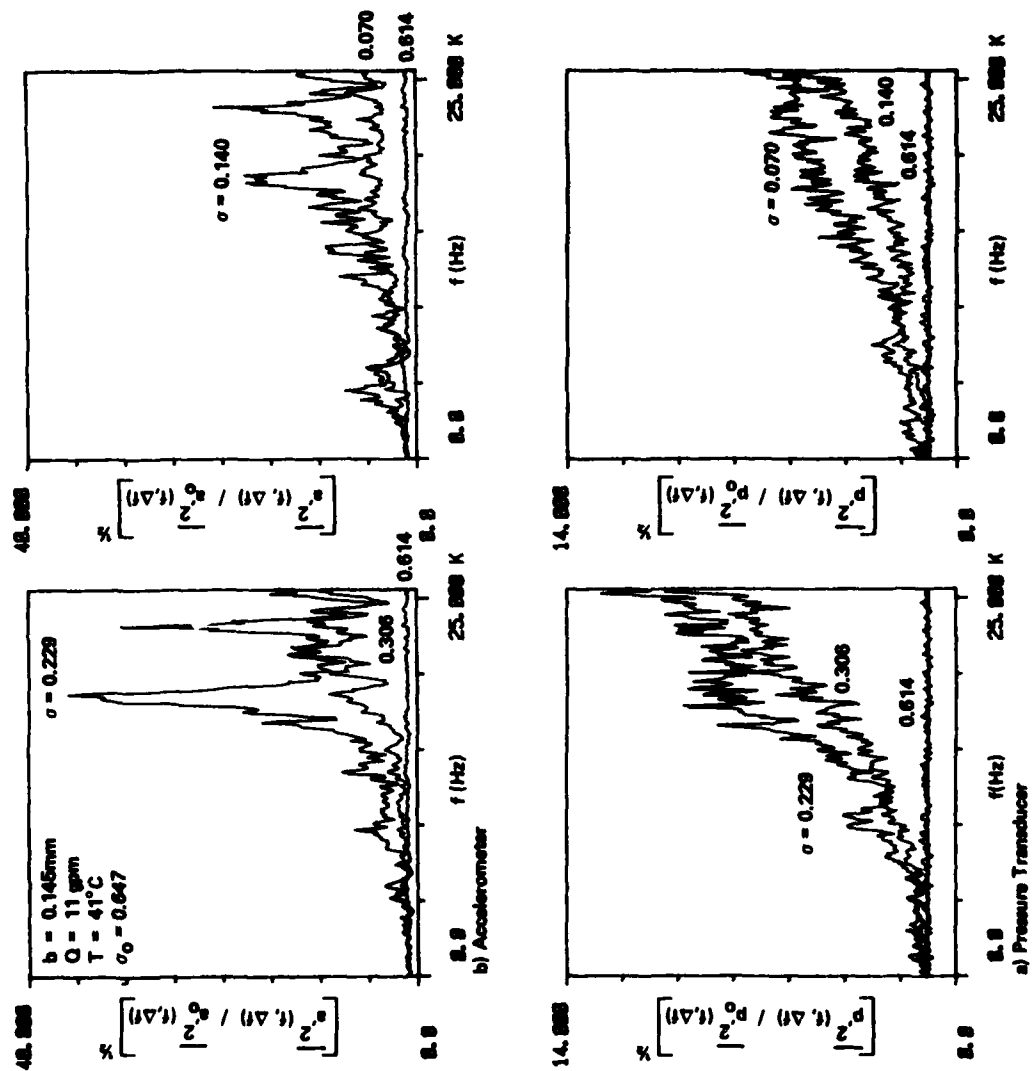


Figure 38. Ratio of Cavitating to Non-Cavitating ($\sigma = 0.647$) Spectral Density for Prototype Valve at a Fixed Opening

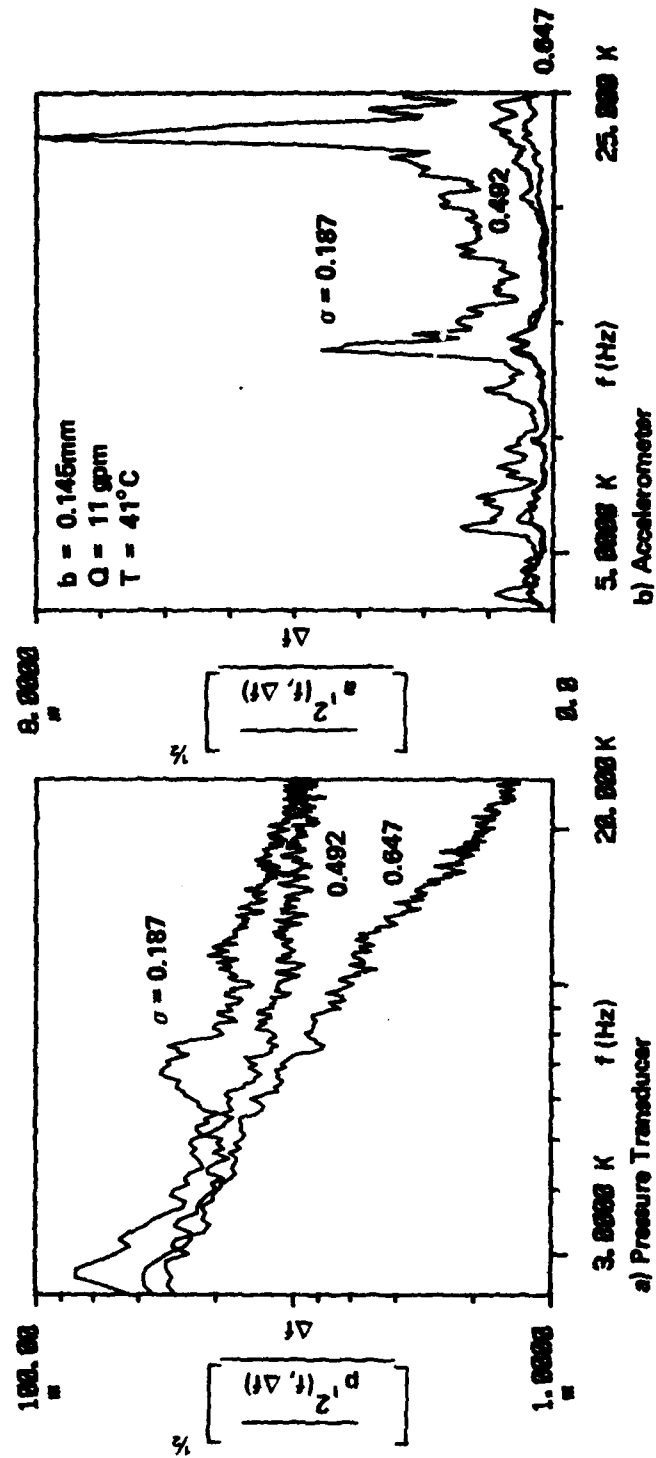


Figure 39. Energy Spectra for Prototype Valve at a Fixed Opening

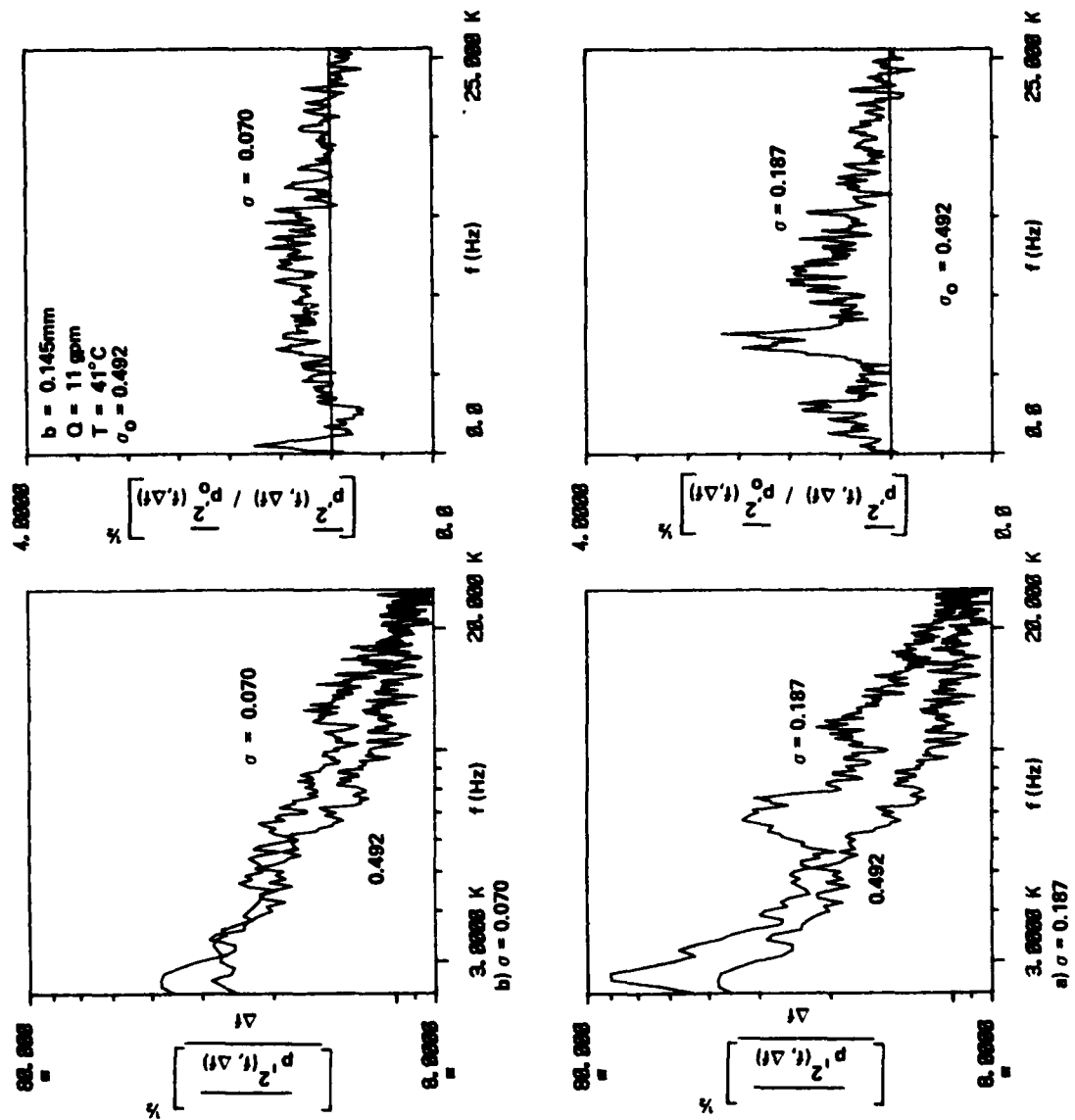


Figure 40. Comparison of Two Cavitating Energy Spectra for Prototype Valve at a Fixed Opening ($\sigma_0 = 0.492$)

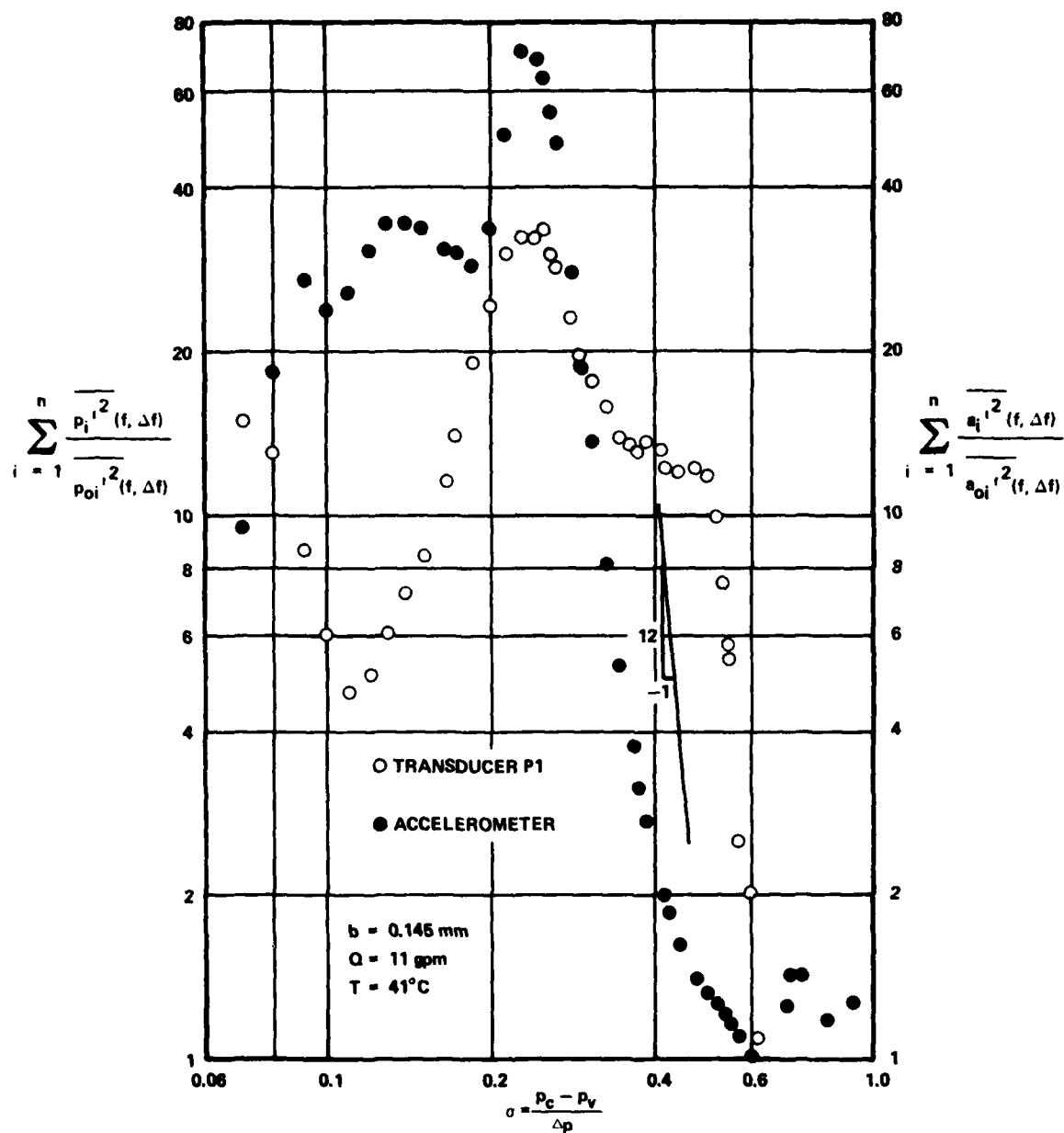


Figure 41. Area under Ratio of Cavitating to Non-Cavitating Mean-Square Spectral Density Curve Versus Cavitation Index for Prototype Valve at a Fixed Opening

the condition of peak noise, and most likely maximum erosion.

Effect of Temperature. -- Although the direct influence of temperature on the Reynolds number and hence on the intensity of pressure fluctuations in a turbulent annular jet was clearly evident in the cavitation inception data of Figure 35, the effect is not as uniform in developed cavitation, as shown by the several sets of data in Figure 42. As expected the mean-square energy under non-cavitating conditions is considerably greater for both instruments at the higher Reynolds numbers. Once cavitation developed toward the condition of maximum fluctuating energy the effect of the lower Reynolds number for $T = 19^{\circ}\text{C}$ became minimal for the pressure spectrum, however. Nevertheless, there appears to be a Reynolds number effect for all values of σ for the accelerometer, and for most of the range for the fluctuating pressure.

The data plotted in Figure 42 for both instruments is presented in order to demonstrate the effect of oil temperature on developed cavitation. Although the effect of temperature on varying the Reynolds number and hence altering the intensity of pressure fluctuations was clearly shown by the cavitation inception data of Figure 35, it is not uniformly evident for the wide range of values of σ associated with the data of Figure 42.

Effect of Valve Opening. -- For a fixed flow rate the effect of varying the opening b is to change the magnitude of the jet velocity V_j , but not the Reynolds number defined by Eq. (9) if the oil temperature remains constant. Mean-square pressure and acceleration energy are plotted versus the cavitation index in Figure 43 for the most common opening used in this investigation ($b = 0.143 \text{ mm}$) and for $b = 0.080 \text{ mm}$. Each set of data points comprises several independent runs. The slight

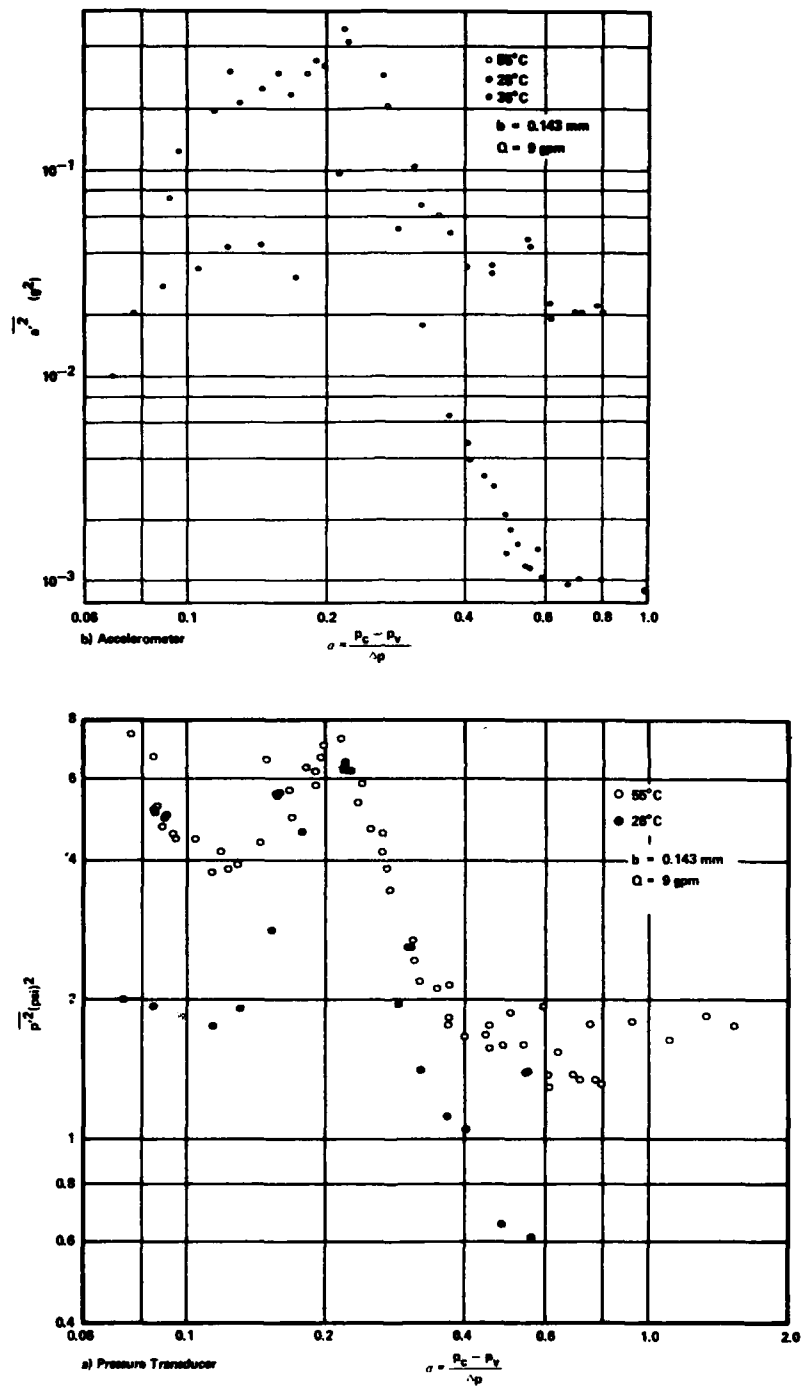


Figure 42. Effect of Temperature on Mean-Square Energy for Prototype Valve at a Fixed Opening

GEORGIA INST OF TECH ATLANTA SCHOOL OF CIVIL ENGINEERING F/6 13/11
CAVITATION DAMAGE MECHANISMS: EXPERIMENTAL STUDY OF CAVITATION --ETC(U)
FEB 80 C S MARTIN, D C WIGGERT, H MEDLARZ F33615-77-C-2036

AFAPL-TR-79-2121

NL

2. 2

$$\frac{1}{2} \left(\frac{1}{2} \right) = \frac{1}{4}$$

END
DATE
FILMED
6 80
DTIC

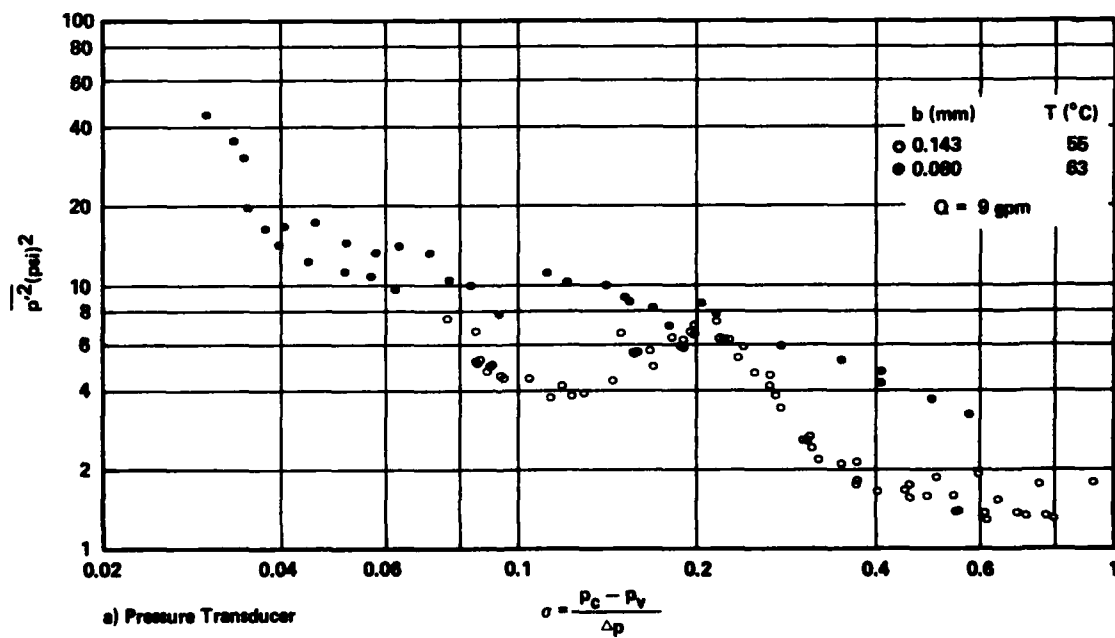
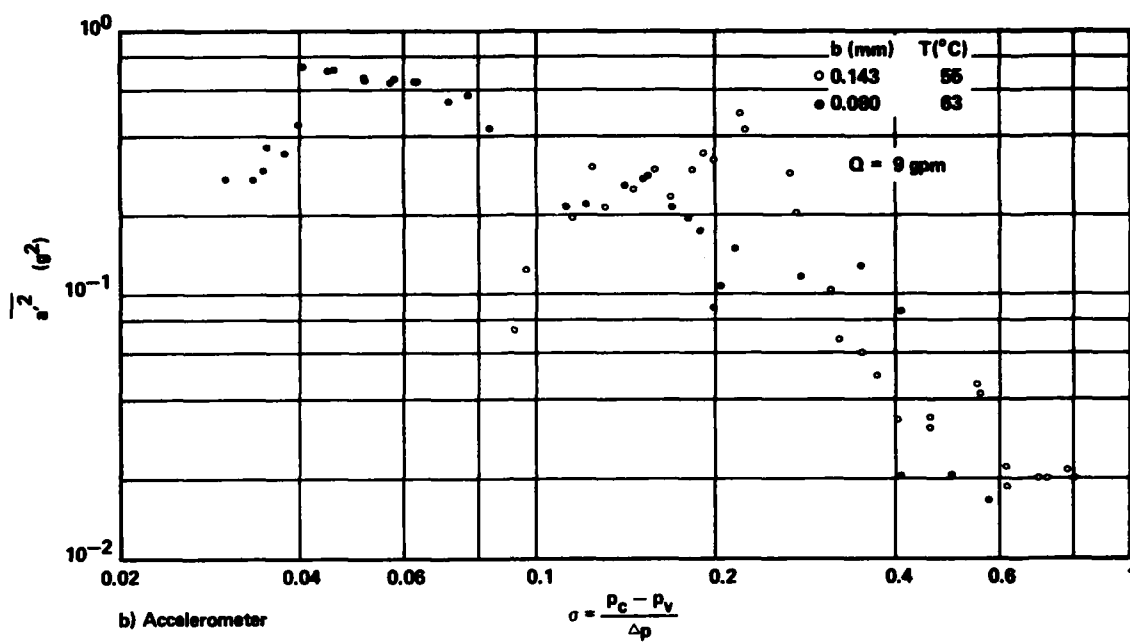


Figure 43. Effect of Valve Opening on Mean Square Energy for Prototype Valve

temperature difference between the two data sets is not believed to be a controlling factor regarding the difference in energy levels. The much greater pressure difference Δp present for the smaller opening allowed for the significantly smaller values of σ . Expected greater values of $\overline{p'^2}$ for the smaller opening materialized except near $\sigma \approx 0.2$, the first peak in energy. There is no clear pattern of the mean-square fluctuating acceleration, however.

Repeatability of Testing. -- Several tests were run under nearly the same conditions in order to ascertain the repeatability of conditions, and the possible effect of such variables as dissolved gas content, oil temperature, and very minor differences in the opening b as computed from Eq. (6). Three complete sets of data taken at a constant flowrate and the same opening, but slightly different temperature, are shown in Figure 44. Although there is some scatter of the mean-square pressure $\overline{p'^2}$ near $\sigma = 0.4$, the test data for both instruments are remarkably close for the independent runs.

Model Valve

The majority of the test data collected for the model valve was for two fixed openings: $b = 0.101$ mm ($Q = 10$ gpm) and $b = 0.207$ mm ($Q = 20$ gpm). One complete set of data obtained by varying σ in very small steps is presented in Figure 45. In contrast to the prototype valve data, for which the background jet noise detected by the pressure transducer was significant, the increase by more than three orders of magnitude of the mean-square energy from non-cavitating to fully cavitating conditions is much more dramatic. Also apparent is the fact that, once cavitation becomes widespread, the total mean-square energy measured by transducers P_1 and P_2

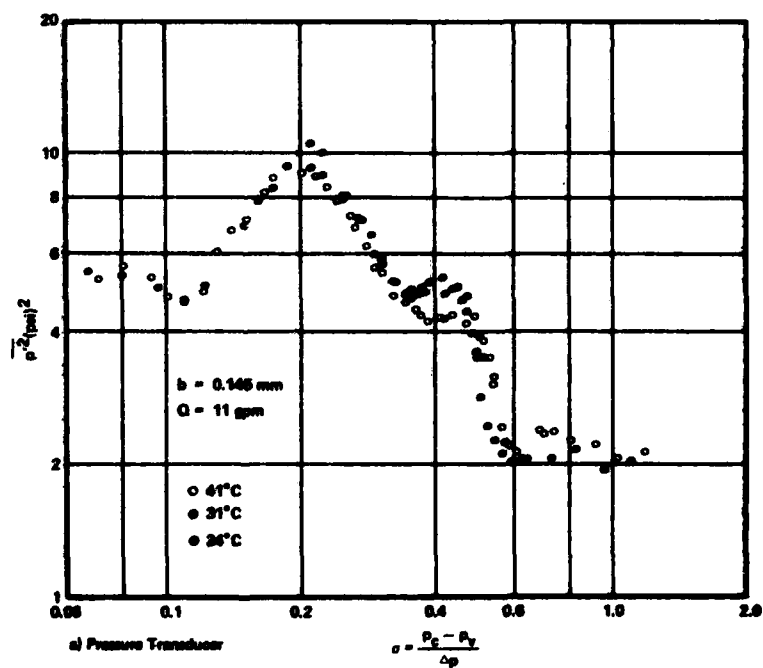
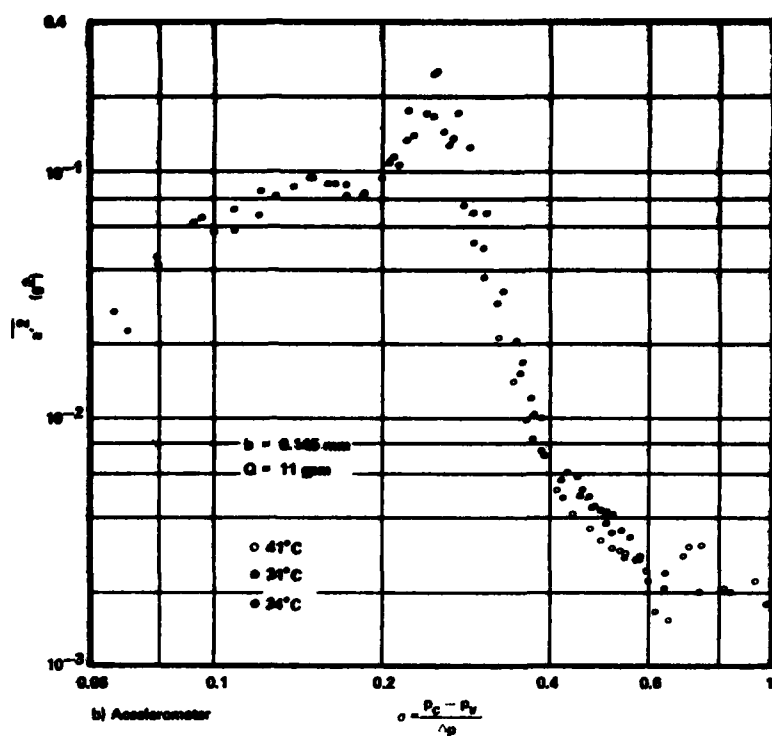


Figure 44. Comparison of Mean Square Energy Results for Tests Run at Different Times under Slightly Different Temperatures

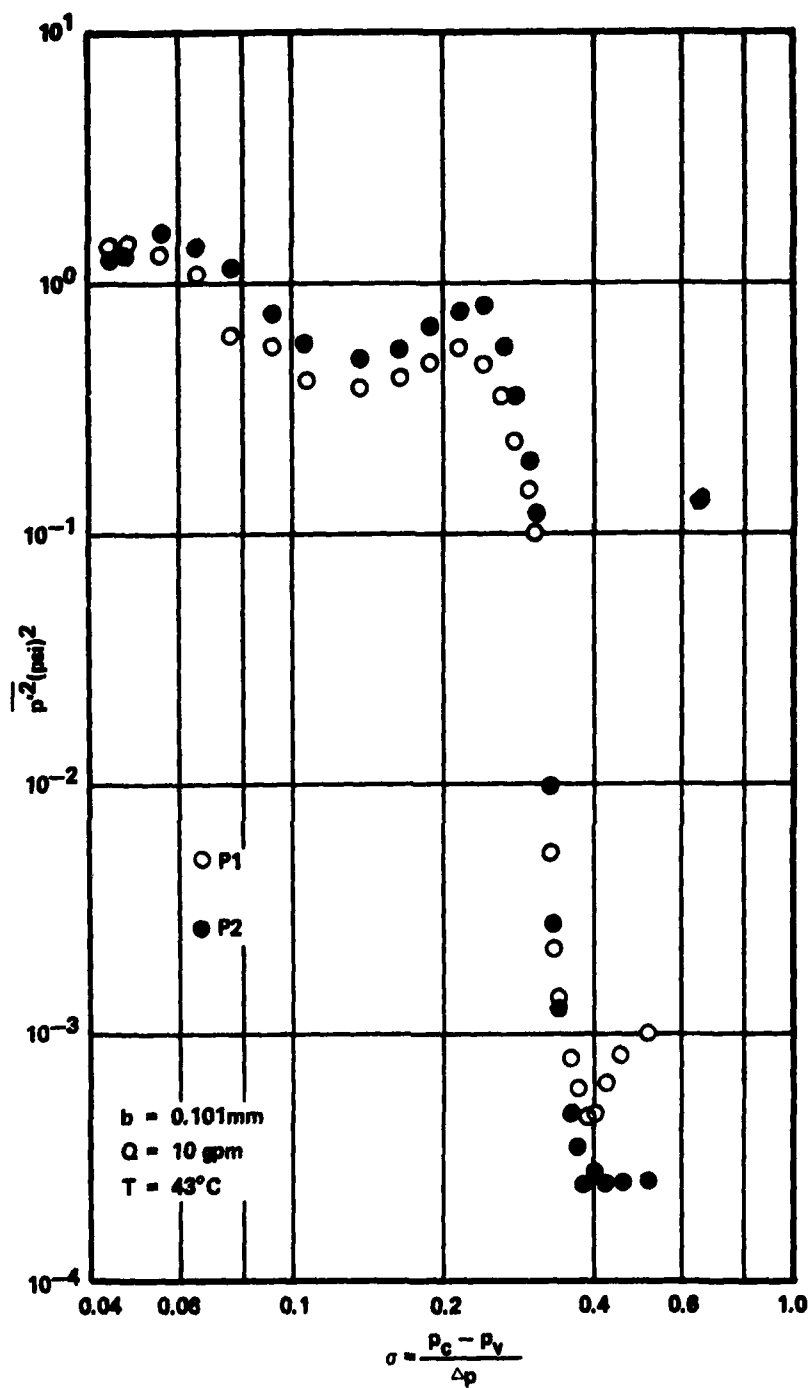


Figure 45. Mean-Square Energy Versus Cavitation Number for Model Valve at an Opening $b=0.101$ mm

are nearly equal. The $\overline{p'^2}$ values at P_2 are most likely greater than those at P_1 because of the close proximity of P_2 to the source of cavitation, even though P_1 experiences a greater effect from the jet than P_2 , as shown by the two energy spectra in Figures 46a and 46b at a non-cavitating condition ($\sigma_0 = 0.421$). Figures 46a and 46b also show that, as σ is successively reduced, the energy spectrum for each transducer gradually rises over the entire band $2.5 \text{ kHz} < f < 25.6 \text{ kHz}$. As σ is lowered below 0.328 the effect of the jet noise at the lower frequencies becomes less and less, resulting finally in nearly white noise over that frequency range at $\sigma = 0.055$. The spectral density ratios are also shown in Figures 46c and 46d for the same spectra, using $\sigma_0 = 0.421$ as the non-cavitating reference spectrum. The corresponding area functions for each transducer are plotted in Figure 47. Although the slope of the area function curves is steeper near σ_1 the area function would not appear to be of any great advantage over $\overline{p'^2}$ in the representation of cavitation in this case.

The variation of $\overline{p'^2}$ with σ is shown in Figure 48 for $b = 0.207 \text{ mm}$ and $Q = 20 \text{ gpm}$. The much greater values of $\overline{p'^2}$ under non-cavitating conditions detected by P_2 than by P_1 are the obvious effect of the jet being directed toward the former transducer, as discussed earlier in Chapter VII. The effect of the jet is apparent for all spectra shown for P_2 in Figure 49b. The corresponding spectra obtained using transducer P_1 , Figure 49a, illustrate the nearly broad band energy distribution as σ is gradually lowered. Figures 49c and 49d are plots of the ratio of spectral density using the non-cavitating reference spectrum for which $\sigma_0 = 0.666$. The direct effect of jet noise is quite obvious at the lower frequencies of Figure 49d. The area function for each of the data points

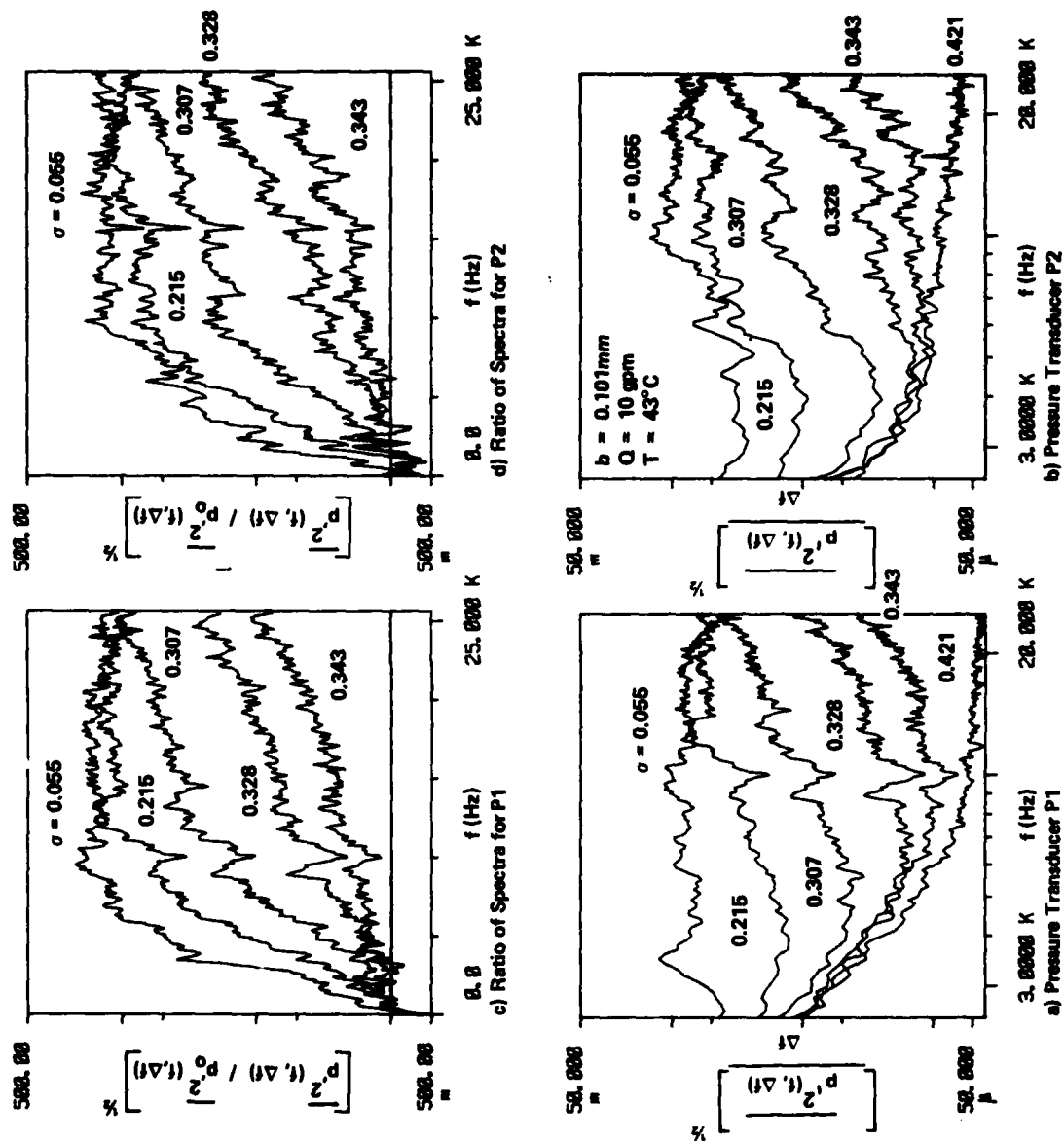


Figure 46. Energy Spectra and Ratio of Cavitating to Non-Cavitating ($\sigma_o = 0.421$) Spectral Density for Model Valve at an Opening $b=0.101$ m

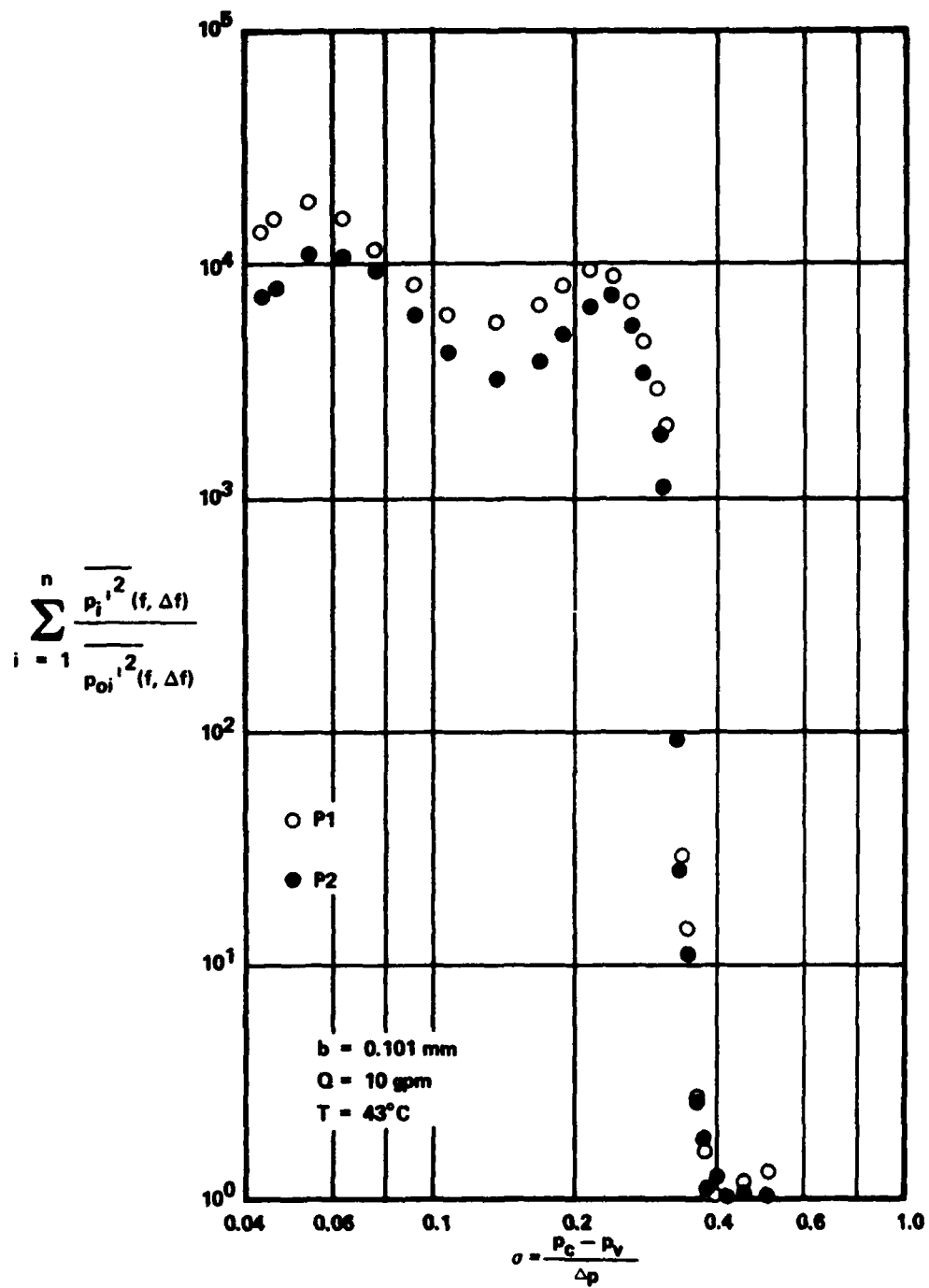


Figure 47. Area under Ratio of Cavitating to Non-Cavitating Mean-Square Spectral Density Curve Versus Cavitation Index for Model Valve at an Opening $b=0.101$ mm

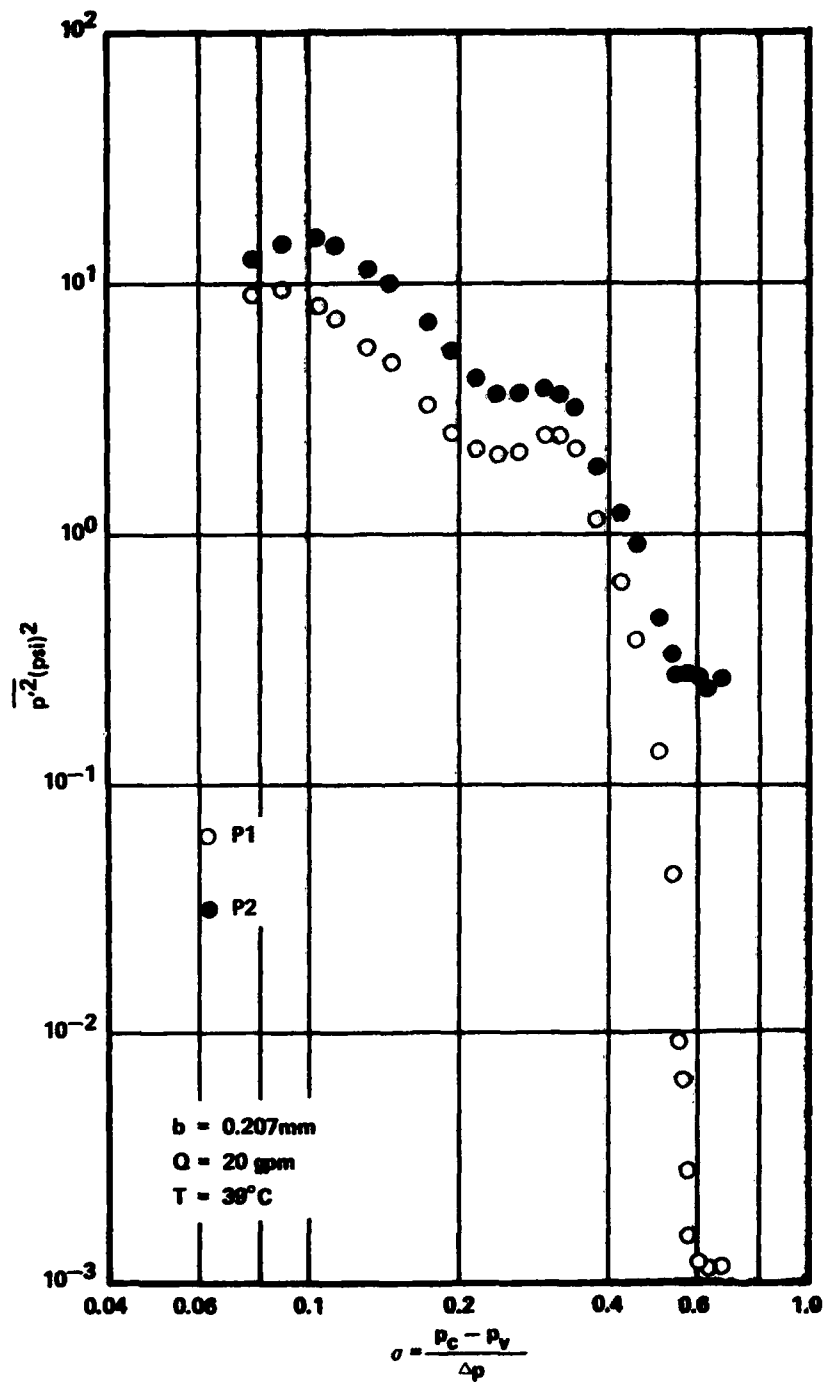


Figure 48. Mean-Square Energy Versus Cavitation Number for Model Valve at an Opening $b=0.207$ mm

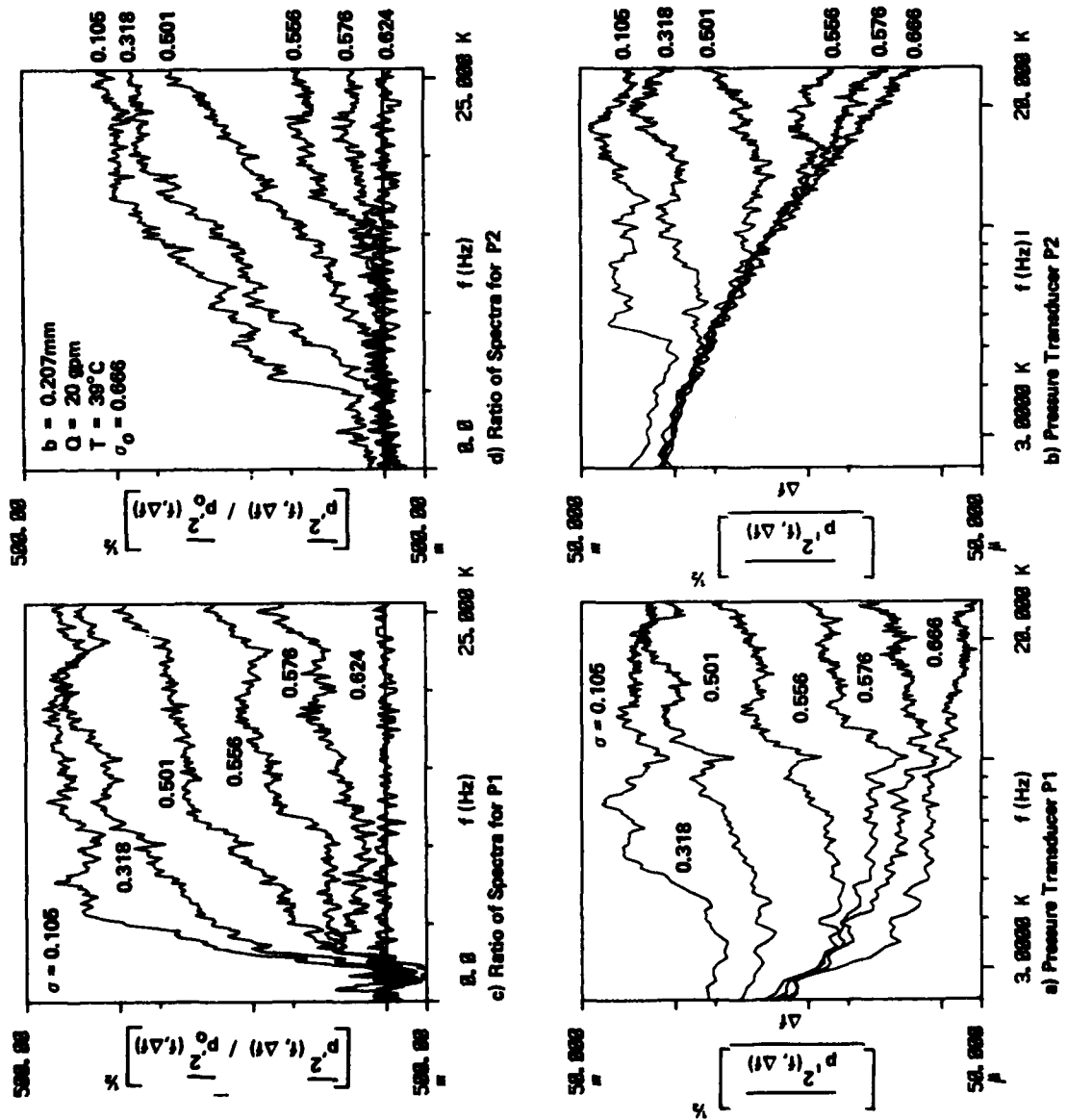


Figure 49. Energy Spectra and Ratio of Cavitating to Non-Cavitating ($\sigma = 0.666$) Spectral Density for Model Valve at an Opening $b=0.207$ mm

is depicted in Figure 50 for each transducer. Again, as for the smaller opening, although the slope of the area function (Figure 50) is greater than that of the mean-square energy curve (Figure 48), there is no significant difference between Figures 50 and 48.

Correlation of Results

An attempt has been made to non-dimensionalize the data in order to obtain a more general correlation of the results. In addition to cavitating test data taken under the conditions of constant flow and fixed opening additional data were collected with (a) fixed opening and variable flow and (b) variable opening and variable flow in order to determine the variation of mean-square energy with flow rate under cavitating conditions.

Figure 51 represents data taken at a fixed opening under conditions of maximum cavitation possible in the prototype valve. As the flow rate increased, the chamber pressure increased, resulting in the cavitation index varying from 0.087 to 0.153. Nevertheless, cavitation was extensive, and probably similar over the entire range of values of σ represented on Figure 51. Interestingly, the sixth-power variation of $\overline{p'^2}$ with Q observed under non-cavitating conditions (Figure 15) is also present under conditions of extensive cavitation (Figure 51), suggesting a dipole source, or Eq. (15). Figure 52 shows the energy spectra for the pressure transducer and the accelerometer, as well as the coherence between the two signals for five of the flow conditions represented on Figure 51. Although the acceleration spectra are difficult to distinguish from one another in Figure 52b, the mean-square acceleration energy is sensitive to flowrate increases (Figure 51). For the entire range of

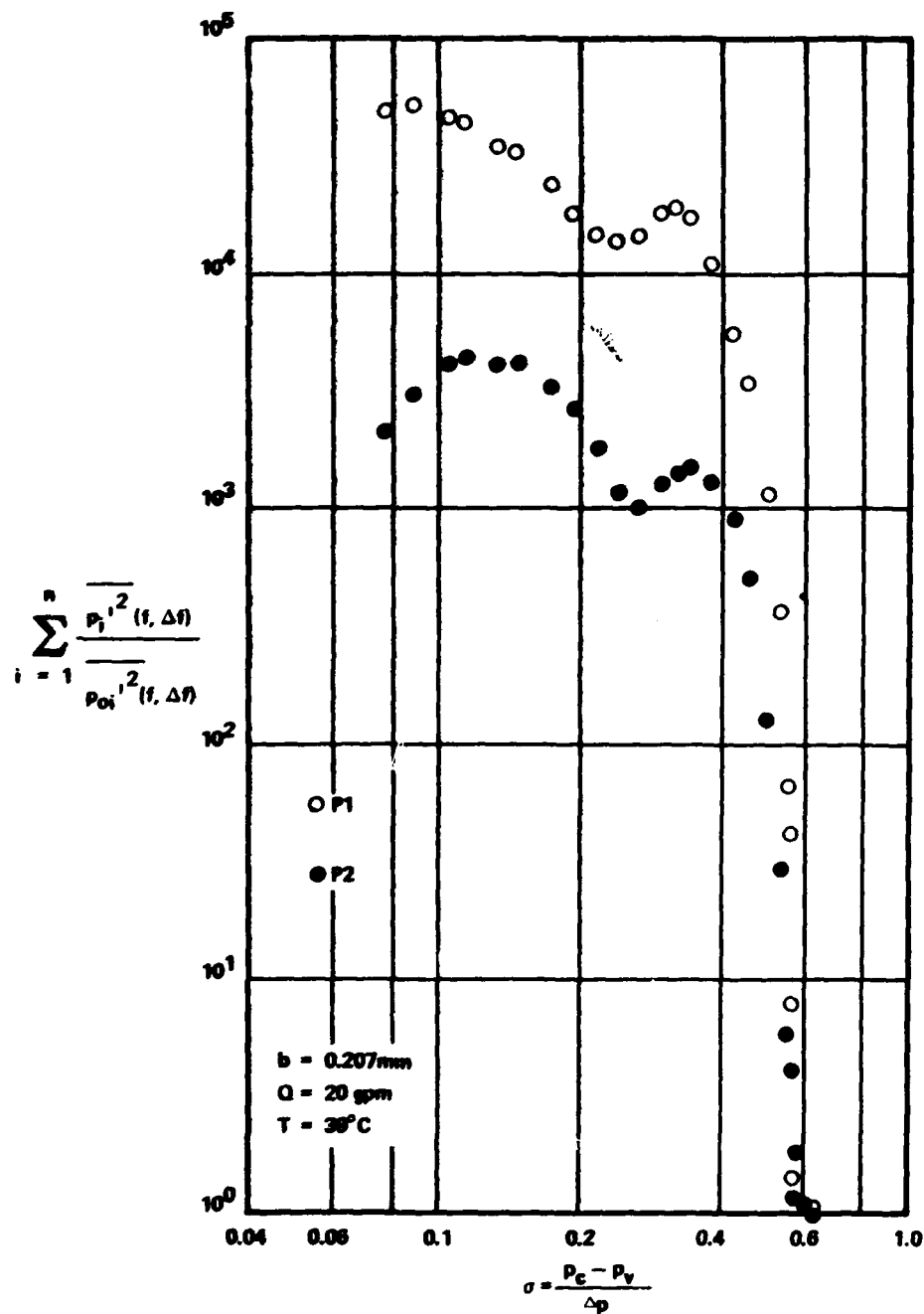


Figure 50. Area under Ratio of Cavitating to Non-Cavitating Mean-Square Spectral Density Curve Versus Cavitation Index for Model Valve at an Opening $b=0.207$ mm

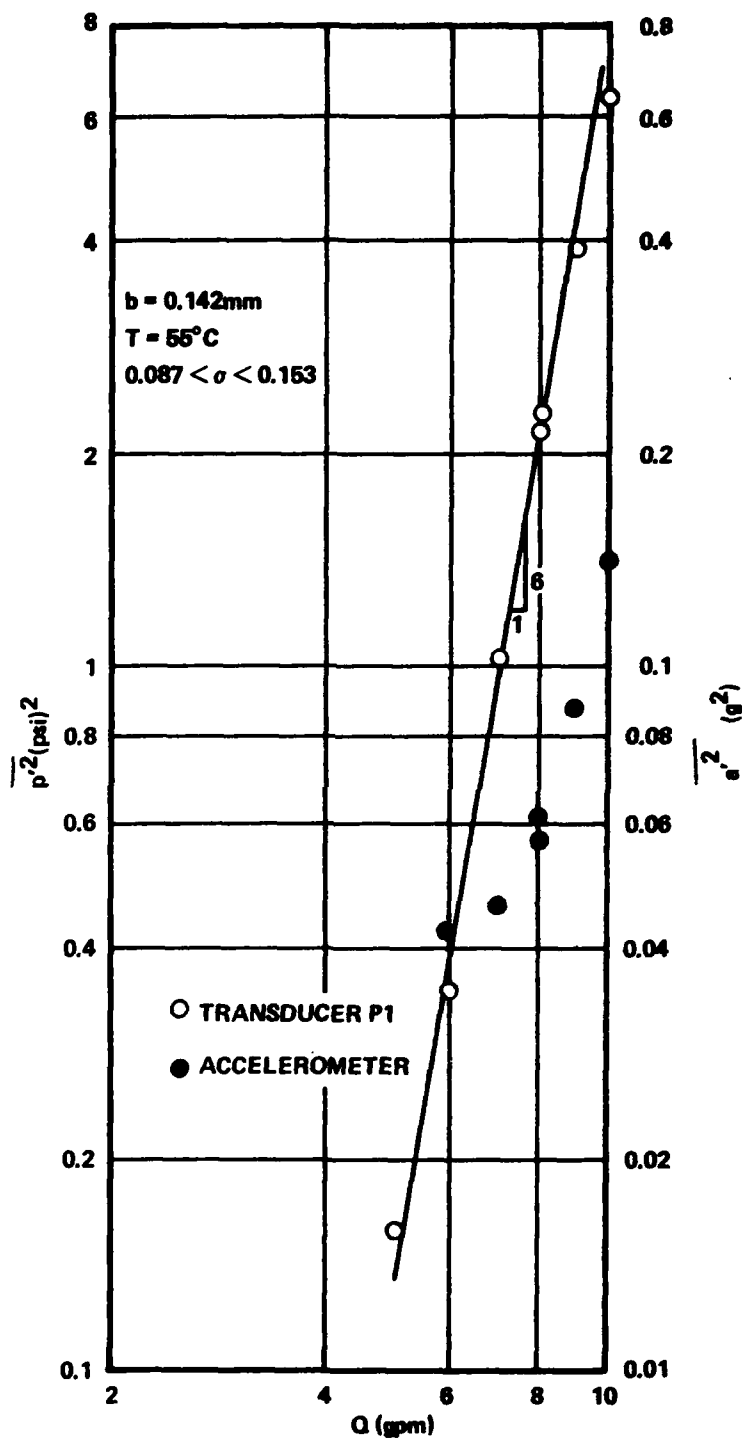


Figure 51. Cavitating Mean-Square Energy Versus Discharge for Prototype Valve at a Fixed Opening

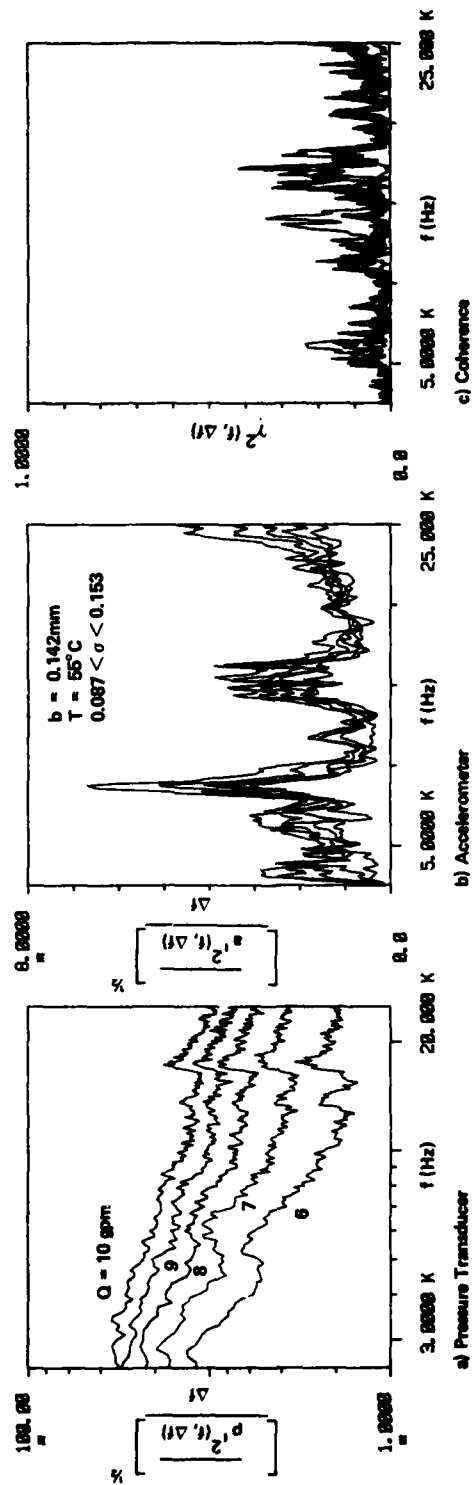


Figure 52. Cavitating Energy Spectra and Coherence Between Fluctuating Pressure and Acceleration for Prototype Valve at a Fixed Opening

flowrates shown on Figure 52c there is very little coherence between the pressure transducer and the accelerometer signals.

Energy spectra were also recorded when the cavitating data plotted in Figure 11 were taken under the test condition of constant pressure difference but variable opening, and hence variable flow rate. The mean-square energy values for the data of Figure 11 are plotted versus flowrate in Figure 53. The constant value of Δp yields a constant value of the velocity in the vena contracta from Eq. (3). The attenuation of the centerline velocity assumed for a non-cavitating jet, Eq. (10), would not necessarily be expected to be valid for severe cavitation. The monopole and dipole source relationships proposed by Eqs. (12) and (13), respectively, for non-cavitating jets would suggest constant mean-square energy if V_j is a constant. The linear variation between $\overline{p'^2}$ and Q on Figure 53 for a constant Δp may be due to an effectively large V_j as b increases, or due somewhat to the effect of varying σ . Further testing is needed at a constant value of σ .

For purposes of comparison and correlation data taken with the model valve at both flow rates, and at different temperatures, are plotted in Figures 54a and b for transducers P_1 and P_2 , respectively. At each flow rate the effect of temperature is especially apparent near the point of cavitation inception, σ_1 . Various non-dimensional ratios were chosen in an attempt to collapse the data of Figure 54. The most successful choice of non-dimensional ratios to date resulted in the correlation of

$$\frac{\overline{p'^2}}{\Delta p^2} \left(\frac{c}{b} \right)^3 = F \left(\frac{\sigma}{\sigma_1} \right) \quad (17)$$

as shown by the data plotted in Figure 55. Normalizing σ by σ_1 took into account the effect of Reynolds number on incipient cavitation. Although

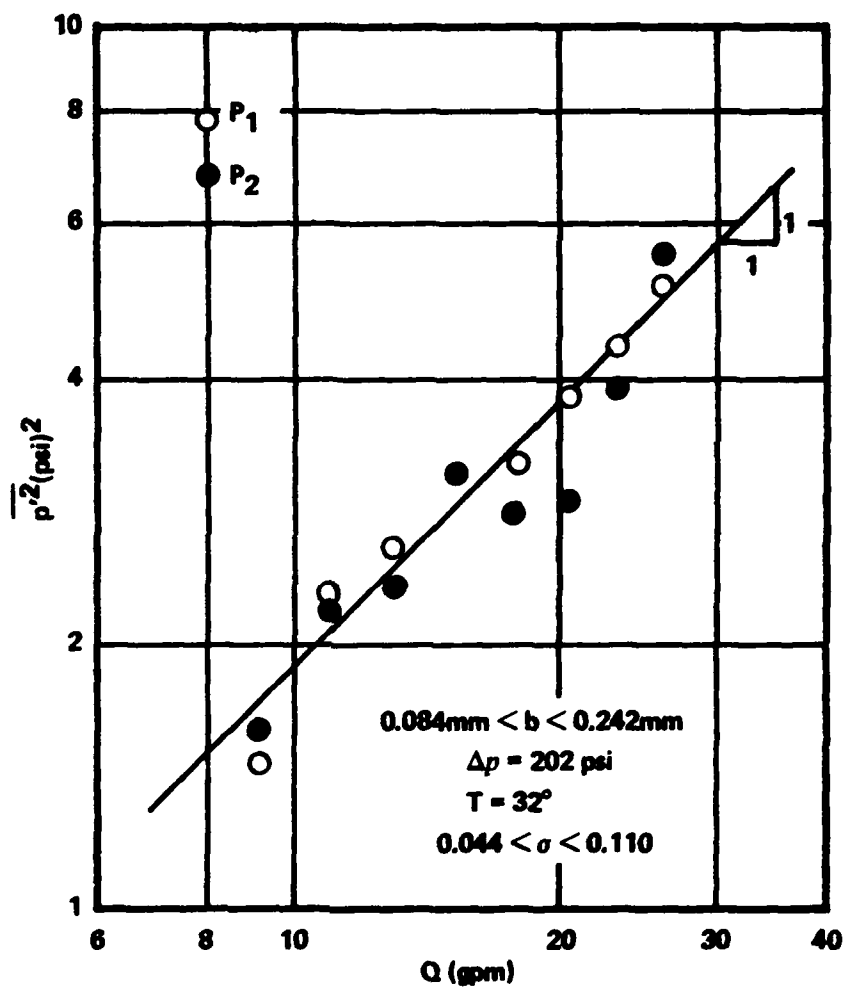


Figure 53. Cavitating Mean-Square Energy Versus Discharge for Model Valve at a Variable Opening

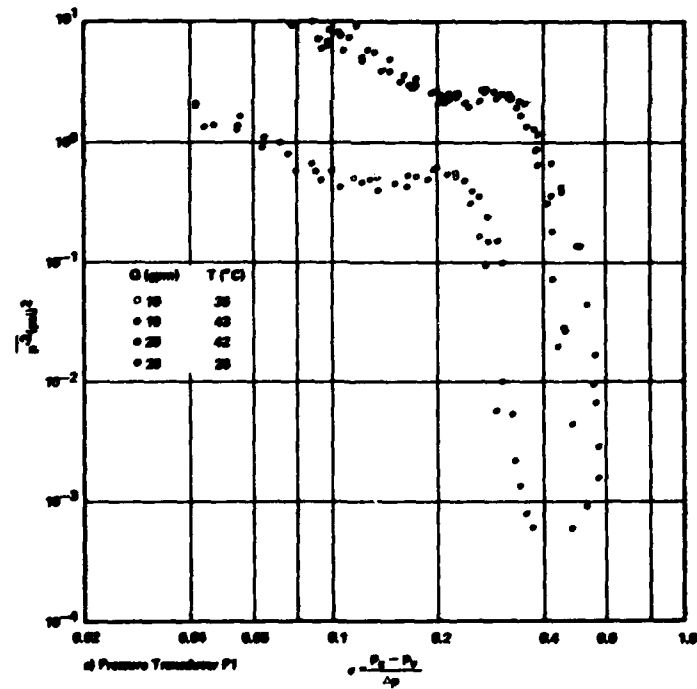
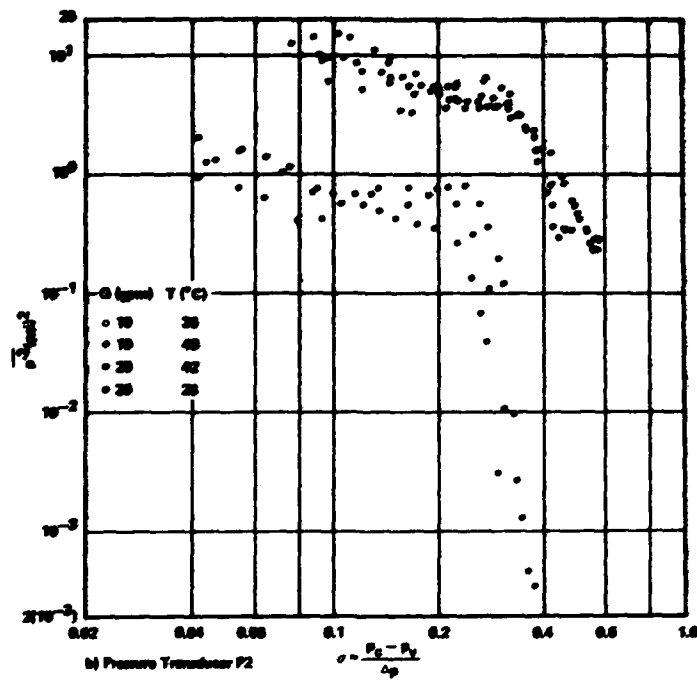


Figure 54. Summary of Test Data Comparing Mean-Square Energy Versus Cavitation Index for Model Valve

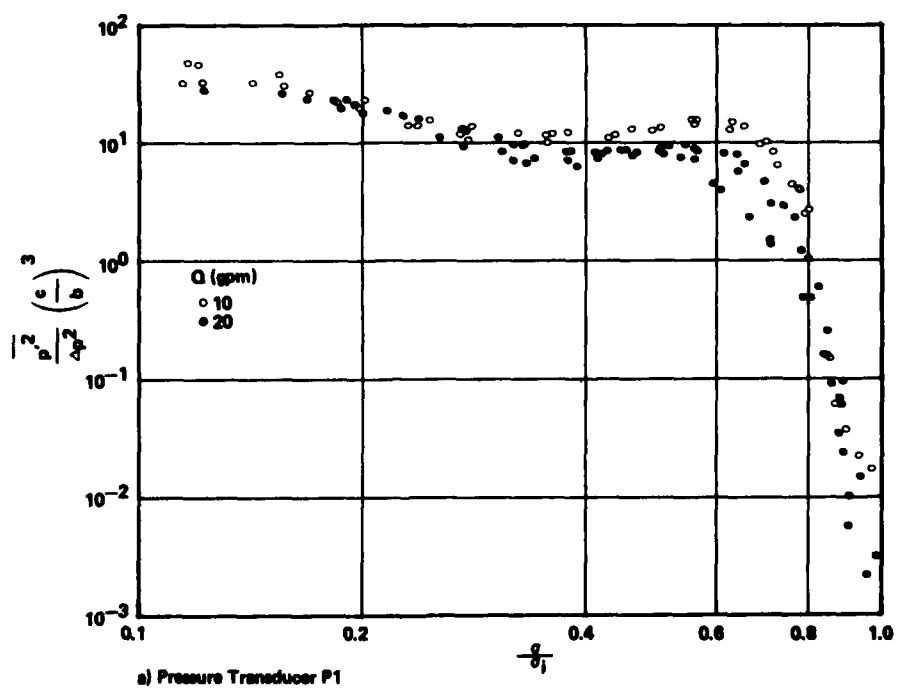
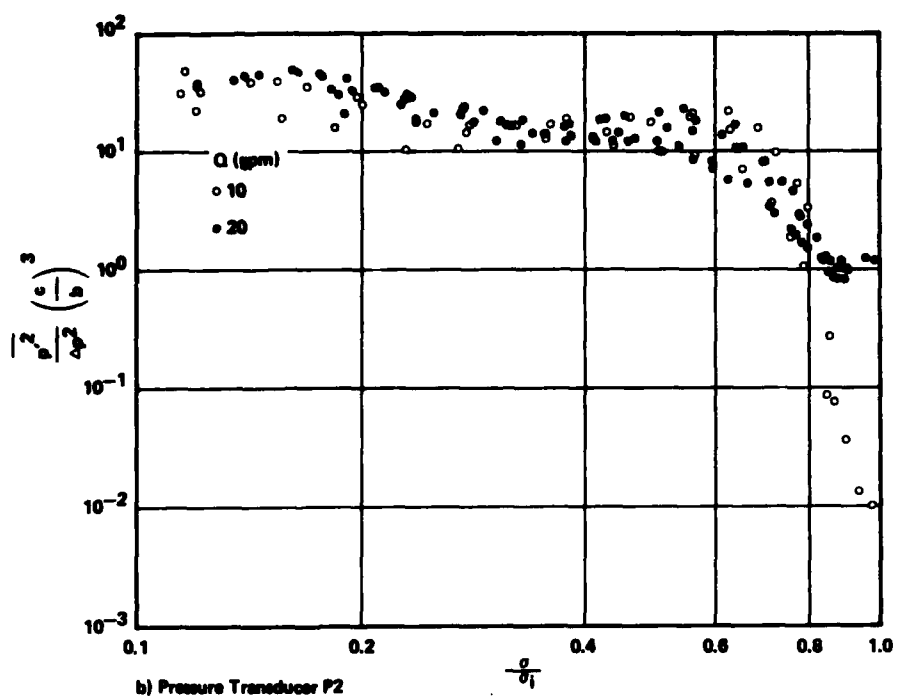


Figure 55. Dimensionless Representation of Test Data for Model Valve

the ratio on the left-hand-side of Eq. (17) does not completely correlate the data for the two flowrates, nor correspond exactly to either a monopole or dipole source in accordance with Eqs. (12) and (13), the data are considerably collapsed by the somewhat empirical relationship.

Effect of Dissolved Gas

The amount of dissolved gas in the test circuit shown on Figure 1 could be lowered to approximately one-half of the saturated value at atmospheric conditions by means of the vacuum tank and spray nozzle scheme described earlier. Portions of the test oil would be pumped from the rubber bag reservoir into the vacuum tank, degassed over a period of several hours, and then transferred back into the reservoir. Then much of the oil in the rest of the test circuit was transferred into the vacuum tank, degassed, and then pumped back, finally resulting in a dissolved gas content of about 4.5% by volume, as measured by the Aire-Ometer.

Without degassing the dissolved gas content attained the saturation value at the prevailing temperature and atmospheric pressure, or about 10% by volume. Figure A3 shows the effect of pressure on the solubility of MIL-H-5606 oil. The amount of dissolved gas in the oil in the test circuit prior to and subsequent to a test was frequently measured by use of the Aerometer.

Tests were conducted with each valve to determine the effect, if any, of dissolved gas content on the energy levels measured by the dynamic instruments. Figure 56 shows the mean-square energy levels obtained by the pressure transducer and the accelerometer for two tests run at virtually the same temperature, but at two different dissolved gas

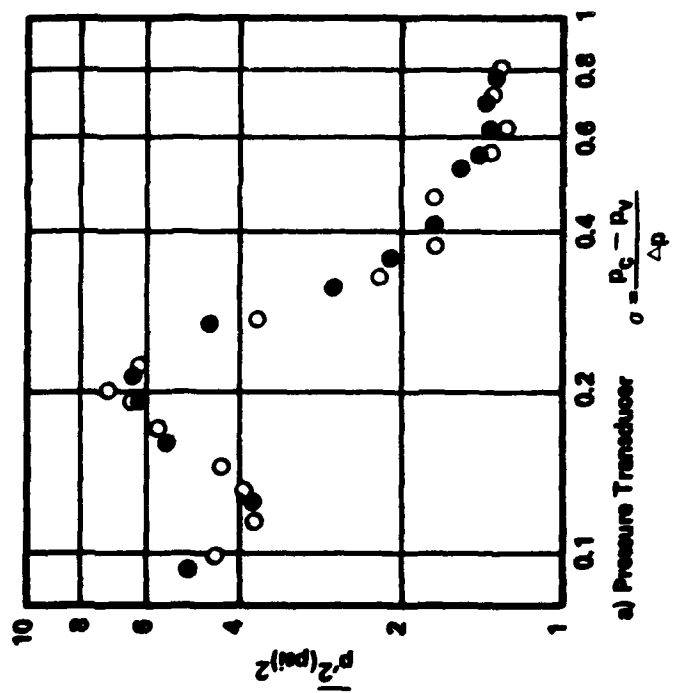
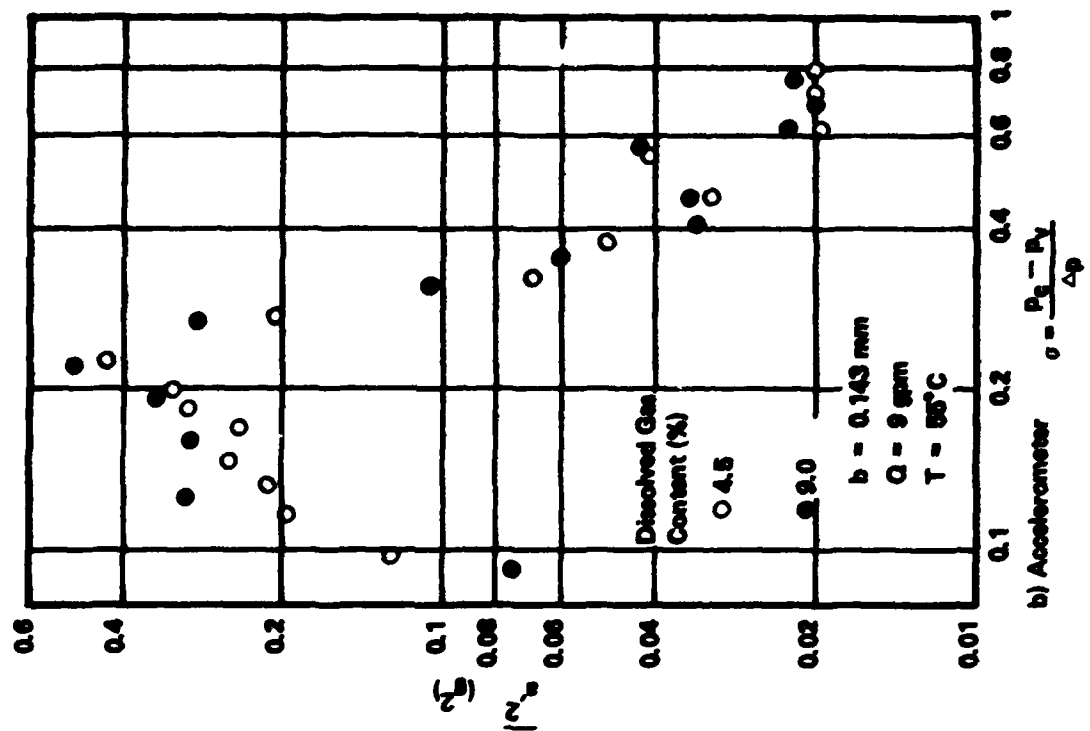


Figure 56. Effect of Dissolved Gas Content on Mean-Square Energy Levels in Prototype Valve

contents, 4.5 and 9.0 percent. The results of two similar tests with the model valve are presented in Figure 57. For the two limiting values of dissolved gas content obtainable in the test circuit there appears to be no discernible effect of the amount of dissolved gas on the fluctuating energy levels measured in each valve.

It is believed that the primary mode of cavitation present in the two test valves was vaporous, not gaseous, because of the relatively short residence time of bubbles in the respective valve chambers. In fact, vapor bubbles that could clearly be seen in the model under conditions of fairly extensive cavitation appeared to disappear as the flow exited the valve return passage.

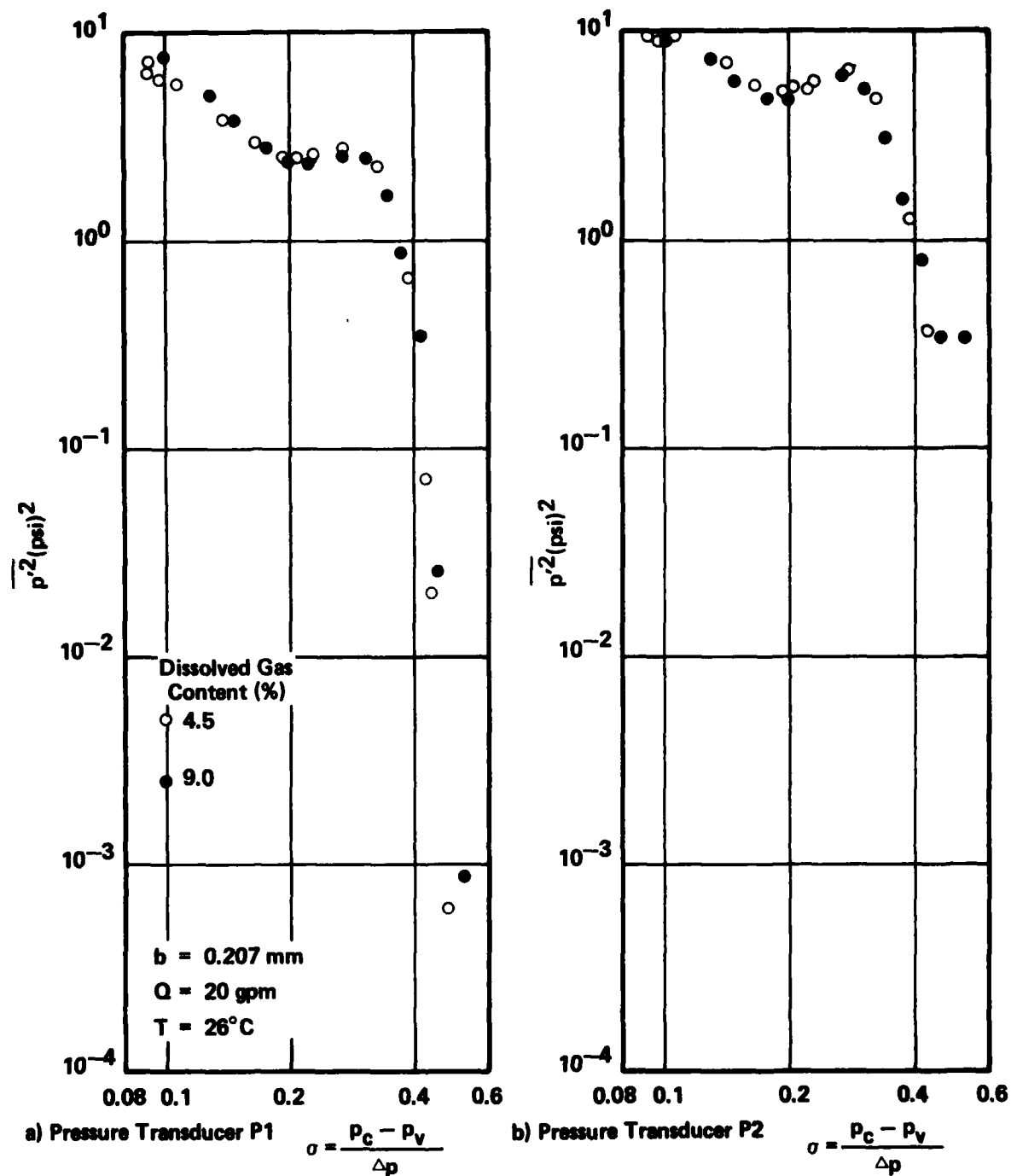


Figure 57. Effect of Dissolved Gas Content on Mean-Square Energy Levels in Model Valve

SECTION X

CAVITATION WITH PULSATING FLOW

Part of the original test plan was the assessment of the effect of steady-state oscillation on cavitation damage mechanisms. The spool of the prototype valve, which was directly attached to the actuator shown in Figure 1, was oscillated simple harmonically by means of a MTS servocontroller and a Moog Model 73-103 servovalve. Initially feedback was supplied by a differential pressure transducer in the hydraulic servosystem and a LVDT mounted on the actuator. For more reliable operation eventually only the LVDT was used as a feedback signal to the servocontroller.

The amplitude of the spool displacement x' about the mean opening of the valve b could be controlled by adjusting the span on the servocontroller. Tests were conducted for three forcing frequencies: $f_f = 10, 20, \text{ and } 30 \text{ Hz}$. For the entire series of tests conducted with the oscillating spool the ratio of x'/b varied from 0.09 to 0.36.

The signals from the various sources -- $p_L, \Delta p, p_c, p_R, Q$, and x -- were fed into the two-channel Digital Signal Analyzer in order to determine the respective amplitudes of oscillation at the selected forcing frequency f_f . A bandwidth of 200 Hz was selected for this analysis. Using the x signal from the LVDT as a reference signal the phase angle between it and the second signal, for example Q or Δp , could be obtained from the cross spectrum. Unfortunately, the two-channel limitation of the analyzer did not allow for the simultaneous collection of data from all of the instruments. It was noticed that the stroke of

the spool remained virtually constant during a series of tests, but on occasion there was a slight change in the mean opening \bar{b} . The average quantities such as \bar{b} and \bar{Q} were obtained by use of the scanner, multi-meter and desktop computer described in Section IV. It was also possible to obtain the mean values of the particular dynamic signal being analyzed by the signal analyzer from the DC value produced by the auto spectrum.

For a given series of tests the valve would be locked in a given position so that the cavitation characteristics at zero frequency could be determined for reference purposes. The dynamic signals from the PCB pressure transducer and the accelerometer were analyzed over a bandwidth of 25.6 kHz using the random signal option. The value was then oscillated at a desired forcing frequency f_f and a constant stroke x' . Using the LVDT signal x as a reference signal the auto spectra and cross spectrum between the remaining signals such as Q , Δp , etc., were sequentially obtained. In order to obtain peak amplitude accuracy the sinusoidal signal input option was chosen for the 200 Hz bandwidth. For the purpose of investigating the effect of valve oscillation on cavitation the signals from the PCB pressure transducer and the accelerometer were again analyzed over a 25.6 kHz bandwidth using a random signal option for data processing.

A summary of the essential pulsating flow tests is listed in Table 4. The fluctuating cavitation index σ' is defined by

$$\sigma' = \frac{p_c'}{\Delta p} \quad (18)$$

in which p_c' is the amplitude of the fluctuating pressure in the chamber of valve at the driving frequency f_f . Both the Kulite semiconductor and

TABLE 4
SUMMARY OF PULSATING FLOW TESTS

<u>Date</u>	<u>Test</u>	<u>f_f</u> <u>(Hz)</u>	<u>Q</u> <u>(gpm)</u>	<u>Δp</u> <u>(psi)</u>	<u>p_R</u> <u>(psi)</u>	<u>σ</u>	<u>σ'</u>	<u>p'²</u>	<u>a'²</u>	HP5420A <u>Tape (Records)</u>
7/31/78	7	10	9.82	1120	6.0	0.061	0.041	9.63	-	1
	8	10	8.37	1142	1.6	0.056	0.040	9.63	-	1
	10	10	7.18	1141	2.4	0.056	0.009	5.74	-	22
	11	20	7.73	1135	3.0	0.057	0.015	6.18	-	43
	12	20	7.60	1137	5.2	0.059	0.015	6.18	-	43
	13	30	7.53	1139	5.4	0.059	0.013	5.54	-	65
8/01/78	2	10	8.83	1237	6.1	0.055	0.012	10.8	-	1
	3	0	8.69	1240	5.0	0.054	0	9.4	-	9
	5	20	8.97	1235	5.4	0.055	0.010	9.5	-	10
	6	0	8.41	1239	5.3	0.054	0	9.5	-	18
	7	30	8.66	1240	5.7	0.055	0.006	9.7	-	19
8/13/78	1	0	8.94	1199	186	0.207	0	7.6	0.244	28-29
	4	10	9.08	1187	166	0.192	0.073	5.6	0.053	38-39
	5	10	8.79	1206	145	0.172	0.071	5.6	0.053	38-39
	6	20	9.16	1170	214	0.236	0.040	4.4	0.181	46-47
	7	20	8.78	1192	195	0.216	0.039	4.4	0.181	46-47
	8	30	9.36	1162	231	0.252	0.046	4.4	0.189	54-55
	9	30	9.14	1175	220	0.240	0.046	4.4	0.189	54-55
8/14/78	3	0	8.99	1192	164	0.190	0	7.2	0.305	62-63
	5	10	8.95	1188	153	0.181	0.082	4.7	0.085	66-67
	9	20	8.93	1184	168	0.194	0.028	5.8	-	77-78
	13	30	9.04	1178	173	0.202	0.039	5.2	0.125	88-89
	17	0	8.91	1184	168	0.194	0	6.6	0.287	99-100

the PCB piezoelectric pressure transducers were used to obtain p_c' . The mean-square energies $\overline{p'^2}$ and $\overline{a'^2}$ are the result of 50 ensemble averages over the frequency range $2.5\text{kHz} < f < 25.6\text{kHz}$. Due to the limited amount of data taken and some uncertainty associated with maintaining steady-state conditions for the various runs at a given condition no attempt was made to determine the unsteady characteristics of the valve. There are some indications of the effect of valve oscillation on cavitation noise, however.

Figure 58 presents some of the results of the tests taken under the condition of the lowest value of the mean cavitation index $\bar{\sigma}$. The data of 8/01/78, for which the fluctuating cavitation index σ' was nominally 0.01 compared to $\bar{\sigma} = 0.055$, indicates virtually no difference in the energy spectra for $f_f = 10$ and 20 Hz compared to no oscillation, $f_o = 0$ Hz. The spectrum at $f_f = 30$ Hz was virtually identical. The ratio of spectral densities shown in Figure 58b using the non-oscillating condition ($f_o=0$) as the reference spectrum also suggests that low frequency modulation has no effect on cavitation for low values of $\bar{\sigma}$.

As the cavitation index is increased to a value close to that corresponding to peak energy levels there is an apparent effect of oscillation on the energy spectra, as shown by Figure 59. Since the value of $\bar{\sigma} = 0.190$ is close to the maximum value of $\overline{p'^2}$ versus σ (see Figures 36, 42 and 43) both positive and negative changes in σ should result in a decrease in energy levels. Both energy spectra for oscillatory flow shown on Figure 59 clearly indicate lower cavitation noise at the high frequency end of the spectrum, especially for $f_f = 10$ Hz, for which σ' is greater than for $f_f = 20$ Hz.

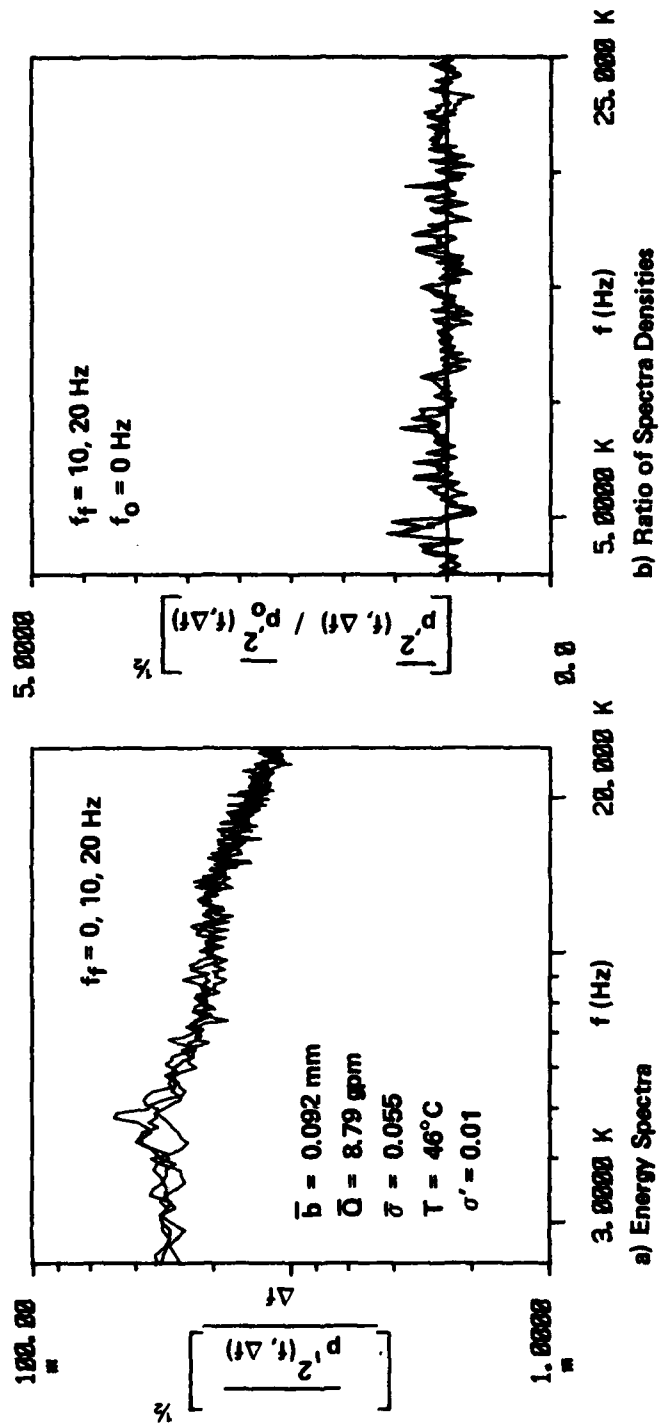


Figure 58. Effect of Spool Oscillation on Energy Spectra ($\bar{\sigma}=0.055$)

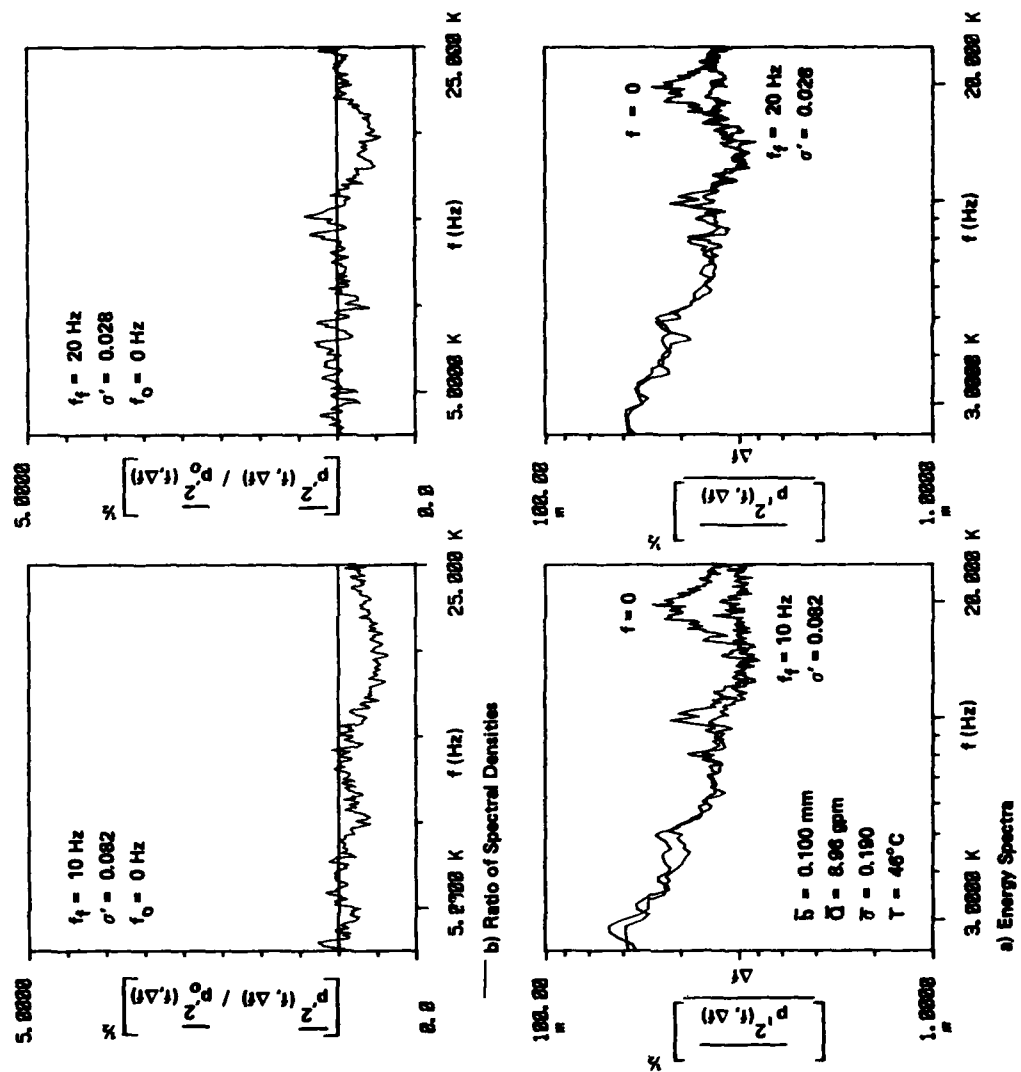


Figure 59. Effect of Spool Oscillation on Energy Spectra ($\sigma = 0.190$)

These somewhat preliminary results indicate that (1) cavitation noise may not be affected by valve modulation if the $\overline{p'^2}$ versus σ curve under steady flow is rather flat and (2) cavitation noise may in fact be suppressed if the valve oscillates about a condition corresponding to $\overline{p'^2}_{\max}$. Further testing is necessary in order to be more conclusive, however.

SECTION XI

IMPACT OF RESULTS ON AIRCRAFT HYDRAULIC SYSTEMS

The three principal manifestations of cavitation on aircraft hydraulic components such as directional control valves are: (1) noise and vibration, (2) material damage to spool or valve body, and (3) effect on performance.

The results for cavitation inception are expected to be applicable for directional control valves operating in the same Reynolds number range as the two valves tested in this investigation. Although the energy levels measured by the pressure transducers and the accelerometer cannot be directly scaled to other valves, the relative effect of cavitation as indicated by the cavitation index should be similar for other directional control valves. The peak fluctuating energy would be expected to occur once the cavitation index becomes less than approximately 0.25.

Regarding damage mechanisms, a number of studies have clearly shown a direct correlation between cavitation noise and material damage. A recent paper by Ramamurthy and Bhaskaran [19] will be referred to to illustrate this point. The principal results of their study are reproduced in Figure 60. Both cavitation noise (Figure 60d) and mass loss (Figure 60c) have a similar dependence upon the cavitation index for flow about the wedge. Furthermore, Figure 60a indicates that there is a good correlation between the cavitation index at peak noise and peak erosion. Their results also suggest that the empirical relationship between mass loss and flow velocity is similar to that between noise and velocity (Figure 60b). Careful testing of cavitation noise

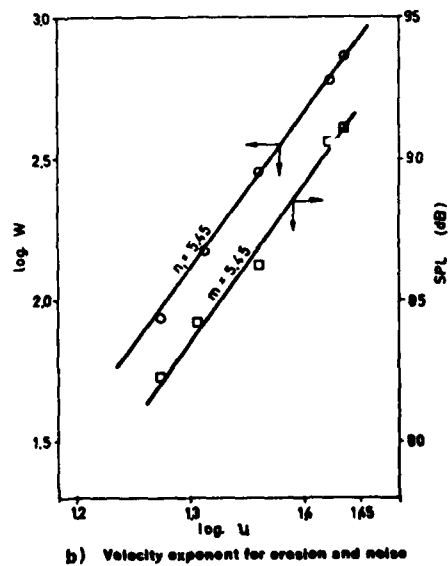
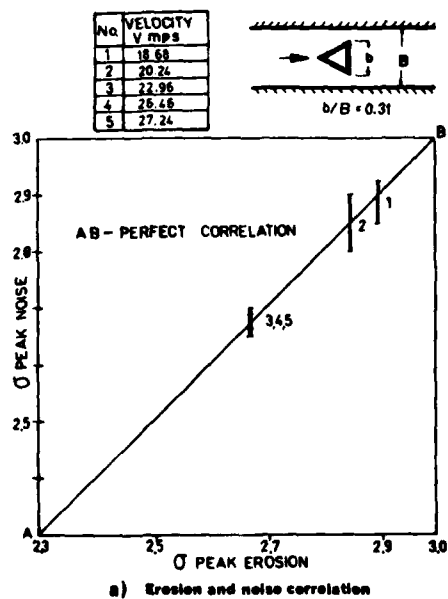
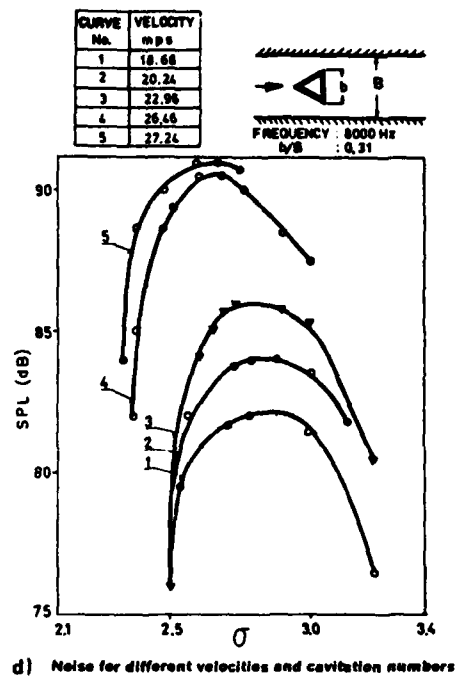
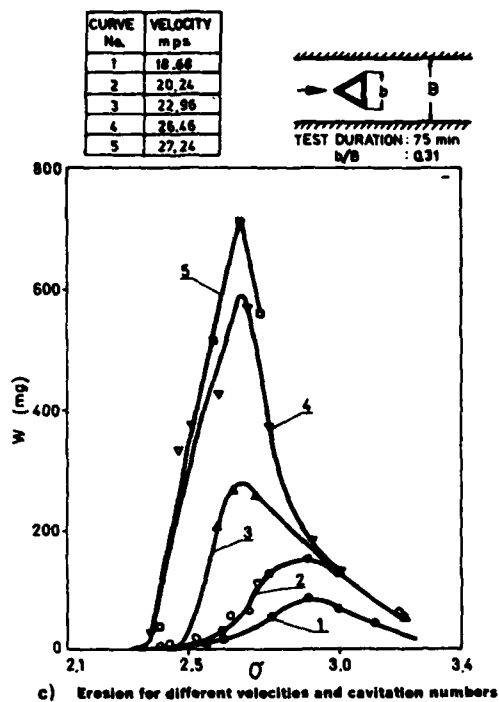


Figure 60. Correlation of Erosion with Cavitation Noise.
(Ramamurthy and Bhaskaran [19])

and erosion in pumps by Varga and Sebestyén [20] and Sebestyén et al. [21] led to a close correlation between erosion intensity and cavitation noise. There is insufficient knowledge at the present time, however, to predict mass loss from noise levels for hydraulic components in general. Recent work by Kleinbreuer [22,23] has enhanced the understanding of the effect of dissolved gas, viscosity, and jet proximity on erosion of various metals by high velocity discharge of hydraulic oil from an orifice. He tested such oils as phosphate esters, mineral oils, water glycol, and oil with various degrees of water content.

As mass loss was not monitored in the current study there is no direct correlation between cavitation noise and damage. Nevertheless, there is no reason to believe that cavitation noise and damage are not closely related in aircraft hydraulic systems. The various correlations of energy levels versus cavitation index for both valves are definitely similar to the cavitation noise level plots of Ramamurthy and Bhaskaran [19]. Peak damage would be expected to occur near the point of maximum fluctuating energy as measured by the pressure transducers and the accelerometer. Fairly extensive cavitation pitting occurred on the radial wall of the body of the model valve in the plane of the opening. No apparent damage occurred on the spool of the model valve after the many hours of operation. The difficulty in dismantling the prototype valve has precluded an inspection of cavitation damage within it.

The limited number of pulsating flow tests indicate that steady-state valve oscillation may have only a minor effect on cavitation noise provided the cavitation index remains low during the unsteady motion. Further testing is necessary to investigate the effect over

a wider range of operating conditions such as oscillating between a non-cavitating and cavitating situation. Of perhaps greater importance is the effect of unsteady cavitation on the frequency response of the valve, and hence the hydraulic system. A knowledge of the transfer function of the valve under various cavitating conditions is essential for the complete frequency response analysis of a given hydraulic system. A complete knowledge of the transfer matrix for a servovalve valve as conducted by Brennen and Acosta [24] for a cavitating pump inducer would also allow for the inclusion of the cavitating valve characteristics into hydraulic transient codes.

SECTION XII

CONCLUSIONS

1. Changes in flow pattern and jet orientation in the chamber of spool valves can be sensed by high-frequency response pressure transducers strategically placed. Under non-cavitating conditions jet noise can frequently be directly correlated with the valve opening and flow rate. For the Reynolds numbers tested in this study there is a definite effect of viscosity on pressure fluctuations emanating from a turbulent non-cavitating jet. For the range of data presented in this paper the critical cavitation number is a function of the Reynolds number.

2. High-frequency response pressure transducers are good diagnostic tools for detection of cavitation inception and cavitation intensity, while a high-frequency response accelerometer is a sensitive indicator of noise levels under cavitating conditions.

3. The ratio of cavitation noise to non-cavitating noise is greater at higher frequencies than at lower frequencies, especially if there is the direct influence of jet noise. Cavitation inception can be identified most easily by (a) comparison of auto power spectra and (b) ratio of cavitating spectra to non-cavitating spectra for the same test conditions.

4. The effect of dissolved gas content on cavitation in spool valves is minimal if the gas content does not exceed that corresponding to atmospheric conditions.

5. The principal effect of temperature is to alter the Reynolds number and hence affect (a) cavitation inception and (b) cavitation noise under certain conditions.

TABLE A-1

TYPICAL PROPERTIES OF MIL-H-5606 HYDRAULIC OIL

Temperature, T (°C)	Density, ρ (kg/m ³)	Specific Heat, c_p (J/kg°K)	Thermal Conductivity, k (W/m°K)
0	883	1814	0.138
20	870	1901	0.136
40	857	1985	0.134
60	843	2069	0.133
80	829	2152	0.132
100	814	2233	0.130
120	796	2323	0.129

APPENDIX A

PHYSICAL PROPERTIES OF HYDRAULIC OIL

The physical properties of the hydraulic oil used in this experimental investigation, MIL-H-5606C, were either obtained by direct testing or from published values in the literature. Not only were the usual hydrodynamic properties such as vapor pressure, mass density, and viscosity of interest, but also some thermodynamic properties; namely, specific heat, latent heat, and thermal conductivity, to name a few. The effect of temperature and pressure on the solubility of air in the oil also was of interest.

Table V lists the variation of density, specific heat, and thermal conductivity of a representative MIL-H-5606 oil with temperature. Figure A1 shows the typical variation of vapor pressure with temperature for MIL-H-5606. Compared to the range of the values of mean pressure in the chamber of each test valve even the value of p_v at the maximum temperature of 65°C is still quite low. The differences in vapor pressure for the various mineral oils would not be expected to affect the cavitation to any noticeable extent.

The sensitivity of viscosity to temperature, as shown by Figure A2, would be of much greater importance as regards cavitation because of the effect of Reynolds number on both cavitation inception and cavitation noise.

The solubility of dissolved air in MIL-H-5606, as well as in water and a synthetic phosphate ester oil, is shown in Figure A3 for various pressure levels. The value measured in the MIL-H-5606C oil used in

APPENDIXES

photography should be employed to obtain a better indication of bubble sizes and cavitation pattern as well as non-cavitating jet orientation.

Limited testing of aerospace hydraulic valves with vastly different designs should be conducted. The effect of small ports and internal sleeves on cavitation inception and cavitation noise should be explored.

Erosion

The direct measurement of mass loss of portions of a directional control valve is probably too difficult to determine experimentally. The direct correlation of noise with erosion could be obtained, however, under the similar conditions of a high velocity jet issuing from an orifice onto a small target or test specimen. As demonstrated in References [6-8, 22,23] various parameters can be closely controlled in this type of test facility. In such an apparatus the effect of various parameters on erosion could be correlated in terms of cavitation noise.

SECTION XIII

RECOMMENDATIONS

Although this investigation resulted in a significant advance in the knowledge of cavitation in a directional control valve, additional effort is necessary for a more complete understanding of the phenomenon. Recommendations for additional work are listed as follows in order of decreasing priority.

Effect of Pulsating Flow

For the purpose of frequency response analyses, tests under steady-state oscillation as well as transient motion should be carefully conducted. The complex transfer function should be determined over a wide range of cavitating conditions using techniques reported in References [24,25]. It is anticipated that these results would be extremely useful in the present codes that deal with hydraulic transients and the frequency response of aircraft hydraulic systems.

Steady-Flow Testing

Although these results clearly show the effect of viscosity on cavitation inception, more research needs to be conducted to assess the effect of temperature on cavitation noise under severe cavitation conditions. Additional testing at various constant values of the cavitation index would aid in the development of scaling parameters to correlate better cavitation noise. Using water in the model valve would allow for testing at higher Reynolds numbers, providing additional correlations. A limited number of tests should be conducted with entrained gas as well as with the oil supersaturated. High-speed

6. Preliminary results indicate that cavitation noise is not significantly altered by an oscillating valve. The effect of an oscillatory flow on the valve characteristics has not yet been established.

7. Peak noise levels occur for values of the cavitation index less than approximately 0.25.

8. Cavitation damage occurred on the body of the model valve.

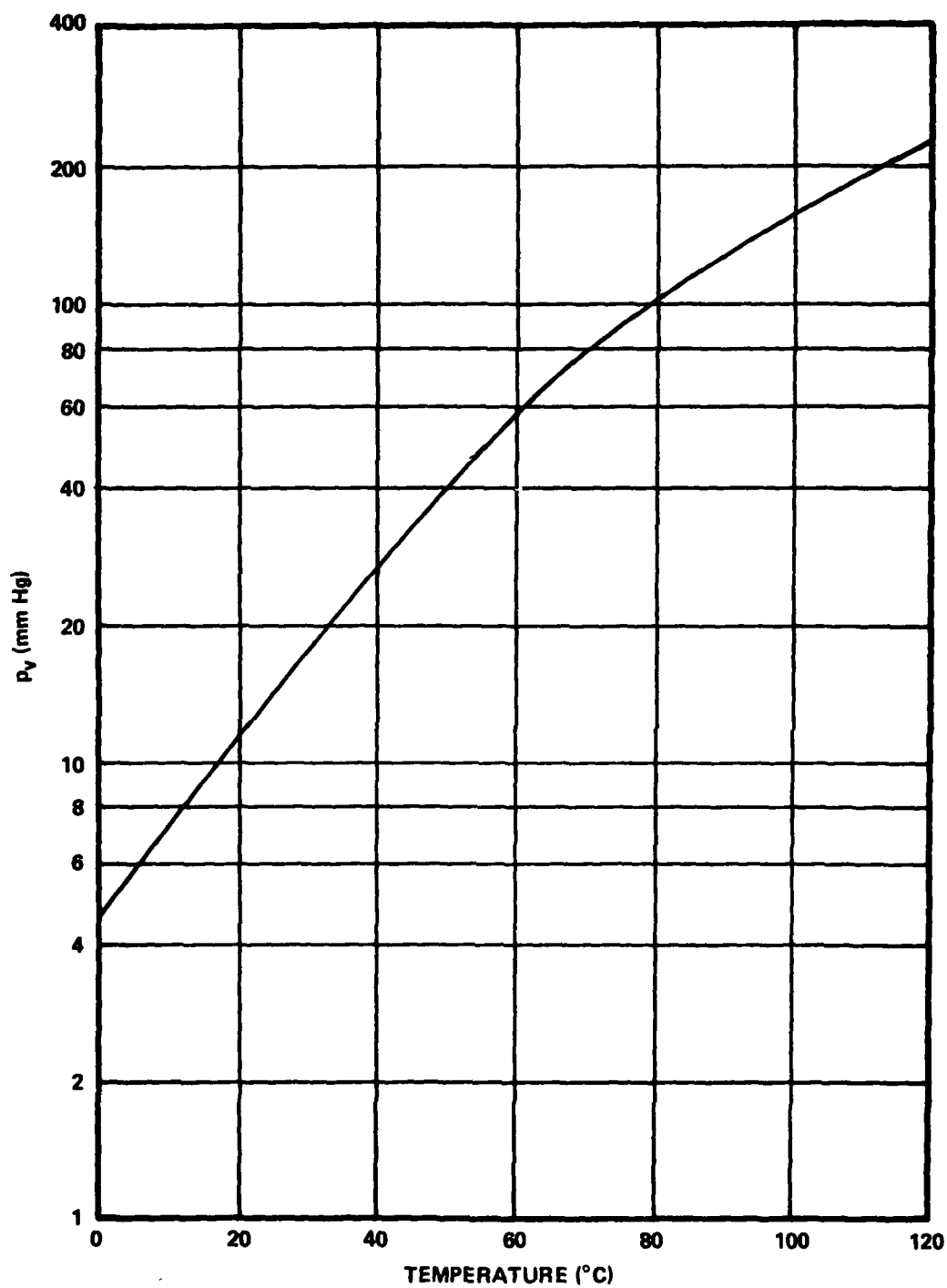


Figure A1. Effect of Temperature on Vapor Pressure of MIL-H-5606 Hydraulic Oil

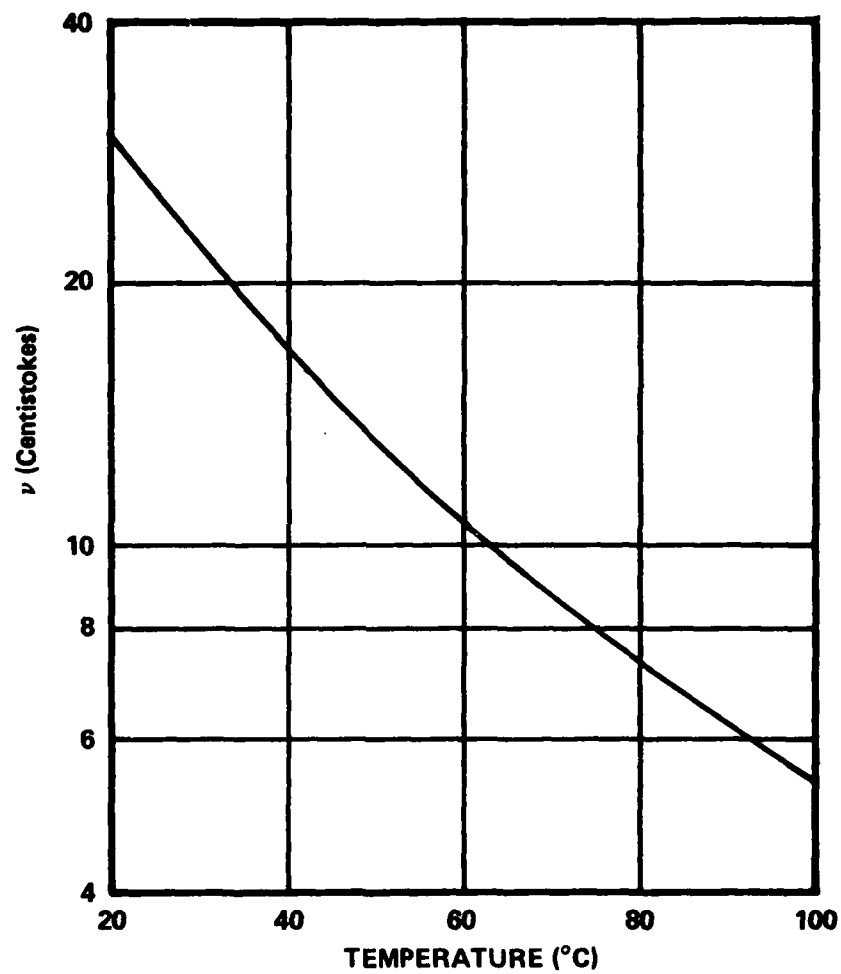


Figure A2. Effect of Temperature on Kinematic Viscosity of MIL-H-5606 Hydraulic Oil

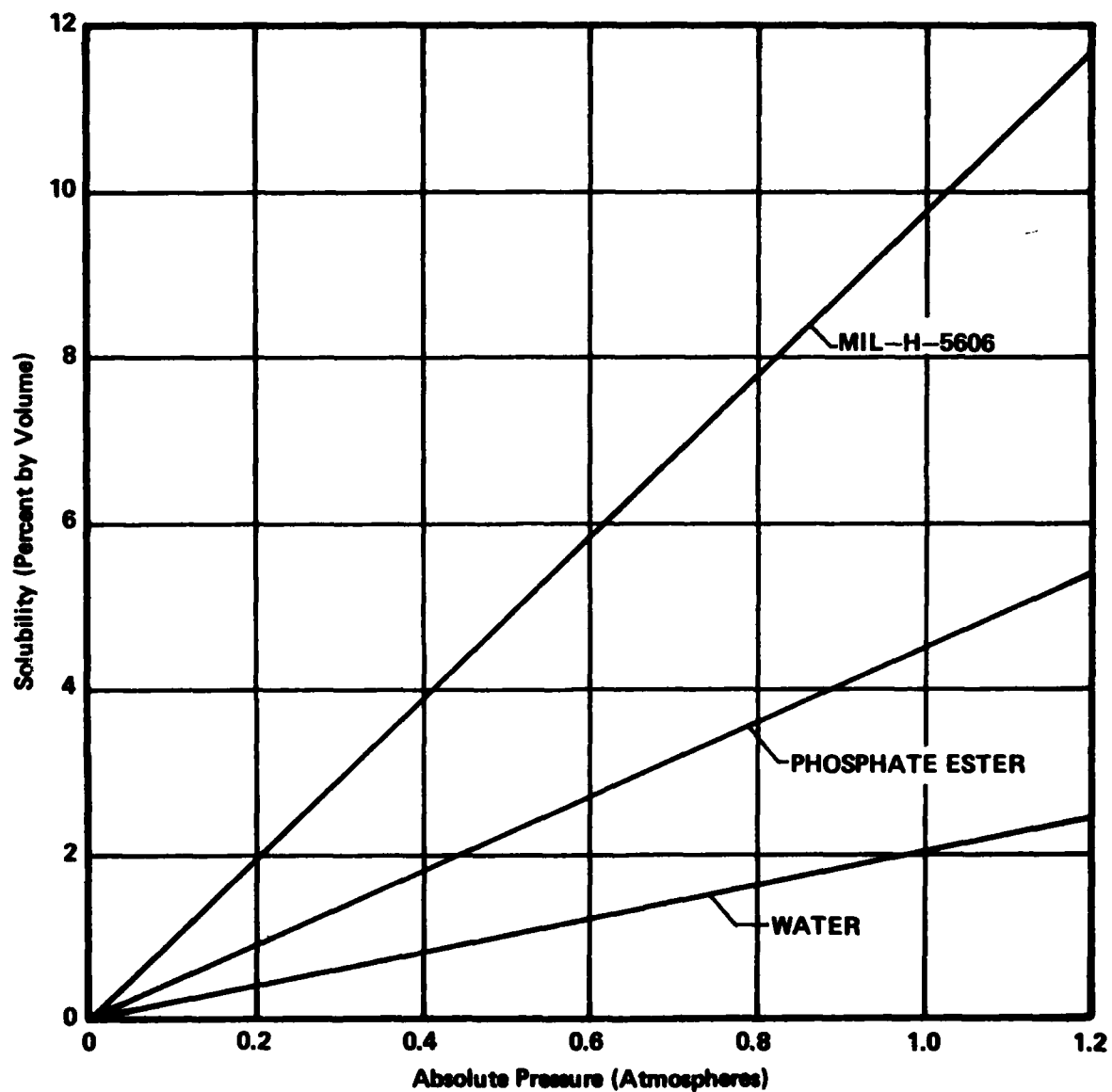


Figure A3. Effect of Pressure on Solubility of Air in MIL-H-5606 Hydraulic Oil

this investigation at atmospheric conditions checked quite closely to the corresponding value on Figure A3.

APPENDIX B
THERMODYNAMIC EFFECT

Bubble formation may not only be affected by hydrodynamic effects, but also thermodynamic factors. Using the theory outlined by Brennen [26] a thermodynamic function was evaluated for MIL-5606 oil to ascertain if there are any potential thermal effects.

As theoretically proven by Brennen [26] the relative effect of thermal to inertia type bubble growth can be expressed in terms of a thermodynamic function

$$\Sigma = \frac{2h_{fg}^2 \rho_v^2}{c_p T \sqrt{\mathcal{D}}} \quad (B1)$$

in which h_{fg} is the latent heat, T is the oil temperature, ρ_v is the density of the oil vapor, c_p and ρ are the specific heat and density of the oil in its liquid phase, and \mathcal{D} is the thermal diffusivity of the oil

$$\mathcal{D} = \frac{k}{\rho c_p} \quad (B2)$$

As values of the latent heat of MIL-H-5606 were not available the Clausius-Clapeyron relationship

$$h_{fg} \rho_v = T \frac{\partial p_v}{\partial T} \quad (B3)$$

was used instead. The derivative $\partial p_v / \partial T$ in Eq. (B3) was determined from Figure A1, allowing for the calculation of Σ , the values of which

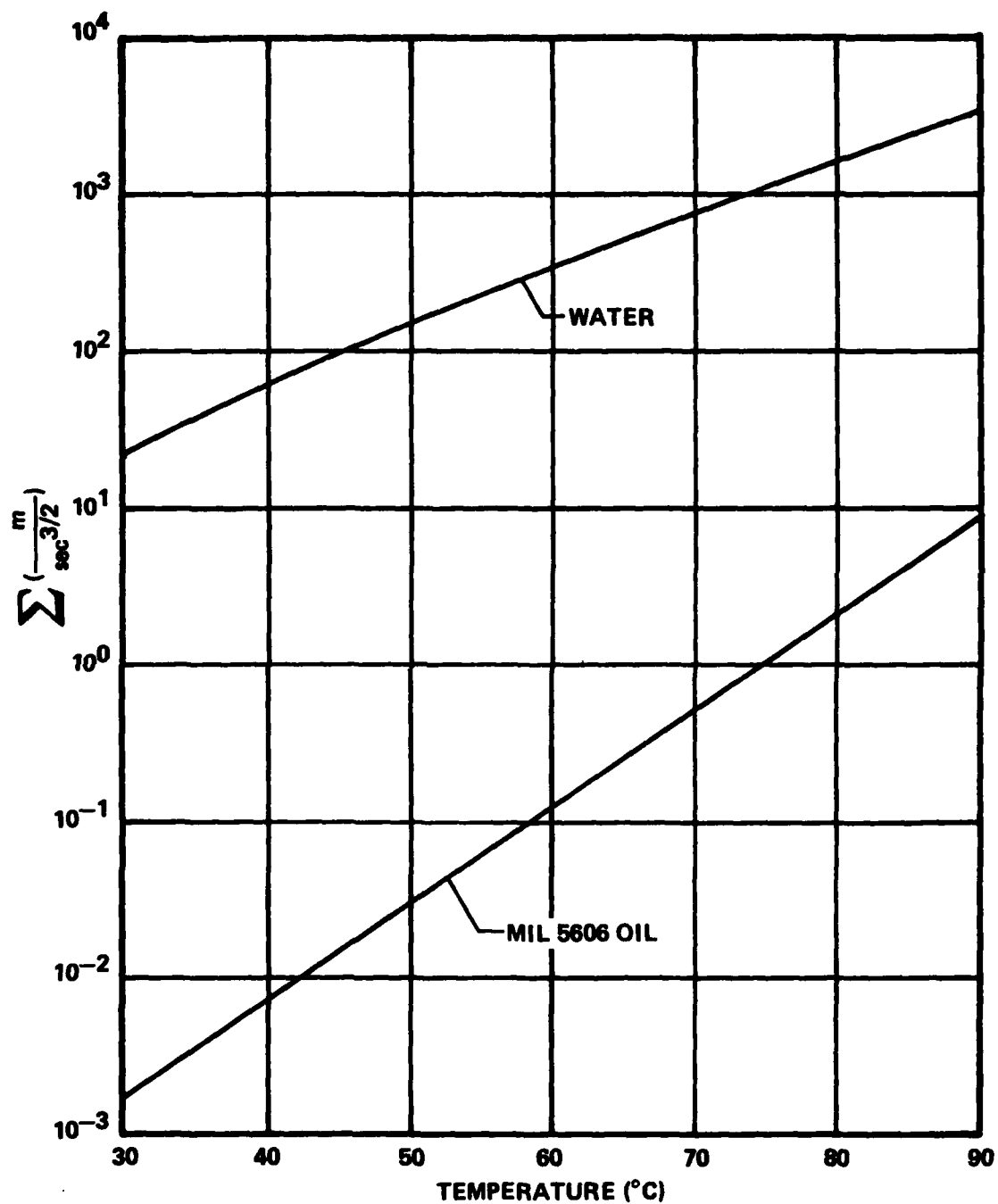


Figure B1. Thermodynamic Function for Water and MIL-H-5606 Hydraulic Oil

are plotted in Figure B1 for a range of temperatures. Corresponding values of Σ for water are included for comparison.

For the temperature ranges of interest it is believed that thermodynamics plays little to no role in bubble formation in cavitation in aircraft type valves because of the relatively low vapor pressure. The low residence time of bubbles in the valve chamber does not allow for any appreciable thermodynamic effect.

APPENDIX C

BUBBLE RESONANCE

In an effort to identify possible peak frequencies on the various energy spectra measured with the pressure transducers the natural frequency of vapor/gas filled spherical bubbles was theoretically calculated.

The natural frequency is obtained by considering a vapor/gas filled bubble of some mean, equilibrium radius r_o which is disturbed by an oscillating pressure of frequency ω and amplitude \bar{p} at an infinite distance from the bubble. The bubble responds with an oscillating radius r . Upon linearizing the perturbations in the Rayleigh equation, Plesset and Prosperetti [27], the natural frequency of the oscillating bubble can be expressed

$$\omega_n = \frac{4}{\rho r_o^3} \left[S + \frac{3(p_\infty - p_v)r_o}{4} - \frac{2\nu^2\rho}{r_o} \right] \quad (C1)$$

in which S is the surface tension, and p_∞ is the mean pressure far away from the bubble. The three terms in the bracket reflect the relative effect of surface tension, pressure, and viscosity, respectively.

For two oil temperatures representative of this study, 25°C and 50°C, and for three values of $p_\infty - p_v$, the theoretical natural frequency f of the oscillating bubble is plotted in Figure C1 as a function of bubble radius r_o .

For a given value of $p_\infty - p_v$ there is an obvious effect of temperature on the natural frequency of small bubbles because of the

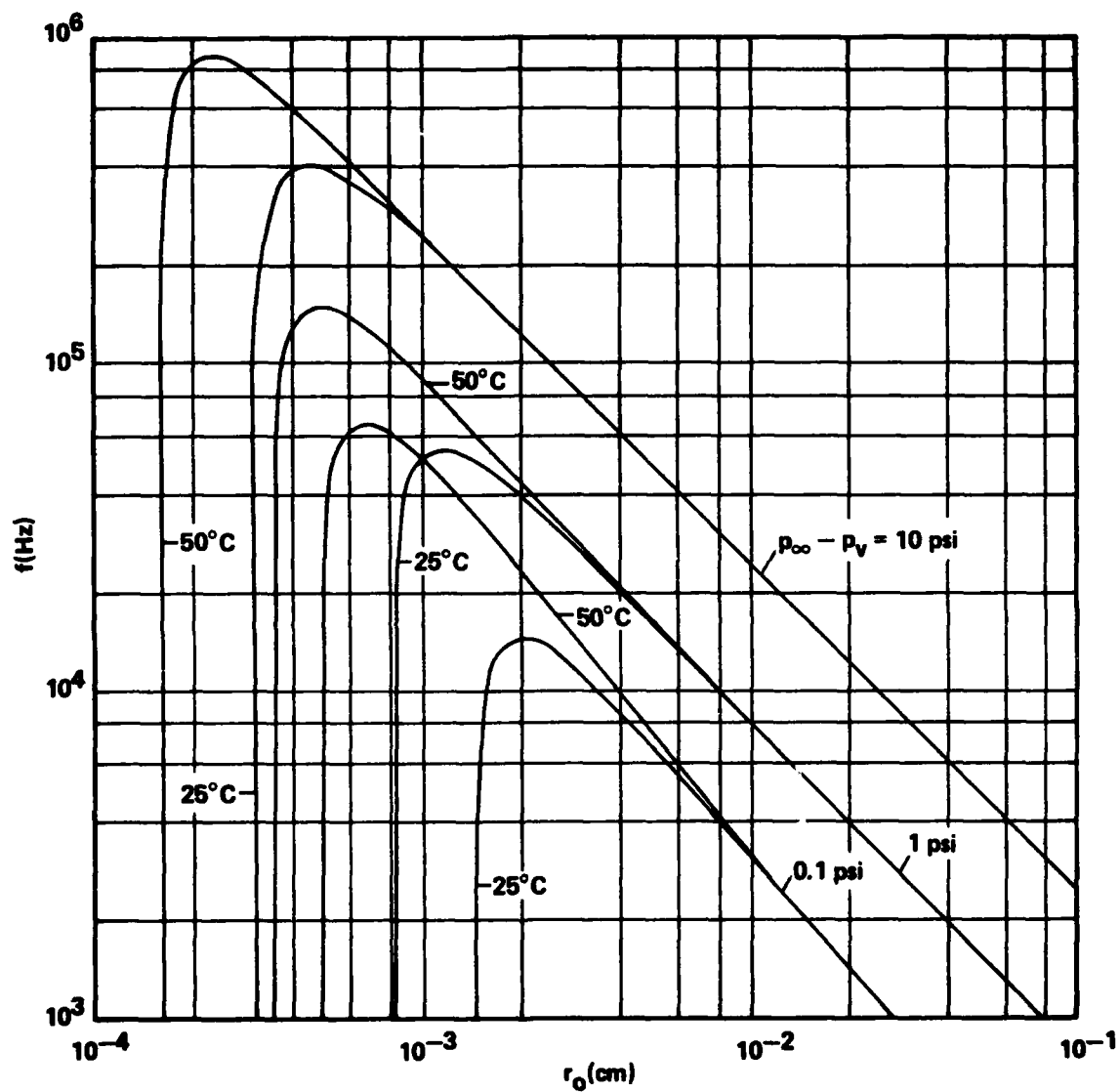


Figure C1. Resonance Frequencies for Bubbles
in MIL-H-5606 Hydraulic Oil

damping effect of viscosity. There is a cutoff radius below which there is no oscillation. The difficulty in applying the results stems from the uncertainty in the value of $p_{\infty} - p_v$ to assume. If p_{∞} were to correspond to p_c in the valve chamber then the minimum value of $p_{\infty} - p_v$ for all tests would be approximately 10 psi. In any event the theory predicts natural frequencies within and greater than the frequency range utilized in the study, 0 to 25.6 kHz.

REFERENCES

1. Wiggert, D.C. and Martin, C.S., "Cavitation Damage Mechanisms: Review of Literature," Technical Report AFAPL-TR-79- , Contract F33615-77-C-2036, Georgia Institute of Technology, November 1979.
2. Knapp, R.T., Daily, J.W. and Hammitt, F.G., Cavitation, McGraw Hill, 1970.
3. McCloy, D. and Martin, H.R., The Control of Fluid Power, Longman, London, 1973.
4. MacLellan, M.A., Mitchell, A.E. and Turnbull, D.E., "Flow Characteristics of Piston-Type Control Valves," Proceedings of the Symposium on Recent Mechanical Engineering Developments in Automatic Control, Institution Mechanical Engineers, London, Jan. 1960, pp. 13-30.
5. Beck, A. and McCloy D. , "Some Cavitation Effects in Spool Valve Orifices," Proceedings Institution Mechanical Engineers, Vol. 182, Pt. I, No. 8, 1967-68, pp. 163-174.
6. Backé, W. and Benning, P., "Über Kavitationserscheinungen in Querschnittsverengungen von ölhydraulischen Systemen," Industrie-Anzeiger, Vol. 63, 1962, pp. 35-42.
7. Backé, W. and Riedel, H.-P., "Kavitation in ölhydraulischen Systemen," Industrie-Anzeiger, Vol. 94, 1972, pp. 153-158.
8. Riedel, H.-P., "Kavitationsverhalten von verschiedenen Druckflüssigkeiten," Industrie-Anzeiger, Vol. 94, 1972, pp. 1724-1727.
9. Lichtarowicz, A. and Pearce, I.D., "Cavitation and Aeration Effects in Long Orifices," Cavitation Conference, Institution Mechanical Engineers, Edinburgh, Sept. 3-5, 1974, pp. 129-144.
10. McCloy, D. and Beck, A., "Flow Hysteresis in Spool Valves," Proceedings of the First BHRA Fluid Power Symposium, Cranfield, 1969, pp. 170-182.
11. Robertson, J.M., Hydrodynamics in Theory and Application, Prentice-Hall, New York, 1965.
12. Albertson, M.L., Dai, Y.B., Jensen, R.A. and Rouse, H., "Diffusion of Submerged Jets," Transactions, ASCE, Vol. 115, 1950, pp. 639-664.
13. Gutmark, E. and Wagnanski, I., "The Planar Turbulent Jet," Journal of Fluid Mechanics, Vol. 73, 1976, pp. 465-495.

14. Reethof, G., "Turbulence - Generated Noise in Pipe Flow," Annual Review of Fluid Mechanics, Vol. 10, 1978, pp. 333-367.
15. Lush, P.A., "Measurements of Subsonic Jet Noise and Comparison with Theory," Journal of Fluid Mechanics, Vol. 46, 1971, pp. 477-500.
16. Arndt, R.E.A., "Pressure Fields and Cavitation," Proceedings of the 7th IAHR Symposium on Hydraulic Machinery, Vienna, 1974, Paper IX.
17. Arndt, R.E.A., "Investigation of the Effects of Dissolved Gas and Free Nuclei on Cavitation and Noise in the Wake of a Sharp Edged Disk," Proceedings of Joint ASME-IAHR-ASCE Symposium on Hydraulic Machinery, Fort Collins, Colorado, 1978, pp. 543-556.
18. Rouse, H., "Cavitation in the Mixing Zone of a Submerged Jet," La Houille Blanche, Vol. 8, No. 1, 1953, pp. 9-19.
19. Ramamurthy, A.S., and Bhaskaran, P., "Velocity Exponent for Erosion and Noise Due to Cavitation," Transactions, ASME, Journal of Fluids Engineering, Vol. 101, March 1979, pp. 69-75.
20. Varga, J., and Sebestyén, G., "Experimental Investigation of Cavitation Noise," La Houille Blanche, No. 8, 1966, pp. 905-910.
21. Sebestyén, G., Stvrteczy, F., and Szabó, A., "Correlation between the Acoustical and Erosion Properties of Cavitation in a Pump," 6th IAHR Symposium on Hydraulic Machinery and Cavitation, Rome, 1972, Part 1, Paper J4.
22. Kleinbreuer, W., "Werkstoffzerstörung durch Kavitation in ölhydraulischen Systemen," Industrie-Anzeiger, Vol. 98, 1976, pp. 1096-1100.
23. Kleinbreuer, W., "Kavitationserosion in hydraulischen Systemen," Industrie-Anzeiger, Vol. 99, 1977, pp. 609-613.
24. Brennen, C., and Acosta, A., "The Dynamic Transfer Function for a Cavitating Inducer," Transactions, ASME, Journal of Fluids Engineering, Vol. 98, 1976, pp. 182-191.
25. Ng, S.L., and Brennen, C., "Experiments on the Dynamic Behavior of Cavitating Pumps," Transactions, ASME, Journal of Fluids Engineering, Vol. 100, 1978, pp. 166-176.
26. Brennen, C., "The Dynamic Behavior and Compliance of a Stream of Cavitating Bubbles," Transactions, ASME, Journal of Fluids Engineering, Vol. 95, 1973, pp. 533-541.
27. Plesset, M.S., and Prosperetti, A., "Bubble Dynamics and Cavitation," Annual Review of Fluid Mechanics, Vol. 9, pp. 145-185.